Aw investigation of the magnetocrystalline anisotropy in some of the heavy rare earth metals

P. H. Bly

AN INVESTIGATION OF THE MAGNETOCRYSTALLINE ANISOTROPY IN SOME OF THE HEAVY RARE EARTH METALS.

by

P. H. BLY, B. Sc.

Presented in candidature for the degree of Doctor of Philosophy.

June, 1967.

P306

ABSTRACT.

The magnetocrystalline anisotropies of gadolinium, terbium, dysprosium and holmium have been investigated using a torque method. Measurements were made on single crystal oblate spheroids, the major planes of which contained either the hexagonal axis or the basal plane of the crystals. The torque magnetometer used automatically balanced the torque produced in the specimen by applying a current through a small coil suspended in a galvanometer magnet, the servomechanism being provided by a light beam and photocell amplifier system. Fourier analysis of the torque curves by computer provided values for the appropriate anisotropy constants.

Torque measurements were made in the temperature range from 55°K to room temperature, and in applied magnetic field strengths up to 12.5 kOe. Because of the comparatively small field strengths available it was not possible to obtain any appreciable movement of the magnetisation from the basal plane in the cases of ferromagnetic Tb, Dy and Ho, and therefore no values could be assigned to the anisotropy constants. In the paramagnetic and antiferromagnetic temperature ranges the torque curves were described completely by one anisotropy constant $\mathcal{K}_1$, although the presence of strain in the specimen could greatly distort the curve. The anisotropy constant in the basal plane, $\mathcal{K}_4$, was measured for Gd, Tb and Dy. The easy directions in the basal plane were the a-axis for Gd, and the b-axis for Tb and Dy, although changes of easy direction were observed in Dy at temperatures where the anisotropy was small. A torque meas-

urement made in the basal plane of holmium just above the critical field showed twelvefold symmetry in the anisotropy energy, but the main energy minimum occurred at the b-axis. Comparison of the temperature variation of $\mathcal{K}_4$ with the prediction of Zener's theory was satisfactory only in the case of Gd.

For torque measurements in the $(10\bar{1}0)$ plane for antiferromagnetic Dy, the occurrence of ferromagnetism as a magnetic field larger than the critical value was rotated across the basal plane enabled the temperature variation of the critical field to be determined. The variation was found to be in agreement with other workers. Determinations of $\mathcal{K}_1$ for Ho showed a change of easy axis from the basal plane to the c-axis in the antiferromagnetic region, and back to the basal plane when the system became ferromagnetic. This behaviour contradicted neutron-diffraction measurements but is confirmed by magnetisation measurements. In the paramagnetic region a variation of $\mathcal{K}_1$ as $H^2/(T-\theta)^2$ was established.

CONTENTS

INTRODUCTION

It is only comparatively recently that the magnetic properties of those rare earth metals which exhibit ferromagnetic ordering have been investigated. The six elements, gadolinium, terbium, dysprosium, holmium, erbium and thulium, are the only ferromagnetic elements known outside the iron group transition elements, but their ordering takes place in a manner very different from that of iron, nickel and cobalt. Gadolinium appears to be a normal ferromagnet, but the other five elements exhibit antiferromagnetism in a certain characteristic range of temperature, and in this region the ordering assumes a structure which is periodic about the C axis, either helicoidal or sinusoidal. This property has aroused great interest in these metals, both theoretical and experimental. In the last few years much experimental data on the physical properties in general, and the magnetic properties in particular, has been collected, while theoreticians have had considerable success in the explanation of these properties. However, production of sufficiently pure materials has only lately permitted the growth of single crystals and therefore the investigation of the crystalline properties. Although magnetisation measurements have indicated that the magneto crystalline anisotropy is large in the five elements following gadolinium, no direct determinations of the anisotropy constants have so far been attempted. It is proposed to report here torque measurements of the anisotropy made on gadolinium, terbium, dysprosium and holmium.

CHAPTER ONE

THE RARE EARTHS

1.1 The Electronic and Physical Properties

The element lanthanum is followed in the Periodic Table by fourteen elements which have virtually identical chemical properties. Because of this similarity the group of fifteen elements is placed in a subgroup separate from the progressive classification of the Periodic Table, under the general name of Lanthanides or Rare Earths. Although these elements occupy the atomic numbers from 57 (lanthanum) to 71 (lutetium) the increase in the number of orbital electrons represented by the increasing atomic number does not take place by the filling of the outer electron orbits, but by the progressive filling of the 4f shell, while the outer shell structure remains unchanged throughout the series. The electronic structure of these elements is indicated by the general formula:-

$$Xe(4d)^{10}(4f)^{n}(5s)^{2}(5p)^{6}(5d)^{1}(6s)^{2}$$

where n increases from o to 14 as the atomic number increases from 57 to 71. Scandium (A.N. = 21) and yttrium (A.N. = 39) are usually included in the series because of the similar structure of the outer electron shells. The 5s and 5p shells thus serve as a screen for the 4f electrons, while the three electrons of the outer shells $(5d)^{1}$ and $(6s)^{2}$ are easily removed to become conduction electrons, leaving a trivalent ion. In certain of the rare earths the electronic configuration has an empty 5d shell, the electron appearing as an additional electron in the 4f shell, but in the trivalent ion the third conduction electron is taken from the 4f shell, so

that the 4f shell reverts to the configuration expected for unitary increase from one element to the next.

The name 'Rare Earths' is somewhat misleading, for the elements are all metals. Moreover, they occur in reasonable abundance, the difficulty arising in separating the different elements, rather than in finding the natural ores. It is only comparatively recently that the development of the ion-exchange method has made possible the separation of the individual elements and hence the preparation of pure rare earth metals (1,2)*.

The rare earth metals are often divided into two sub-groups on the basis of the total electron spin in the 4f shell (3); the first group is from cerium to gadolinium, in which the seven vacant states for spins of +1/2 are successively filled. Lanthanum may be included in this group, although it is not, strictly speaking, a rare earth, since it has no 4f electrons. The second sub-group corresponds to the successive filling of the -1/2 spin states, and extends from terbium to lutetium. Such a division is rather artificial, since there is no marked difference in physical properties between the first group, the 'light' rare earths, and the second, the 'heavy' rare earths: indeed, from the standpoint of an investigation of magnetic properties, gadolinium must be included in the second sub-group.

The density of the metals generally increases with increasing atomic number; as the growing nuclear charge has a larger attraction for the orbital electrons, so the mean atomic radius decreases. The decrease is small however, the radius being 1.87Å for lanthanum, and

* Numbers in brackets indicate references on page 113.

Table 1.1

Element		Atomic No.	Mol. Wt.	Density gm/cm³	Crystal Structure	Lattice Parameters a, Å	Lattice Parameters c, Å	Transition Temp. °C	M. Pt. °C	Atomic Radius Å
Scandium	Sc	21	44.96	2.90	hcp	3.309	5.273	α→β 1450	1530	1.655
Yttrium	Y	39	88.92	4.50	αY hcp βY bcc	3.647 4.11	5.731	α→β 1490	1502	1.778
Lanthanum	La	57	138.92	6.18	αLa hcp βLa fcc γLa bcc	3.77 5.30 4.26	12.16	α→β 310 (β→α) 220 β→γ 864	920	1.885
Cerium	Ce	58	140.13	6.79	αCe fcc βCe hcp γCe fcc δCe bcc	4.85 3.68 5.16 4.11	11.92	α→γ 113 γ→α 178 β→γ 100 γ→β 10 γ→δ 725	797	1.825
Praseodymium	Pr	59	140.92	6.71	αPr hcp βPr bcc	3.67 4.13	11.84	α→β 792	935	1.836
Neodymium	Nd	60	144.27	6.96	αNd hcp βNd bcc	3.66 4.13	11.80	α→β 862	1024	1.829
Samarium	Sm	62	150.35	7.50	αSmromb βSm bcc	8.97 4.07	α=23°13′	α→β 917	1072	1.811
Europium	Eu	63	152.0	5.30	bcc	4.58			826	1.994
Gadolinium	Gd	64	157.26	7.80	αGd hcp βGd bcc	3.64 4.06	5.78	α→β 1264	1312	1.810
Terbium	Tb	65	158.93	8.19	αTb hcp	3.60	5.69	α→β 1326	1364	1.801
Dysprosium	Dy	66	162.51	8.35	hcp	3.59	5.65		1407	1.795
Holmium	Ho	67	164.94	8.65	hcp	3.58	5.62		1461	1.789
Erbium	Er	68	167.27	9.01	hcp	3.56	5.59		1497	1.779
Thulium	Tm	69	168.94	9.20	hcp	3.54	5.55		1545	1.769
Ytterbium	Yb	70	173.04	7.02	αYb fcc βYb bcc	5.49 4.45		α→β 798	824	1.940
Lutetium	Lu	71	174.99	9.79	hcp	3.50	5.55		1652	1.752

1.73Å for lutetium (3). Both europium and ytterbium have atomic radii appreciably greater than this, but these metals are believed to be divalent in the metallic state. The values of the atomic radii and the densities for the rare earth metals are listed in Table 1.1.

It is not only the outer electrons which take part in the interionic bonding, but also the electrons of more deeply lying shells, as is the case in all the transition-group metals. This very strong bonding results in great strength and hardness, high melting points and high metallic electrical resistivity.

Table 1.1 lists the crystal structures of the rare earths, and it can be seen that at room temperature almost all have hexagonal close-packed structures; the exceptions are europium and ytterbium, which may be divalent, and cerium. The majority of the rare earths have a simple hexagonal close packed structure with a c/a ratio of approximately 1.6. More complicated structures, which are still basically h.c.p., exist for lanthanum, praesodymium and neodymium, where because next nearest layers are not of the same orientation the c/a ratio is 3.2. Samarium has a crystal structure with a c/a ratio of 7.2, since although each basal plane layer of ions is hexagonal, the variation in the orientation of these layers is only repeated after nine layers.(4)

1.2 Magnetic Properties of the Rare Earth Metals

The magnetic properties of the rare earth metals are closely related to the character of the unfilled 4f shell, since it is this shell which gives rise to uncompensated electron spins, in a manner similar to the unfilled 3d shell in the iron group transition elements. In the

Table 1.2

Element	Magnetic Susceptibility at 25°C x10⁻⁶ emu/mole	Curie-Weiss Constant x10⁻⁴ emu.°K.gm	Asymptotic Curie Point θ °K	Curie Point T_c °K	Néel Point T_n °K	Electronic State of 3⁺ion S	L	J	Effective Moment Theory Hund M_s	Theory VV-F M_s	Expt. 3⁺ion M_s	Expt. Metal M_s	gJ M_s	Obs. M_s
Sc	8.08	-												
Y	191	-												
La	101	-				0	0	0	0	0	0	0.49	0.0	
Ce	2430	55.3	-46		12.5	½	3	2½	2.54	2.56	2.52	2.51	2.14	
Pr	5320	119.8	-21			1	5	4	3.58	3.62	3.60	3.56	3.20	
Nd	5650	94.7	-16		7.5	1½	6	4½	3.62	3.68	3.50	3.3	3.27	
Pm		-				2	6	4	3.68	2.83	-	-	2.40	
Sm	1275	-			14.8	2½	5	2½	0.85	1.55	-	1.74	0.72	
Eu	33100	414	15		(90)	3	3	0	0.00	3.40	-	7.12	0.0	
Gd	356000	476	310	289		3½	0	3½	7.94	7.94	7.80	7.95	7.0	7.12
Tb	193000	739	236	220	228	3	3	6	9.72	9.70	9.74	9.7	9.0	9.25
Dy	99800	867	151	87	178.5	2½	5	7½	10.64	10.6	10.5	10.64	10.0	10.2
Ho	70200	911	87	20	132	2	6	8	10.60	10.6	10.6	10.89	10.0	9.7
Er	44100	667	42	20	80	1½	6	7½	9.58	9.6	9.6	9.5	9.0	8.3
Tm	26200	434	20	22	53	1	5	6	7.56	7.6	7.1	7.52	7.0	
Yb	71	-				½	3	3½	4.53	4.5	4.4	0.41	4.0	
Lu	17.9	-				0	0	0	0	0	0	0.21	0.0	

latter case, however, the unfilled shell is outermost in the metallic ion, and interaction of the electron orbits with the crystalline field quenches the orbital angular momentum. In the rare earths the unfilled 4f shell is screened from the cyrstalline field by the 5s and 5p shells, even in the trebly ionised atom, and the orbital angular momentum contributes to the total magnetic moment. Further, the screening effect of these outer orbits might be expected to inhibit severely the direct ion to ion interactions which give rise to magnetic ordering in the iron group transition elements, and other mechanisms for interaction must be sought to explain the ordering present in some of the rare earth metals. The very small radii of the 4f shells will also tend to minimise such direct interactions.

The 4f shell, with quantum number l=3, has seven orbitals whose magnetic quantum numbers are -3, -2, -1, 0, 1, 2 and 3. These can be filled by fourteen electrons, half with spin of +1/2, and half with negative spin, the seven positive spin orbitals being filled first. The quantum numbers for the shell, S, L and J are denoted for each element in Table 1.2. Since the energy gap between the first excited state and the ground state is large, only the latter need be considered at moderate temperatures. These values may then be used to determine the Landé splitting factor or gyromagnetic ratio g, and also the effective magnetic moment:

$$M_{eff} = g\sqrt{\{J(J+1)\}}\,M_B,$$

where M_B is the Bohr magneton, which is the magnetic moment of the electron, $\frac{eh}{4\pi mc}$. These theoretically derived values are listed in Table 1.2. The effective moment is compared in Figure 1.1 (5) with experimentally obtained

Fig. 1.1 The dependence of the atomic magnetic moments on the number of electrons in the 4f shell for the trivalent rare earth ions and the rare earth metals. Also shown are the values predicted by the Hund and Van-Vleck-Frank theories.

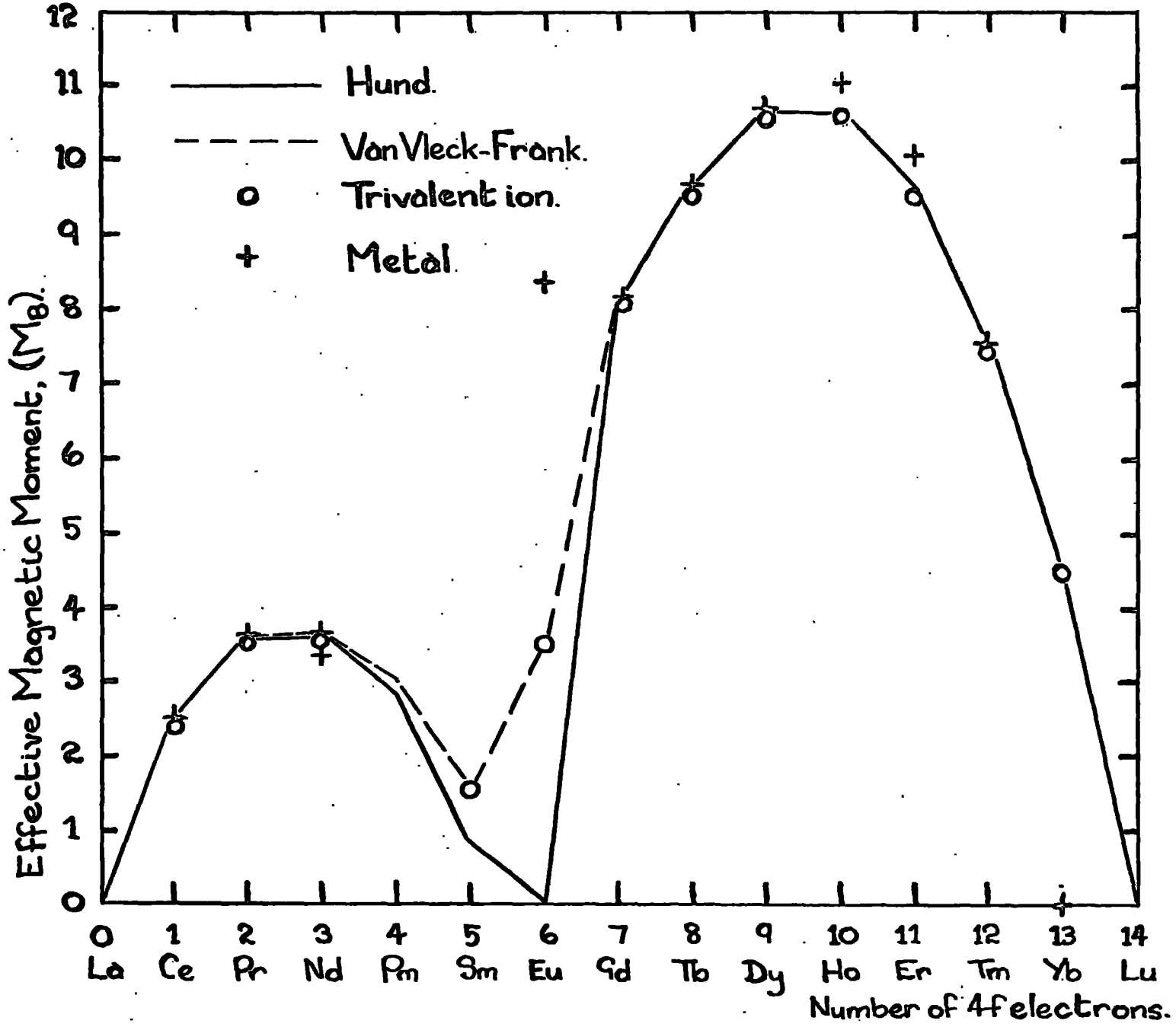

values of the magnetic moment obtained from the temperature dependence of the susceptibility of rare earth salts (6). Agreement is excellent except in the cases of europium and samarium, and these discrepancies have been explained by Van Vleck (7) in terms of the small energy separation between the ground state and the first excited state, occupation of which, because of the larger J value, increases the effective magnetic moment. The corrected values are also shown in Figure 1.1.

Also plotted in Figure 1.1 are the magnetic moments determined experimentally for the rare earths in the metallic state (8) and here again the agreement with theory is good. The points for europium and ytterbium are far from the ionic values, but both elements have very large atomic radii, and consequently the overlapping of electron orbits of neighbouring atoms could increase the effective number of electrons in the 4f shell and raise the electronic configurations to those of gadolinium and lutetium respectively (5).

The great similarity of the magnetic moments for the ionic and metallic rare earths indicates that the 4f shell is unaffected by the valance electrons, unlike the iron group transition metals, where the unshielded 3d electrons cannot be considered to be completely localised in the atom.

Except for those elements at the beginning and at the end of the rare earth series, the elements have very large paramagnetic susceptibilities: this is especially true in the case of the elements from gadolinium through to thulium. It is these elements which are found to exhibit ferromagnetism, the Curie temperatures decreasing with

increasing atomic number. Gadolinium becomes ferromagnetic just above room temperature; the other elements have ferromagnetic Curie points well below room temperature.

Magnetisation measurements have been made on all the ferromagnetic rare earth metals by various workers: gadolinium (9,10,11, 12,13); terbium (14, 15, 16, 17); dysprosium (14, 18, 19, 20, 21); holmium (14, 20, 22, 23, 24); erbium (20, 25, 26, 27, 28); and thulium (14, 23, 29, 30). The absolute saturation magnetic moments determined from these measurements agree well with the theoretical value gJ; comparison is made in Table 1.2. The temperature dependence of this saturation moment obeys the $T^{3/2}$ law proposed by Bloch (31) in the case of gadolinium and holmium, but terbium, dysprosium and holmium, together with gadolinium at low temperatures, show a dependence of the saturation moment which agrees better with a T^2 law, which is a dependence predicted by Niira(32), who considered the effect of the magnetocrystalline anisotropy on the magnetisation.

Perhaps the most remarkable feature of the magnetism exhibited by the heavy rare earth metals is that in a temperature region above the Curie point the elements Tb, Dy, Ho, Er and Tm become antiferromagnetic. This behaviour is clearly visible in the magnetisation data: as the temperature is decreased while the metal is paramagnetic, the magnetisation increases in such a manner that the inverse susceptibility is proportional to temperature, in common with most paramagnetic materials. The magnetisation passes through a maximum, and then decreases with decreasing temperature as the system becomes antiferromagnetic, the maximum indicating the Néel temperature. Then as the temperature decreases

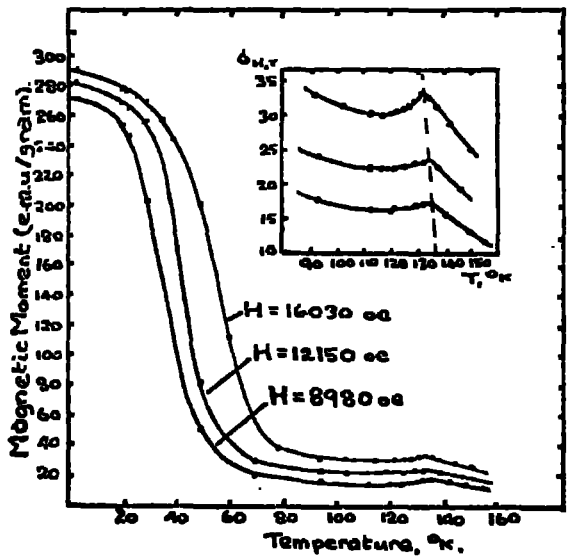

Fig. 1.2 Magnetic field and temperature dependence of the magnetisation of holmium.

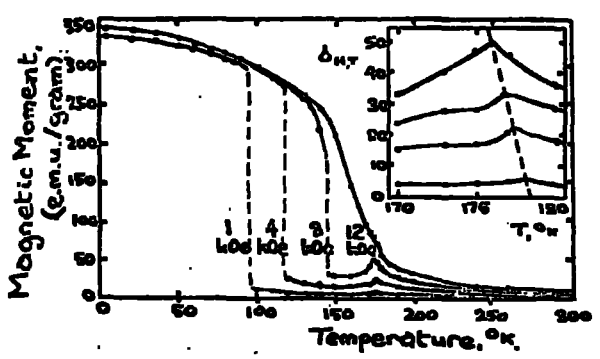

Fig. 1.3 Magnetic field and temperature dependence of the magnetisation of dysprosium.

further, below the ferromagnetic Curie point, the metal becomes ferromagnetic, and the magnetisation increases rapidly. This behaviour of the magnetisation in the case of holmium (23) and dysprosium (19) is shown in Figures 1.2 and 1.3.

It can be seen from these graphs that the Néel temperature is slightly field-dependent, the magnetisation maximum moving to lower temperatures as the magnetic field strength is increased. Further, it can be seen for dysprosium that if the magnetising field is of the order of 12kOe or larger, the transition to ferromagnetism occurs at the Néel point, and there is no antiferromagnetic region. For magnetising field strengths below 12kOe, the temperature range of the antiferromagnetic region decreases as the field strength is increased, the antiferromagnetic transition moving to higher temperatures.

The magnetocrystalline anisotropy is very large for the elements terbium to thulium, and consequently the magnetisation lies close to the preferred crystalline direction, even when fields of some tens of kilo-oersteds are applied. High field work by Henry (33,34) has shown that in the case of dysprosium and holmium, where the easy directions for magnetisation lie in the basal plane, magnetic fields of the order of 80 kOe are necessary to produce magnetic saturation along the C axis. Terbium also has an easy direction in the basal plane, but in the cases of erbium and thulium it is the C axis which is the easy direction (28,30).

Neutron diffraction studies have been carried out by Koehler et al (35, 36, 37) in order to determine the magnetic ordering which exists in the antiferromagnetic rare earth metals. For the metals from terbium through to thulium the antiferromagnetic ordering shows a sinusoidal

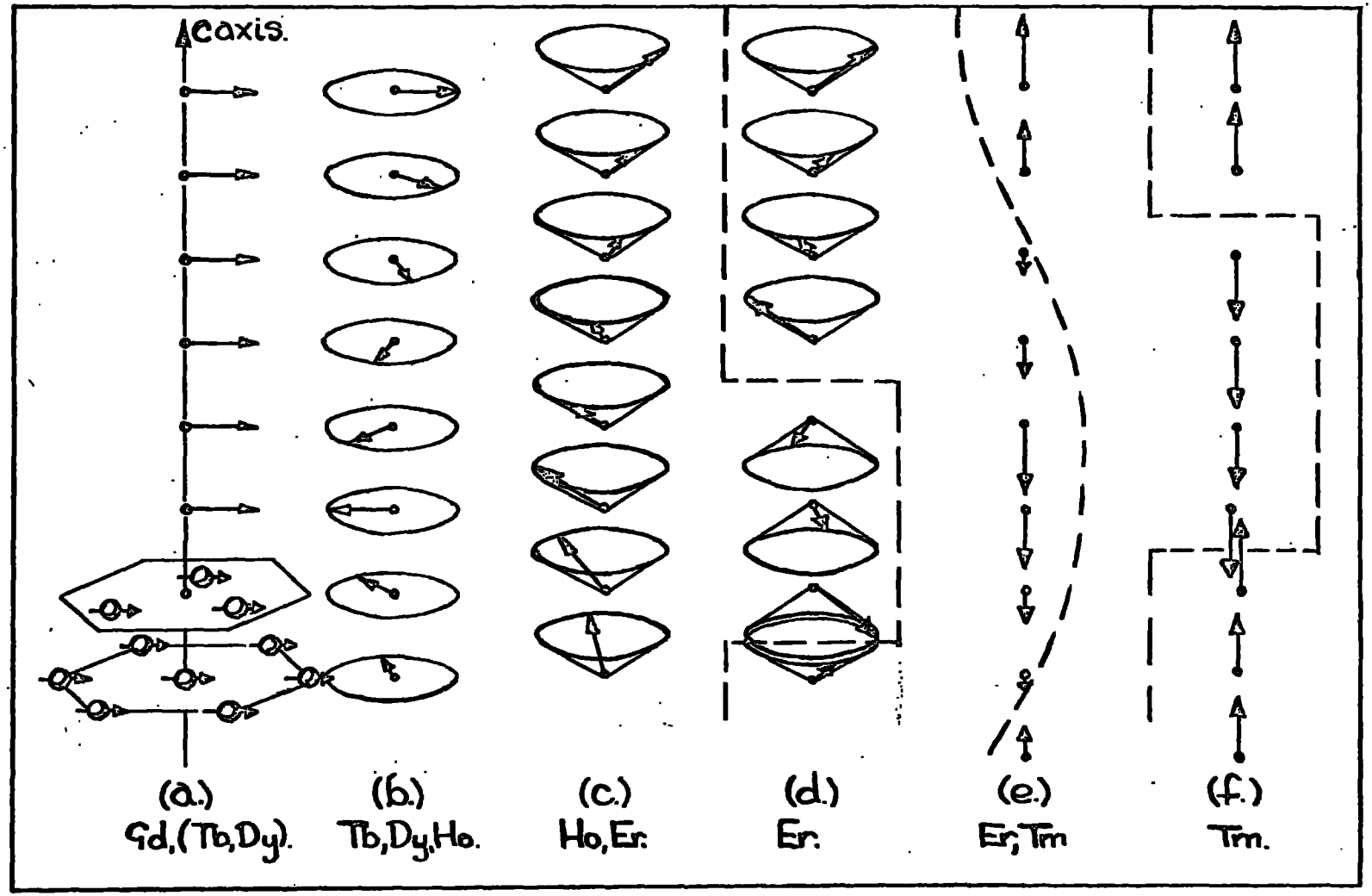

Fig. 1.4 Spin structures found in the heavy rare earth metals in the antiferromagnetic state, as determined by neutron diffraction techniques.

variation along the C axis and, except for thulium, ferromagnetic ordering within the a-b planes. The various types of spin structures determined by neutron diffraction are illustrated schematically in Figure 1.4. In terbium and dysprosium the spins lie entirely within the basal plane, and the ordering in each of the basal plane layers is ferromagnetic. However, the direction of magnetisation in the plane rotates through a constant angle from one layer to the next. This results in a spiral structure about the C axis, as indicated in Figure 1.4(b). For holmium, the studies of Koehler et al indicated that in the antiferromagnetic region the spins are arranged in a simple spiral or screw structure about the C axis, as for terbium and dysprosium. Below the ferromagnetic Curie point, $20^{\circ}K$ this screw structure is retained, in zero applied field, but there is a small ferromagnetic component parallel to the C axis. This results in a conical spiral, as illustrated in Figure 1.4(c). However, the application of a small magnetic field in the basal plane results in ferromagnetism in the basal plane, where the full saturation moment of $10M_B$ is developed (37).

In the case of erbium and thulium, a different type of ordering exists. In the previous metals the easy direction for magnetisation has been in the basal plane, there being a large magnetocrystalline anisotropy between this plane and the C axis, but only a comparatively small anisotropy existing within the basal plane itself. In erbium and thulium the large anisotropy is still present between the C axis and the basal plane, but it is such as to make the C axis the easy direction. If the exchange effects involved produce a periodic variation of the spin order along the C axis, a spiral can exist where the spins are confined to the plane and have two degrees of freedom, but where the spins are confined close to the C axis, only a periodic variation of the C axis component of the spins is

Table 1.3

	Paramagnetic Curie Point, ^{o}K	T_n, ^{o}K	Structure and Turn Angle T_a			T_c, ^{o}K	Ferromagnetic Structure
Tb	$\theta = 237$		Simple spiral, $\angle 20.5^{o} \rightarrow 18^{o}$, $\mu \perp c$			220	$\mu \perp c$
Dy	$\theta = 121$ $\theta = 169$	175	Simple spiral $\angle 43^{o} \rightarrow 35^{o}$	140	Spiral plus 2nd harmonic $\angle 35^{o} \rightarrow 26^{o}$	87	$\mu \perp c$
Ho	$\theta = 88$ $\theta = 85$	132	Simple spiral $\angle 50^{o} \rightarrow 36^{o}$	35	Non-sinusoidal arrangement $\angle \sim 36^{o}$, spacing 10 layers. Small $\mu \parallel c$	20	$\mu \perp c$ induced by field
Er	$\theta = 42$	80	Sinusoidal $\mu \parallel c$	52	Sinusoidal plus harmonics. Antiphase domain at low temperatures, Spiral $\angle 51^{o} \rightarrow 43^{o}$	20	Spiral with ferro. $\mu \parallel c$ Spiral $\mu \perp c$ $\angle = 41^{o}$
Tm	$\theta = 20$	53	Antiphase domain arrangement almost constant period of $\sim 63^{o}$:			20	Ferro. $\mu \parallel c$

produced. In erbium, between 84°_{K} and $53{\cdot}5^{\circ}_{K}$, and in thulium between 56°_{K} and 40°_{K}, a sinusoidal variation of the spin component along the C axis is observed (37). In this arrangement the components of the moments in the C axis direction are aligned parallel, while there is no order among thebasal plane components. This is shown in Figure 1.4(e). Below $53.5^{\circ}K$ in erbium, the components in the basal plane begin to order into some helical arrangement, while higher order harmonics appear in the sinusoidal form of the C axis components, which at lower temperatures have an "antiphase domain" type of structure, with the moments parallel for several layers, followed by several layers with the moments parallel in the opposite C axis direction, as shown in Figure 1.4(d). Thulium, on the other hand, never shows any ordering of the moments within the basal plane until the Curie temperature is reached, but below 40°_{K} the C axis components begin to assume the antiphase domain structure, where three layers of moments pointing one way are followed by four layers with moments pointing in the opposite direction, as in Figure 1.4 (f). The type of structure during the transition is unclear, many additional harmonics developing in the original sinusoidal variation.

It has been suggested by Belov et al (38, 39, 40) that gadolinium has a Néel point of 290°_{K}, below which lies an antiferromagnetic region, with a ferromagnetic Curie point at 210°_{K}, the antiferromagnetism being destroyed by applied magnetic fields above a few tens of oersteds. Neutron diffraction studies have shown no evidence of any periodic arrangement of the spins, even at zero field (41). The ordering appears to be purely ferromagnetic, the easy direction for magnetisation being dependent on temperature. This arrangement is indicated in Figure 1.4(a) which shows

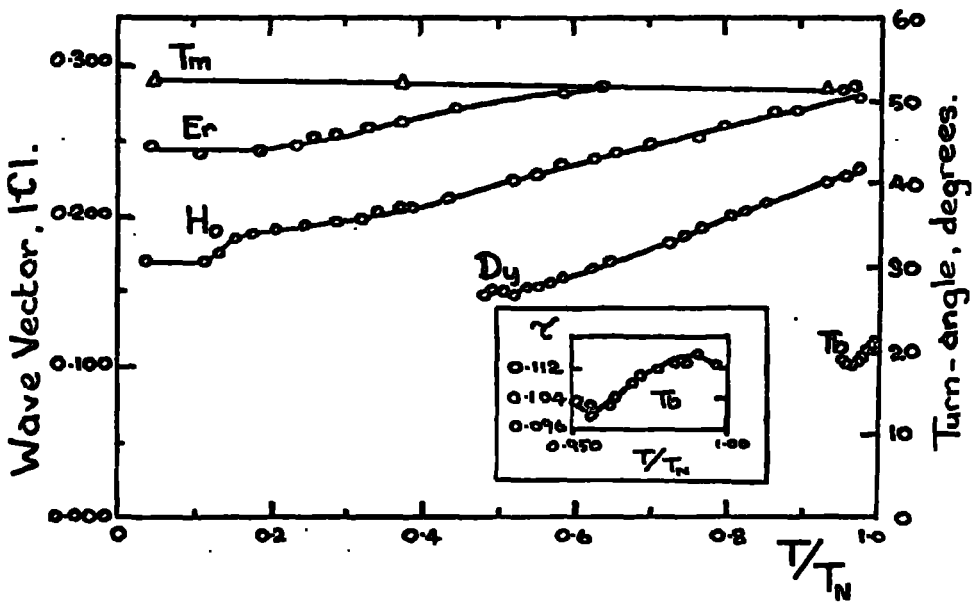

Fig. 1.5 Temperature dependence of the periodicities of the spiral spin structures in the rare earth metals.

the positions of the individual spins in the hexagonal lattice, although, of course, the spins do not necessarily lie in the basal plane.

The periodicity of the spin structures in the antiferromagnetic rare earth metals was found to be strongly temperature dependent by Koehler et al (37). In the case of the spiral spin structures, the turn angle decreases as the temperature decreases below the Néel point, until the spiral becomes unstable and ferromagnetism results. For holmium this does not happen unless an external magnetic field is applied. The magnetic structure and its dependence on temperature is summarised in Table 1.3 and the nature of the variation in the periodicity is shown in Figure 1.5.

CHAPTER TWO

Basic Concepts

If a magnetic field H is applied to a substance, a magnetic moment of σ_g per unit mass of the substance will be induced. σ_g is related to the magnetising field by the equation:

$$\sigma_g = \chi_g H \qquad 2.1$$

where the coefficient χ_g, which is scalar if measured in the direction of H, is called the magnetic susceptibility, and will in general be a function of H and temperature. This equation describes all magnetic states; for diamagnetic substances χ_g is small and negative, and very nearly field and temperature independent. For paramagnetic substances χ_g is rather larger and positive, and field independent, the magnetisation being proportional to the applied magnetic field. The classical theory of Langevin (42), when modified by consideration of the quantised nature of the possible orientations of the atomic magnetic moments, leads to an expression for the susceptibility in the form (see, for example 43):-

$$\chi_g = \frac{Ng^2 J(J+1) M_B^2}{3kT} \qquad 2.2$$

where J is the quantum number for total angular momentum, which is non-zero for substances exhibiting strong paramagnetism, g is the Landé splitting factor

$$g = 1 + \frac{J(J+1)+S(S+1)-L(L+1)}{2J(J+1)} \qquad 2.3$$

N is the number of atoms per unit mass, M_B is the Bohr magneton and k is Boltzmann's constant. The susceptibility is inversely proportional to the absolute temperature T in this expression, a relationship which is not generally valid; a more universal relationship is known as the Curie-Weiss law:-

$$\chi_g = \frac{C_g}{T-\theta} \qquad 2.4$$

where Cg is the Curie constant per unit mass, and θ is a constant known as the paramagnetic Curie temperature.

The bulk magnetisation of a paramagnet will increase with increasing field or decreasing temperature: for a magnetic field H and absolute temperature T the statistical distribution of spins about the mean direction leads to a value of the magnetisation of a material with N atoms per unit mass, of:-

$$\sigma_g = NgM_B J B_J(x), \quad \text{where} \quad x = \frac{gJM_B H}{kT} \qquad 2.5$$

Here B_J is the Brillouin function defined by:-

$$B_J(x) = \frac{2J+1}{2J}\coth\frac{(2J+1)x}{2J} - \frac{1}{2J}\coth\frac{x}{2J} \qquad 2.6$$

Thus for perfect parallelism of the atomic dipoles, when $\frac{H}{T} \to \infty$, the magnetisation will reach a saturation value of:-

$$\sigma_{sat.} = NgJM_B \qquad 2.7$$

Certain substances exhibit ordering of the atomic magnetic moments even when no magnetic field is applied. Antiferromagnetic substances exhibit an ordering of the atomic moments in an antiparallel arrangement, with zero resultant magnetisation. χ_g is positive, and shows a temperature dependence well above the Néel point (the temperature at which the transition from paramagnetism to antiferromagnetism takes place) identical with the Curie-Weiss law. However, in this case the asymptotic Curie temperature is generally negative. χ_g reaches a maximum at the Néel point, and at lower temperatures decreases with decreasing temperature.

In ferromagnetic substances the susceptibility is positive, very large, and dependent on both magnetic field strength and temperature below the ferromagnetic Curie point, Tc. Above the paramagnetic Curie point, which is normally a few degrees above Tc, the Curie-Weiss law is obeyed.

Below Tc the atomic magnetic moments order and become parallel. If no external magnetic field is applied, a macroscopic specimen of the material will contain many small regions (domains) which are each spontaneously magnetised but may be so arranged relative to one another as to give zero or small total magnetisation, thus minimizing the magnetic energy. Application of an increasing magnetic field will favour energetically the domains with magnetisation in the direction of the field, and these domains will increase in size at the expense of the other domains, thus progressively increasing the total magnetisation in the direction of the field. When this domain growth is completed and the material has only one domain, further magnetisation increase takes place slowly by a pulling of the spins into the field direction and away from the easy direction for magnetisation in the crystalline lattice. Ferromagnetic materials display hysteresis, in that if the magnetising field is reduced to zero, the total magnetisation in the direction of the field still has a finite value; that is to say, the domain distribution has not returned to its original state.

The actual magnetic field effective in orientating the atomic dipoles is much larger than the externally applied field: Weiss (44) postulated the existence of an 'internal molecular field' expressed as:-

$$H_m = H_a + \lambda M \qquad 2.8$$

where Ha is the applied field, M is the magnetisation, and λ is a proportionality constant. The molecular field is an expression of the exchange interaction which exists between the atomic dipoles and tends to align them. The equations which were derived for paramagnetic materials on the basis of the Langevin theory may be applied to ferromagnets if the

magnetising field is written as 2.8, to include the effect on each atomic magnetic moment of the surrounding atomic moments. The term λM is equivalent to an internal magnetic field of the order of 10^7 oersteds.

CHAPTER THREE

MAGNETOCRYSTALLINE ANISOTROPY

3.1 Phenomenology

In the foregoing brief remarks on ferromagnetism, the nature of the magnetic material was not considered. The atomic moments or spins will lie in a crystal lattice, and the exchange interactions involved will be affected by the direction in which the spins are pointing relative to the lattice. Thus there will in general be certain crystal directions in which magnetisation is easier than in others; that is to say, the energy required for magnetisation is less. Such 'easy' directions are usually crystallographic axes. Directions in which the energy for magnetisation is maximum are, conversely, known as 'hard' directions. In measuring the energy of magnetisation, it is not difficult to obtain the difference in energy for magnetisations along the easy axis and along the hard axis; the total magnetisation energy involves also the energy for magnetisation along the easy axis as a constant which is not involved when changes in direction only of the magnetisation are being investigated.

For polycrystalline substances the effect of the crystalline anisotropy is to add a further perturbation to the parallelism of the magnetic spins and consequently a further dependence of magnetisation on magnetic field and temperature. For a single crystal the magnetisation in the direction of the magnetising field will be dependent on the direction of this field relative to the easy axis, being maximum when the field is in the easy axis and the magnetisation lies in this easy direction, and minimum when the field lies in the hard axis, and the magnetisation lies

between the magnetic field and the easy axis. As the field is increased, the magnetisation will move closer to the field direction. The variation of the energy for magnetisation involved here might be expected to depend on the crystal symmetry, and an expression for the energy must contain terms involving the orientation of the magnetisation relative to the crystal lattice. For cubic crystals, such as iron or nickel, this orientation may be expressed in terms of the direction cosines $\alpha_1, \alpha_2, \alpha_3$ with respect to the three cube edges. Directions in the crystal which are identical through the symmetry of the crystal would be expected to have the same magnetisation energy, and this consideration allows only those terms in α which satisfy cubic symmetry. (For a discussion of magnetic anisotropy see for example, references 5, 45 or 46). The first term must therefore have the form $\alpha_1^2 + \alpha_2^2 + \alpha_3^2$, which is unity, terms in odd powers of α being eliminated. The fourth order term $\alpha_1^4 + \alpha_2^4 + \alpha_3^4$ can also be expressed in terms of $\alpha_1^2\alpha_2^2 + \alpha_2^2\alpha_3^2 + \alpha_3^2\alpha_1^2$ as can the sixth order term, if an additional term $\alpha_1^2\alpha_2^2\alpha_3^2$ is included. Thus, for cubic crystals, the energy for magnetisation can be written to the sixth order as:-

$$E_k(\alpha) = K_0 + K_1(\alpha_1^2\alpha_2^2 + \alpha_2^2\alpha_3^2 + \alpha_3^2\alpha_1^2) + K_2\alpha_1^2\alpha_2^2\alpha_3^2 + \ldots\ldots \quad 3.1$$

For iron and nickel, the two constants K_1 and K_2 are found sufficient to determine the variation of magnetisation energy with direction of the magnetisation.

Cobalt has a hexagonal crystal structure, the easy direction for magnetisation being parallel to the C axis. The magnetisation energy will therefore increase as the magnetisation is rotated away from the C axis reaching a maximum when Θ, the angle between the

magnetisation and the C axis, is 90°, and thereafter decreasing to its original value when $\Theta = 180°$. For cobalt it is found sufficient to use an expansion for E_k only to fourth order, keeping only the terms with the necessary symmetry:

$$E_k(\Theta) = K_0 + K_1 \sin^2\Theta + K_2 \sin^4\Theta + \ldots\ldots \qquad 3.2$$

The angle Θ does not specify completely the direction of the magnetisation in the crystal: this is also dependent on the azimuthal angle ϕ about the C axis. Because of the hexagonal symmetry in the basal plane, no term in ϕ appears until the above expression is taken to the sixth order, whereupon two further coefficients appear:

$$E_k(\Theta,\phi) = K_0 + K_1 \sin^2\Theta + K_2 \sin^4\Theta + K_3 \sin^6\Theta + K_4 \sin^6\Theta \cos 6\phi + \ldots\ldots \qquad 3.3$$

If the last term is small compared with the preceding terms, it will merely introduce a slight sixfold undulation in the anisotropy energy surface in the region of the basal plane. This 'energy surface' is a three-dimensional representation of the variation of anisotropy energy (obtained by setting Ko=0 in the previous equations) with crystallographic direction, the energy being indicated by the distance of the surface from the origin for any particular direction.

Generally K_1 will dominate, a positive value of K_1 indicating the C axis as the easy direction, a negative value indicating that the easy direction lies in the basal plane. In the latter case the sign of K_4 will indicate the position in the basal plane of the easy direction. If ϕ is measured from the $\langle 11\bar{2}0 \rangle$ or a axis, then a negative value of K_4 indicates that the easy direction is the a axis, while a positive value indicates that the easy direction is the $\langle 10\bar{1}0 \rangle$ or b axis.

The term 'anisotropy constant' applies to a constant K in an expression such as equation 3.3 only if all the spins in the crystal are orientated in the direction (θ,ϕ). Any determination of the anisotropy constants should be done, therefore, in an infinite applied magnetic field, so that a saturation magnetisation will exist along the field direction in the crystal. Consequently, in fields less than those necessary to produce saturation, the apparent anisotropy constants would be expected to increase with increasing field strength; that this is not necessarily so in gadolinium, where the easy direction can be dependent on field strength, has been shown by Graham (47). It is therefore of interest to study the effect of magnetic field strength on the constants, which are also very temperature dependent.

The expressions 3.1 to 3.3 for the magnetocrystalline anisotropy arise purely from a consideration of the symmetry of the crystal, and in no way involve a theory of the physical origin of anisotropy. Such a theory must use as its starting point a knowledge of the interactions which exist between the individual atomic moments and the crystalline lattice.

3.2 Origin of Anisotropy

The simple classical concept of ferromagnetism as a parallel array of atomic dipoles gives an exchange interaction which is independent of the orientation of the moments relative to the lattice. An attempt was made by Mahajani (48) in 1929 to explain the anisotropy by consideration of the shape of the electron spin distribution in the atom, producing results which were qualitatively correct.

Van Vleck (49) considered the problem in terms of the energy

of the exchange interactions between pairs of atomic magnetic moments, and the dependence of this on the direction of the moment, Θ, as measured from some crystallographic axis. Since each atomic moment is situated in the symmetry of the crystal potential, it is to be expected that the variation of the exchange energy will exhibit the same symmetry as the crystal. In general this energy can be expanded in spherical harmonics of even order, since for both hexagonal and cubic crystals there is even symmetry.

Then the pair energy can be expressed as:

$$W(\theta) = A_o^o + A_2^o Y_2^o(\theta) + A_4^o Y_4^o(\theta) + \ldots\ldots \qquad 3.4$$

where $Y_2^o = \frac{\sqrt{10}}{4}(3\cos^2\theta - 1)$

$Y_4^o = \frac{3\sqrt{2}}{16}(35\cos^4\theta - 30\cos^2\theta + 3)$

and A_o^o, A_2^o and A_4^o are constants.

Then the first term is independent of Θ, and should be considered to include the exchange energy. The second term has the same form as the magnetic interaction between two dipoles. If this is the sole explanation for such a dependence of the pair energy, we can equate the co-efficient A^o_2 with that for the dipole pair interaction:

$$A_2^o = -\frac{M^2}{\sqrt{10}\pi\mu_o r^3} \qquad 3.5$$

where M is the atomic magnetic moment, μ_o is the permeability of free space, and r is the separation of the atomic dipoles under consideration. The value obtained for A^o_2 calculated from 3.5 is of the order 10^2 - 10^3 smaller than the value estimated from anisotropy or magnetostriction observations (5). Obviously some other effect must be looked for, in which a much stronger interaction is involved. It is now accepted that this must arise through spin-orbit coupling. Values of the g factor

obtained for the iron-group ferromagnets indicate that the orbital angular momentum L does not contribute to the atomic magnetic moment: the orbital angular momentum is 'quenched' by the crystalline field. This means that the electron orbits are polarised by the molecular field, and cannot be rotated by the application of an external field. If the wave functions of neighbouring electron orbits can be considered to overlap, then such an interaction is intuitively reasonable. However, not all the orbital angular momentum is quenched, because the value of the g factor is known to be slightly less than 2, which is the value for a pure electron spin contribution. Thus there remains some orbital angular momentum to interact with the electronic spin magnetic moment, and consequently a change in the direction of the spin magnetic moment will affect the inter-orbit coupling and hence the energy of the system. The various θ-dependent terms arising from this mechanism have been calculated by Van Vleck, and by analogy with the purely magnetic interactions, the quantum-mechanical equations are called pseudodipolar pseudoquadrupolar, etc.

The situation arising in the rare-earth metals is rather more complex. Here there is virtually no quenching of the orbital magnetic moment because the shielding provided by the complete outer shells weakens the direct exchange coupling between the magnetic 4f shells, and other forms of exchange interactions must be considered. However, the charge distributions of the orbitals are aligned by the crystalline fields by interactions to be considered later, and the effect is similar to that outlined above.

Regardless of the origin of the pair anisotropy energy, the

expression for this energy is still in the form 3.4, because of the symmetry considerations. Then a summation of the energy of the interaction between nearest neighbours, and possibly between next nearest neighbours over all the atoms in the lattice, will give the total energy of magnetisation:

$$E_k = \sum_i w_i(\theta) \qquad 3.6$$

over all i lattice sites.

If the energy is summed for a cubic lattice, over all the direction cosines α_1, α_2 and α_3, then the lowest order term is $\alpha_1^2\alpha_2^2 + \alpha_2^2\alpha_3^2 + \alpha_3^2\alpha_1^2$ as expected from 3.1. The dipolar term with coefficient A^o_2 disappears in the summation, and the anisotropy constant K_1 is a function of A^o_4. In fact Van Vleck pointed out that in second order perturbation theory, the dipole-dipole interaction does exist in a cubic lattice, since the dipolar interaction itself, between individual pairs of atomic moments, disturbs the parallelism of the system. Such a consideration leads to a value for the constant K_1 of the right order of magnitude.

For a hexagonal crystal, which has also been treated by Van Vleck, the lower symmetry of the crystal leads to the existence of a dipole term in the summation, as well as the quadrupole term. Since the coefficient of the dipole term is, generally, much larger than that of the quadrupole term, the crystalline anisotropy tends to be larger for lower symmetry crystals. On the basis of Van Vleck's treatment, a value obtained for the anisotropy of cobalt is of the correct order of magnitude. The temperature dependence of this calculated anisotropy is, however, much gentler than that observed experimentally.

3.3 Temperature Dependence of Magnetocrystalline Anisotropy

An explanation of the temperature dependence of the anisotropy constants was attempted on a classical basis by Zener (50). His basic assumptions were that the effect of temperature was to cause deviations of the local atomic magnetic moments from the direction of the bulk magnetisation of the specimen, the magnitude of the magnetisation vector J remaining unchanged. Then for each individual magnetic dipole, which we are considering to sample an anisotropy which is unaffected by temperature, the anisotropy energy can be expressed in spherical harmonics in the polar angles of the direction of the dipole, with coefficients which are those for zero temperature:

$$w(\theta,\phi) = \sum_n k_n(0) Y_n^0(\theta,\phi) \qquad 3.7$$

A summation of these energies for the whole crystal will produce the bulk anisotropy energy, which is expressed as a series identical with 3.7, but involving the mean values of the polar angles, $\bar{\theta}$ and $\bar{\phi}$ of the bulk magnetisation direction, and with values of the anisotropy constants appropriate to the temperature T. Thus a summation of 3.7 over the whole crystal is equivalent to $K_n(T)\ Y_n^0(\bar{\theta},\bar{\phi})$ for the order n, where $K_n(T)$ is the bulk anisotropy constant at temperature T occurring in an expression in spherical harmonics for the anisotropy energy. If the anisotropy is determined at 0°K to find $K_n(0)$, then there will be no deviation of the dipoles from the average direction, and a summation over the whole crystal is equivalent to:

$$\sum w_n(\bar{\theta},\bar{\phi}) = K_n(0) Y_n^0(\bar{\theta},\bar{\phi}) \qquad 3.8$$

To proceed further it is necessary to determine the average value of $w_n(\theta,\phi)$. Zener assumed that the distribution of the atomic

moments about the mean direction was a random walk function, symmetrical about $(\bar{\theta},\bar{\phi})$. By expressing the energy in spherical harmonics in terms of the polar co-ordinates relative to the mean direction, Zener showed that the average value of $w_n(\theta,\phi)$. with respect to the random walk function (R.W.) is given by:

$$\langle w_n(\theta,\phi)\rangle_{R.W.} = \langle P_n(\cos\theta)\rangle_{R.W.} w_n(\bar{\theta},\bar{\phi}) \qquad 3.9$$

where $P_n(\cos\theta)$is the nth order Legendre polynomial, arising from the use of spherical harmonics in the expression. Random walk theory gives the result that

$$\langle P_n(\cos\theta)\rangle_{R.W.} = e^{-n(n+1)\tau} \qquad 3.10$$

where the temperature variation is included in τ which determines the spread of the distribution function.

The magnetisation M(T) at the temperature T is obtained from a summation over the whole crystal of the product of the individual atomic moments and the cosine of the angle between the moment and the direction of the bulk magnetisation:

$$M(T) = \sum_i J\cos\theta_i = M(0)\langle\cos\theta\rangle_{R.W.} \qquad 3.11$$

The average, with respect to the random walk function, of cos θ is identical with that of the first order Legendre polynomial, P_1 (cos θ). Then from 3.10

$$\frac{M(T)}{M(0)} = \langle P_1(\cos\theta)\rangle_{R.W.} = e^{-2\tau} \qquad 3.12$$

Combining 3.10 and 3.12:

$$\langle P_n(\cos\theta)\rangle_{R.W.} = \left\{\frac{M(T)}{M(0)}\right\}^{\frac{n(n+1)}{2}} \qquad 3.13$$

Expressing the summations of the individual atomic dipole energies in terms of the bulk anisotropy constants, Zener's dependence is obtained:

$$\frac{\sum\langle w_n(\theta,\phi)\rangle_{R.W.}}{\sum w_n(\bar{\theta},\bar{\phi})} = \frac{K_n(T)}{K_n(0)} = \left\{\frac{M(T)}{M(0)}\right\}^{\frac{n(n+1)}{2}} \qquad 3.14$$

Such a comparison between the temperature dependence of the anisotropy constants and that of the magnetisation was successful in the case of iron, where, for n= 4, $\frac{K_1(T)}{K_1(0)}$ must be compared with $\left\{\frac{M(T)}{M(0)}\right\}^{10}$ since it was the fourth order term in the spherical harmonics which gave rise to K_1. In the cases of nickel and cobalt there was no agreement, but Carr (51) obtained a sufficiently close fit to the experimental results by taking into account the thermal expansion of the lattice. Zener's assumption of a crystalline anisotropy unaffected by temperature does not hold, of course, if there is any change in the dimensions of the lattice: because the dimensions of the lattice are dependent on the direction of magnetisation also, due to magnetostriction, Zener's equation cannot be expected to be valid if these effects are large.

Callen and Callen (52) have performed a similar calculation for the temperature dependence of the anisotropy, assuming a distribution of the Boltzmann form. This work predicts Zener's form for the temperature dependence at low temperatures, where

$$1 - \left\{\frac{M(T)}{M(0)}\right\} \ll \frac{1}{S} \qquad 3.15$$

For the rare earth metals, where the orbital angular momentum remains unquenched, S must be replaced by (g-1)J. Keffer (53) had previously shown that Zener's theory was only valid for low temperatures, Van Vleck's theory (49) holding at high temperatures.

If the Zener dependence is valid, it must be remembered that the coefficients to which it applies are those of the expansion in spherical harmonics, equation 3.7, and not those of the simple power series normally used to express magnetocrystalline anisotropy, as in equations 3.1, and 3.2.

In general the anisotropy constants K_n will contain more than one of the constants κ_n, though if one constant is dominant the temperature dependence will not be much affected. For the hexagonal basal plane which is likely to be of most interest here, the expression for the anisotropy energy in terms of spherical harmonics is:

$$E_k(\phi) = \kappa_0 + \kappa_2 Y_2^0(\phi) + \kappa_4 Y_4^0(\phi) + \kappa_6 Y_6^0(\phi) + \ldots\ldots \qquad 3.16$$

where ϕ is the azimuthal angle in the basal plane, and

$$Y_2^0(\phi) = (3\cos 2\phi + 1)/4$$

$$Y_4^0(\phi) = (35\cos 4\phi + 20\cos 2\phi + 9)/64$$

$$Y_6^0(\phi) = (231\cos 6\phi + 126\cos 4\phi + 105\cos 2\phi + 50)/512$$

This expression can be written in terms of $\cos 6\phi$, $\cos 4\phi$ and $\cos 2\phi$, and differentiated with respect to ϕ to obtain the torque $L(\phi)$ produced by the specimen when the magnetisation is held at an angle ϕ to the easy direction:

$$L(\phi) = \frac{693}{256}\kappa_6 \sin 6\phi + \left[\frac{35}{16}\kappa_4 + \frac{63}{64}\kappa_6\right]\sin 4\phi + \left[\frac{3}{2}\kappa_2 + \frac{5}{8}\kappa_4 + \frac{105}{206}\kappa_6\right]\sin 2\phi \qquad 3.17$$

where, according to Zener, the temperature dependences of the constants would have the relationship:

$$\kappa_6 \propto \left\{\frac{M(T)}{M(0)}\right\}^{21} \quad ; \quad \kappa_4 \propto \left\{\frac{M(T)}{M(0)}\right\}^{10} \quad ; \quad \kappa_2 \propto \left\{\frac{M(T)}{M(0)}\right\}^{3} \qquad 3.18$$

For basal plane torque measurements the coefficient K_4 of the $\sin 6\phi$ term would also have the $\left\{\frac{M(T)}{M(0)}\right\}^{21}$ temperature dependence, but the coefficients of $\sin 2\phi$ or $\sin 4\phi$ terms present would contain κ_6 and would therefore have no simple temperature dependence. Although these last two terms might be expected to be small in the basal plane, the coefficients κ_2 and κ_4 can be appreciably large, if they are opposite in sign to κ_6.

Callen and Callen (52) have also shown, using quantum mechanical

methods, that in the paramagnetic region (T>Tc)

$$K_n(T) \propto \left\{\frac{M(T)}{M(0)}\right\}^n \qquad 3.19$$

Consequently, for the axial anisotropy

$$K_2 \propto K_1 \propto \left\{\frac{M(T)}{M(0)}\right\}^2 \qquad 3.20$$

and for the basal plane:

$$K_6 \propto K_4 \propto \left\{\frac{M(T)}{M(0)}\right\}^6 \qquad 3.21$$

Since in the paramagnetic region the magnetisation is proportional to the strength of the applied field, and inversely proportional to $(T-\theta)$, this relationship provides a field and temperature dependence for the anisotropy constants.

CHAPTER FOUR

THEORY OF MAGNETISM IN THE RARE EARTH METALS

4.1 The Magnetic Structure

Although no sufficient theory for magnetic anisotropy in the rare earth metals has so far been advanced, as is the case for other ferromagnetic materials, the general magnetic structures of the heavy rare earth metals have been explained qualitatively, and in some cases quantitatively, notably by Kaplan (54), Elliott (55), and Miwa and Yosida (56). Elliott has also written a useful review of the theories (57).

Whatever the exchange interaction involved, it must be capable of producing the helical spin structures observed in terbium, dysprosium, holmium, erbium and thulium. Such structures were predicted in rutile type structures by Yoshimori (58), on the basis of an exchange interaction between the localised ionic electrons and the conduction electrons. The conduction electrons are polarised by the spin of the ion, and, because of this polarisation, tend to align the neighbouring ions. Thus in second order perturbation theory there is an effective interaction between the ionic moments. Rudermann and Kittel (59) determined the interaction to be of the form:

$$\frac{9\pi K^2}{2}(g-1)^2(\underline{J}_i \cdot \underline{J}_j)\ F(2\underline{k}_o \cdot \underline{R}_{ij})/E_o \qquad 4.1$$

for a spherical Fermi surface, where E_o is the Fermi energy and $\underline{k}_o$ the electron wave vector at the surface, $\underline{J}i$ and $\underline{J}j$ the total angular momenta of the ith and jth ions, $\underline{R}ij$ the separation of the ions, and K is the coupling constant. The function F has the form $(x\cos x - \sin x)/x^4$,

which gives the interaction an oscillatory form; that is, the coupling between the ions will be alternately ferromagnetic and antiferromagnetic as ions further from the ith ion are considered. The interaction is also long-range, supplying the ingredients necessary for the formation of the observed spiral type structures.

This type of interaction has also been developed by Yosida (60) while Kasuya (61) and de Gennes (62) first proposed this interaction as applicable in the case of the rare earths.

The coupling constant K, being related to the overlap of the conduction and ionic electrons, probably varies but little along the rare earth series. The main variation is likely to arise from the factor $(g-1)^2J^2$, which falls rapidly, in agreement with the observed trend, the Néel temperature decreasing along the series.

The direct Heisenberg exchange due to overlap of the ionic shells is expected to be very small for the rare earth metals, because of the screening provided by the 5s and 5p shells: even in the transition metals where the unfilled 3d shell is outermost, the direct exchange contribution is now thought to be small. Because the charge clouds are highly anisotropic in the lattice, the exchange is no longer of a simple $\underline{J}_i.\underline{J}_j$ form, but has complicated terms containing higher powers of J. Since the dependence of the coupling in the rare earths appears to be relatively simple, the direct exchange can play no very large part.

On the assumption of a simple Heisenberg form for the exchange where the coupling is of the type

$$-\mathcal{J}(\underline{R}_i - \underline{R}_j)\ (g-1)^2\ \underline{J}_i.\underline{J}_j \qquad 4.2$$

the exchange energy can be derived for the longtitudinal wave type ordering as

$$E_x = -\frac{1}{2}N\mathcal{J}(\underline{q})\ (g-1)^2\ J_z^2 \qquad 4.3$$

where J_z is the component of the total angular momentum along the C axis, and

$$\mathcal{J}(\underline{q}) = \sum_R \mathcal{J}(\underline{R}) \cos(\underline{q}.\underline{R}) \qquad 4.4$$

where $\underline{R}$ is the interionic separation for the ions under consideration, and $\underline{q}$ is a vector parallel to the C axis which determines the periodicity of the ordering. For the helically ordered spins:

$$E_x = -N\mathcal{J}(\underline{q}) \ (g-1)^2 \ J_{xy}^2 \qquad 4.5$$

where Jxy is the component of $\underline{J}$ in the basal plane. The factor of 1/2 is necessary in the expression for the longtitudinal wave because in layers where J_z is small (at the nodes) there is very little ordering. To minimise the energy $\mathcal{J}(\underline{q})$ must be a maximum: if $\mathcal{J}(\underline{R})$ is large only for nearest neighbours then this occurs at $\underline{q} = 0$, resulting in ferromagnetism for positive $\mathcal{J}(\underline{R})$ and antiferromagnetism of the normal type for negative $\mathcal{J}(\underline{R})$. For the spiral structures observed $q \neq 0$ and this requires $\mathcal{J}(\underline{R})$ to be long range and oscillatory, indicating the Rudermann-Kittel interaction.

If such spiral structures are energetically favourable compared with a ferromagnetic arrangement (and in the case of the longtitudinal wave structure the larger entropy compared with a ferromagnetic structure can lower the free energy and so stabilise the system) it is the anisotropy energy which determines which configuration will be stable. If the easy direction lies in the basal plane, then the helical structure will result; if the easy direction is along the C axis, then the longtitudinal wave is stable.

If summation is carried out only as far as second nearest neighbour layers, assuming each basal plane layer to be ferromagnetic, then

$$\mathcal{J}(q) = (A_o + 2A_1\cos\tfrac{1}{2}qc + 2A_2\cos qc) \qquad 4.6$$

where A_o, A_1, and A_2 are the coupling constants for self-energy of a layer, between nearest neighbour layers, and between next-nearest neighbour layers, respectively. The intervals along the C axis are of $c/2$, since the unit cell contains two interlayer distances. Then the maximum for $\mathcal{J}(q)$ occurs at

$$\cos\tfrac{1}{2}qc = -A_1/4A_2 \qquad 4.7$$

The values of the paramagnetic Curie temperature and the Néel temperature are sufficient to determine the A values: for dysprosium the values are (57) : $A_o/k = -24^oK$; $A_1/k = 44^oK$; and $A_2/k = -15^oK$, indicating the type of oscillation necessary to produce these structures.

By taking into account the effect of an applied field on the energy of the system, the variation with temperature of the critical field necessary to send the system ferromagnetic can be calculated, and the derived dependence has the same form as the experimental curve (55). Nagamiya et al (63, 64) have suggested that the transition at the critical field H_c is incomplete, there remaining a fan-structure in the spins, about the field direction. Further increase in the field reduces the spread of the fan, until full ferromagnetic ordering is obtained at $H=2H_c$.

Kaplan (54) has considered the longtitudinal wave structure in the molecular field approximation and shown that the basal plane

components would be expected to order at some temperature below the Néel point T_N, as is seen in erbium. Yosida and Miwa (56) have also indicated that it is possible for a cycloidal spin structure to exist, resulting in a simple spiral in the basal plane, together with a sinusoidally varying C axis component.

The fact that the periodicity of the spin structures decreases with temperature has been treated by de Gennes and St. James (65) from the point of view of scattering of the conduction electrons due to the 4f spin disorder, and by Elliott and Wedgewood (66) on the basis of the existence of 'superzone boundaries' in the Brillouin zones, introduced by the periodicity of the spin structures. These latter produce energy gaps in the conduction electron spin wave spectrum. The variation of the energy gaps with magnetisation, and therefore with temperature, produces a variation inthe exchange interaction, and therefore in the periodicity of the ordering, which agrees well with the observed temperature dependence. Miwa (67) has also produced a unified theory to combine the effects of both the above theories.

4.2 The Magnetic Anisotropy

The crystal field, which gives rise to the magnetic anisotropy, is of interest. Since the susceptibilities close to the ordering temperature approximate to the free ion values the exchange interactions must dominate over the crystal field; magnetic fields approaching a hundred kilo-oersteds are necessary to produce saturation in crystal directions other than the easy directions, however, and the contribution of the crystal field must be large.

The potential energy of an electron at position (r,θ,ϕ) in the hexagonal lattice can be expanded for a particular J manifold as:-

Table 4.1

	Tb	Dy	Ho	Er	Tm
$V_2^0 \alpha$	$\perp$	$\perp$	$\perp$	$\parallel$	$\parallel$
$V_4^0 \beta$	$\parallel$	$\angle$	$\angle$	$\parallel$	$\parallel$
$V_6^0 \gamma$	$\parallel$	$\angle$	$\parallel$	$\angle$	$\parallel$
$V_6^6 \gamma$	30	0	30	0	30

Symbols $\perp$, $\angle$, and $\parallel$ indicate the tendency of the crystal field to orientate the moments perpendicularly, at an angle, or parallel to the c-axis. For V_6^6 the angles indicate the orientation with respect to the a-axis.

$$V = V_2^0\langle r^2\rangle\alpha Y_2^0(\underline{J}) + V_4^0\langle r^4\rangle\beta Y_4^0(\underline{J}) + V_6^0\langle r^6\rangle\gamma Y_6^0(\underline{J}) + V_6^6\langle r^6\rangle\gamma\left[Y_6^6(\underline{J}) + Y_6^{-6}(\underline{J})\right] \qquad 4.8$$

where the $Y_n^m(\underline{J})$ are the operator equivalents on $\underline{J}$ of spherical harmonics, and α, β and γ are constants which can be evaluated. The $\langle r^n\rangle$ are mean values of r^n over all the 4f electrons, and the V_n^m are constants depending on the form of the lattice, and on the distribution of the charges: since this is not known precisely, only approximate values for the terms $V_n^m\langle r^n\rangle$ may be obtained. It is in fact the signs of the constants α, β and γ which determine the anisotropy, the other factors varying but slightly along the series. The dominant V_2^0 term is equivalent to

$$\sum_i (3z_i^2 - r_i^2) = \langle r^2\rangle\alpha\left[3J_z^2 - J(J+1)\right] \qquad 4.9$$

and has the form of the dipole term in the anisotropy expression. The values obtained for the V_n^m factors indicate that in all cases the charge clouds lie largely in the basal plane. If α is positive this produces a moment in the z direction, i.e. along the hexagonal axis. If α is negative then the moments lie in the basal plane.

For each element, the tendencies of the various terms to produce moments parallel or perpendicular to the C axis may be calculated. These contributions are shown in Table 4.1 (55), where it can be seen that the term V_2^0 in all cases describes the experimentally observed behaviour, Tb, Dy and Ho having moments in the basal plane, and Er and Tm along the C axis. Er has a secondary tendency to have some moment in the plane, and Ho to have some moment along the C axis; hence the

observed conical spirals. The term V_6^6 predicts the easy direction in the basal plane, and these too are in general agreement with experiment.

Although the theory still leaves something to be desired in the way of quantitative results, it supplies a satisfactory explanation of the observed magnetic behaviour in the heavy rare earth metals.

CHAPTER FIVE

PREVIOUS MEASUREMENTS

5.1 The Measurement of Magnetocrystalline Anisotropy

There are various methods available for the measurement of the anisotropy constants. The most fundamental is a determination of the energy from an integration of the magnetisation curves, since the energy for magnetisation in the direction (θ,ϕ) is given by:

$$E(\theta,\phi) = \int_0^{I_s} H \, dI \qquad 5.1$$

where the magnetisation is in the direction of the magnetising field. The anisotropy constants may then be determined from an examination of the difference in energies required for magnetisations in the different crystallographic directions. For this method either a precise knowledge of the demagnetising factor for the specimen is required, or the specimen may be cut in the form of a 'picture frame', when the closed magnetic circuit eliminates the involvement of a demagnetising factor. In this case a separate specimen is required for each crystallographic direction investigated.

A determination of the anisotropy constants can also be made for a single crystal using ferromagnetic resonance techniques at microwave frequencies. The magnetic field necessary for resonance is dependent on the crystal direction in which it acts, since the existence of anisotropy is equivalent to an additional external magnetic field pulling the spins into the easy direction. From the variation of the resonance field with the crystallographic direction of magnetisation an analysis can be made for the anisotropy constants. The method is not satisfactory for constants higher than first order, however. If the

sample is polycrystalline, then the anisotropy will affect the shape of the resonance, as the magnetic field is swept through the resonance, but an analysis of the line shape for the anisotropy constants is not very precise.

The most commonly used method for measuring crystalline anisotropy is that of the torque magnetometer, as described by Williams (68). In its simplest form the apparatus consists of a torsion fibre and rotatable head. The specimen, in the shape of a thin disc of known orientation, is suspended from the fibre in a magnetising field. If this field is applied in a direction other than the easy direction, a torque develops as the specimen tries to rotate until the easy direction lies in the field direction, this being the minimum energy position. The torsion head can then be rotated until the specimen returns to its original position, when the torque developed is known from the angle through which the head has been turned, and the constants of the torsion wire. By determining the torques developed as the field is applied over a complete range of crystallographic directions, a simple analysis of the torque curve obtained will supply the anisotropy constants.

The energy for magnetisation in a hexagonal crystal is defined in equation 3.3. The torque developed is equal to the rate of change of magnetisation energy with crystallographic direction:

$$L(\Theta) = -\frac{\partial E_k}{\partial \Theta}(\Theta,\phi) \qquad 5.2$$

if the field is rotated in a plane including the C axis, and

$$L(\phi) = -\frac{\partial E_k}{\partial \phi}(\Theta,\phi) \qquad 5.3$$

if the field is rotated in the basal plane of the crystal.

The resultant expressions for the torques developed, obtained by

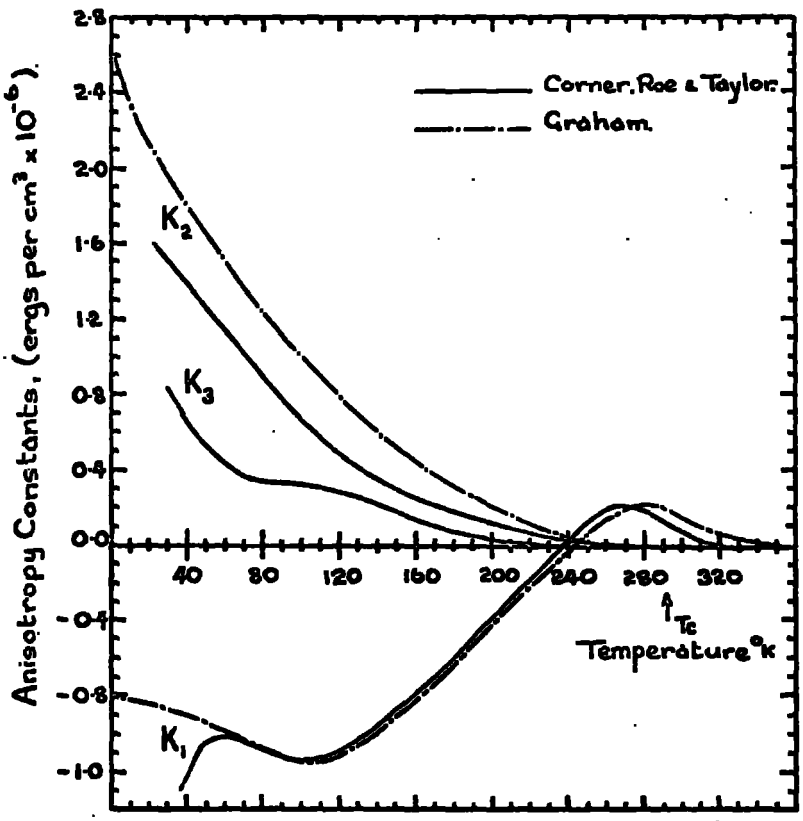

Fig. 5.1 Temperature variation of the anisotropy constants K_1, K_2, and K_3 for gadolinium, as determined by Corner et al, and Graham.

differentiation of equation 3.3 are:

$$L(\theta) = -\left[K_1+K_2+\frac{15}{16}(K_3+K_4\cos 6\phi)\right]\sin 2\theta + \left[\frac{K_2}{2}+\frac{3}{4}(K_3+K_4\cos 6\phi)\right]\sin 4\theta - \frac{3}{16}(K_3+K_4\cos 6\phi)\sin 6\theta + \ldots . \qquad 5.4$$

for the plane containing the C axis, and

$$L(\phi) = 6K_4\sin 6\phi \qquad 5.5$$

for the basal plane. This method of investigation of the anisotropy was employed in the measurements reported here.

5.2 Previous Torque Measurements on the Rare Earths

Torque determinations of the anisotropy constants of gadolinium have been made by Corner, Roe and Taylor (69) and Graham (70, 71) for the constants K_1, K_2 and K_3. Graham (47) has also investigated the field dependence of the constants. Corner et al found it necessary to employ the third constant K_3 to fully describe the torque curves obtained, whereas Graham used only the first two constants. The values obtained are not in perfect agreement: the easy direction is the C axis above 240^{ok}, and lies on a cone about the C axis below this. However Graham reports the easy direction is in the basal plane below 225^{ok}, whereas Corner et al report the angle between the easy direction and the C axis to be a maximum of 70° at 220^{ok}, and the spins lie at an angle of 30° to the C axis at 37.5^{ok}, the lowest temperature used. This latter behaviour has been confirmed by Will et al (41) using neutron diffraction techniques, but Birss and Wallis (72) have made torque measurements which indicate that the easy direction is intermediate between the directions found by Corner et al and Graham, tending to move towards the basal plane at higher field strengths. The variation of the anisotropy constants determined by Corner et al and Graham are

shown in Figure 5.1.

The anisotropy in the basal plane, constant K_4, has also been determined by Darby and Taylor (73) and by Graham (74). This was found to be smaller by a factor of at least 100 than the anisotropy constant K_1, and the easy direction in the basal plane is the a axis.

In considering gadolinium it must be remembered that it is essentially different from the other ferromagnetic rare earth metals in that the ordering transition, though not sharp, appears to be from paramagnetism to ferromagnetism with no antiferromagnetic phase. Belov et al (38, 39, 40) have suggested that in fact gadolinium exhibits antiferromagnetic ordering in applied fields below a few oersteds, with a Néel point at 290^{ok} and a ferromagnetic Curie point at 210^{ok}, but there seems to be no strong evidence for this. The large temperature range of the proposed antiferromagnetic state would appear as an exception to the behaviour of the series, where this temperature interval is decreasing with decreasing atomic number. Although the exchange interactions in gadolinium are similar to those in the other heavy rare earths, the anisotropy is much smaller (the constants α, β and γ in equation 4.8 being zero (57), although a small periodic crystalline potential persists), and is insufficient to stabilise the oscillatory spin structures.

CHAPTER SIX

THE APPARATUS

6.1 The Specimens

The specimens used for torque measurement must be single crystal, and have cylindrical symmetry about the axis of rotation relative to the applied magnetic field. The specimens used by Graham (47, 70, 71, 74) were in the form of thin discs, but an oblate ellipsoidal shape produces a more uniform field within the specimen, and it is this form which has been preferred for previous torque measurements at Durham (69, 73).

For measurement of the anisotropy constants K_1, K_2 and K_3 the plane containing the major axes of the ellipsoid must also contain the C axis of the crystal (the C-axis specimen) while for determination of the basal plane anisotropy constant K_4 the plane of the ellipsoid must contain the basal plane of the crystal (the basal plane specimen). In order that the specimen should have a reasonably small demagnetising factor, the ratio of the major axis to the minor axis of the ellipsoid must be large, or, if a disc, the ratio of the diameter to the thickness must be large. The specimens used had a diameter to thickness ratio of approximately 10 to 1, with a diameter of approximately 5 mms.
The gadolinium C axis specimen used by Corner, Roe and Taylor (69) in their determination of the anisotropy constants K_1, K_2 and K_3 was machined to shape by a process of electrolytic polishing in a solution of orthophosphoric acid, the specimen being mounted on a rotating spindle to preserve the cylindrical symmetry. The outline of the specimen was

projected on to a screen and compared with an enlarged version of the required ellipsoidal cross-section, machining continuing until this shape was achieved. The gadolinium crystal was originally cut from a single crystal provided by Johnson Matthey and Co. Ltd. (Wembley).

The gadolinium basal plane specimen used by Darby and Taylor (73) for a determination of K_4 was also used for further torque measurements in the present investigation. This specimen, and specimens of terbium, dysprosium, holmium and erbium, were prepared using the procedure described above by Metals Research Ltd. (Cambridge) from single crystals grown by Metals Research from polycrystalline material provided by Johnson Matthey. Single crystals of terbium, dysprosium, holmium and erbium were produced under a joint research contract with the Physics Department of the University of Oxford. The crystals were obtained by zone melting the 99.9% pure metals. After some difficulty when the zone refined samples contained many closely aligned crystallites with a spread of 5 to 10 degrees, rather than a true single crystal, C axis specimens of terbium, dysprosium and holmium and basal plane specimens of terbium, dysprosium, holmium and erbium, were obtained. Of these, the dysprosium C axis specimen contained crystallites with an angular spread in the plane of the ellipsoid of 3-4°, and a second holmium C axis specimen with a rather more severe crystallite spread (10°) was produced.

After initial measurements on the terbium and dysprosium basal plane specimens it became apparent that the torques produced at nitrogen temperatures were too large to be held by the counter-torque system. Consequently, to make measurements at these temperatures it was necessary

to obtain specimens of smaller volume. These Metals Research were unable to provide, the raw material then available not being suitable for the production of good single crystals. However, samples in the form of very thin discs had been prepared for the Physics Department of the University of Oxford, and were then being used in the Physics Department of Sheffield University. Basal plane specimens of terbium and dysprosium and also a C axis specimen of terbium, were made available from this source by Dr. D.M.S. Bagguley of Oxford University and Professor E. W. Lee of Sheffield University. Because these specimens were so thin, the cylindrical symmetry in each case was poor, there being indentations in the circumferences. X-ray diffraction also indicated that there was an overall crystallite spread in each crystal of the order of 7°.

The orientation of each specimen used was examined by X-ray diffraction, using the Laue back-reflection technique. The ellipsoidal specimen was mounted on the end of a small brass tube, which was clamped on a goniometer, the carefully machined end of the tube ensuring that the plane of the ellipsoid was perpendicular to the axis of the tube; a fine hole down the centre of this tube was used as a collimator for the X-ray beam, so that the system could be aligned prior to the mounting of the specimen, which was examined with a microscope to centre it on the mounting. The orientations of the crystal axes could then be determined to within $\pm 1^{\circ}$. In many cases difficulty was experienced because of the existence of a surface layer on the crystals. Although these films were generally polycrystalline, in a few instances the film showed a crystalline alignment with the rare earth crystal, which resulted on the X-ray photograph in multiple spots around each spot position for the underlying lattice, presenting the appearance of a preferentially aligned system of crystallites,

Table 6.1

Specimen	Maximum Diameter cms.	Maximum Thickness cms.	Mass $\times 10^3$ gms.	Demagnetising Factor, $N/4\pi$	Remarks
Gadolinium basal plane ellipsoid	0.441±0.002	0.0290±0.0005	25.85±0.05	0.052	
Terbium c-axis ellipsoid	0.490±0.001	0.0580±0.0005	53.10±0.05	0.091	
Terbium c-axis disc	0.408±0.003	0.0282±0.0005	28.65±0.05	0.012	Indentations in circumference
Terbium basal plane ellipsoid	0.492±0.002	0.0540±0.0005	50.00±0.05	0.079	
Terbium basal plane disc	0.377±0.002	0.0240±0.0005	20.95±0.05	0.012	Indentations in circumference
Dysprosium c-axis ellipsoid	0.476±0.004	0.0467±0.0005	42.75±0.05	0.070	crystallite spread 3-4°
Dysprosium basal plane ellipsoid	0.493±0.002	0.0605±0.0005	52.95±0.05	0.091	
Dysprosium basal plane disc	0.423±0.003	0.0115±0.0005	12.15±0.05	0.003	Indentations in circumference
Holmium c-axis ellipsoid	0.489±0.003	0.0427±0.0005	43.30±0.05	0.068	
Holmium c-axis ellipsoid	0.495±0.002	0.0460±0.0005	45.35±0.05	0.068	Crystallite spread ~10°
Holmium basal plane ellipsoid	0.497±0.003	0.0445±0.0005	49.80±0.05	0.068	

rather than a single crystal. A quick etch in an etching fluid consisting of 50% nitric acid and 50% acetic acid removed such layers to reveal the true natures of the specimens, which were generally true single crystals, except in the above-mentioned cases for dysprosium and holmium, and for the thin discs of terbium and dysprosium, where continued etching failed to remove the crystallite spread, and in fact revealed grain boundaries. In all the specimens used the required crystal axes were in the plane of the ellipsoid, within the accuracy with which such orientations could be determined.

The ellipticity of the specimens was checked by using a photographic slide projector to throw a focussed shadow of the ellipse on to a screen, where the shape was traced on to graph paper and could then be compared with a plotted ellipse of the appropriate dimensions.

The physical dimensions of the specimens were determined using a travelling microscope, and the specimens were weighed on a chemical balance. It was not necessary to know the volume of the crystals, since although previous anisotropy constants for gadolinium have been expressed per unit volume, it is more convenient to express the constants per unit mass, when corrections for thermal expansion become unnecessary. This has been pointed out by Graham (74), when the constants determined by him were expressed in ergs per gram. Such constants will be denoted by the script letter, as $\mathcal{K}$.

The specifications of the crystals used here are listed in Table 6.1. The demagnetising factor for each specimen was obtained as $N/4\pi$ from Bozorth (45). The saturation magnetisation in the rare earth metals is of the order of 300 e.m.u. per gram, which corresponds to 2 kilogauss.

Taking the demagnetising factor as 0.07, a demagnetising field of approximately 1.5 KOe is indicated where saturation exists. The field strengths quoted throughout this report remain uncorrected for this.

6.2 The Torque Magnetometer

As mentioned previously, a convenient method of measuring the anisotropy constants is by a determination of the torque developed when a single crystal of the material under investigation is suspended in a magnetic field, the torque being measured as that provided by the suspending fibre when the specimen is returned to the position occupied in the absence of the magnetic field. Manual rotation of a torsion head (68) to provide the necessary restoring torque is apt to prove tedious: an automatic method of balancing this torque would be desirable, and such a system has been described by Croft, Donahoe and Love (75). In this apparatus the specimen is attached to the coil of a moving coil galvanometer. Current is fed to this coil, which moves in the appropriate galvanometer permanent magnet, and sufficient counter-torque is thus developed to bring the specimen back to the null position. The necessary feed back is provided by the use of a mirror attached to the specimen mounting: a fixed lamp shines on to the mirror, the reflected beam of light illuminating a pair of photocells, the difference signal from which is amplified and fed to the counter-torque coil. Appropriate calibration of the counter-torque coil supplies a measurement of the torque produced by the specimen, through a determination of the current in the coil. A further advantage of the system is that the suspension does not move appreciably since it is held in the equilibrium position, and change in the torsional constants of the suspending wires due to temperature changes

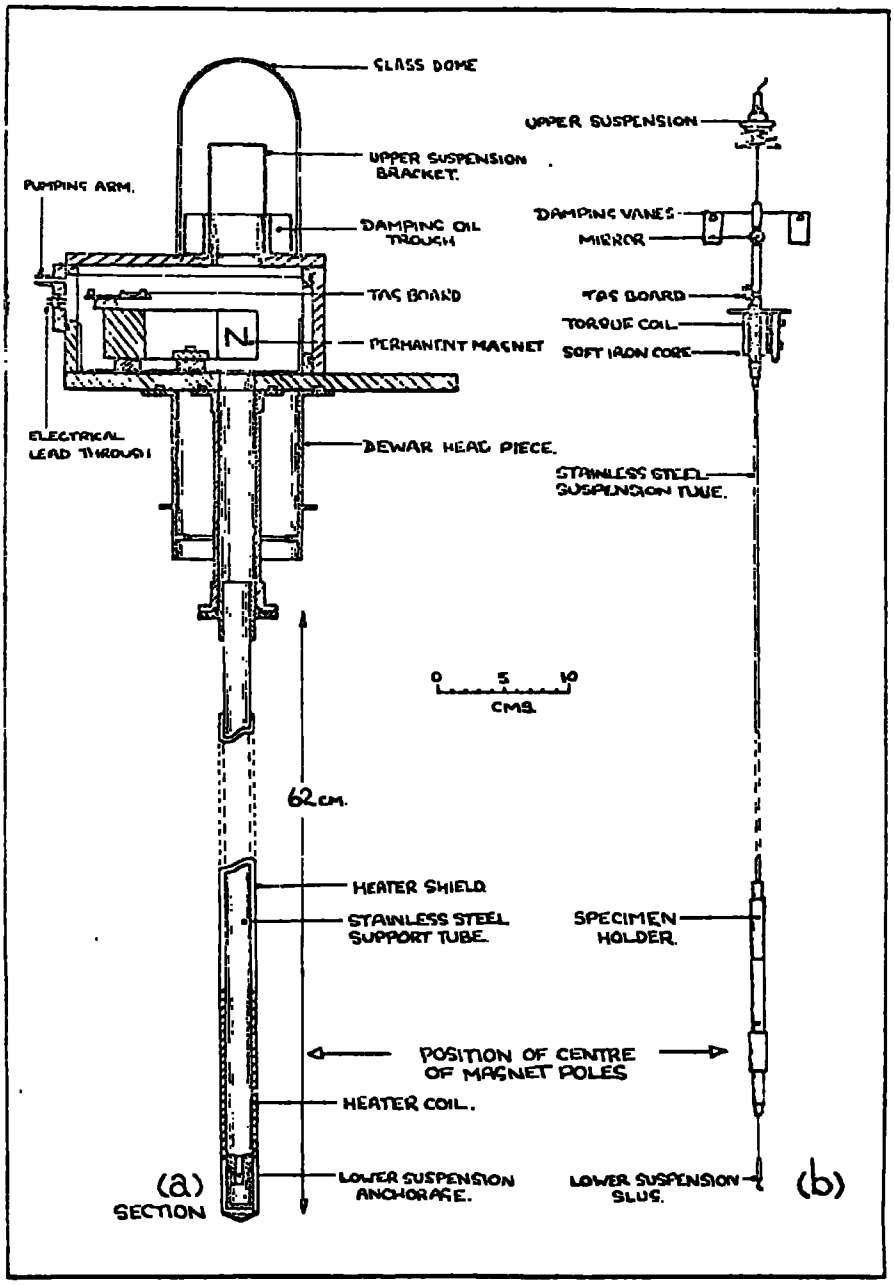

Fig. 6.1 The torque magnetometer.

is not important, as it is when the restoring torque is supplied by a twisting of the suspension.

This system was further developed by Penoyer (76) and by Pearson and Guildford (77,78); the torques measured here were larger than in the above system, and the resulting torque curves were plotted directly on an X-Y recorder. This latter refinement was not adopted; since the torque curves were to be subjected to computer analysis numerical values of the curves had in any case to be obtained, and the extra complexity introduced by such a system was not considered to be justified.

Previous determinations of the anisotropy constants of gadolinium have been made at Durham by Corner, Roe and Taylor (69) and Darby and Taylor (73). The torque magnetometer used for these measurements was constructed originally by Roe (79). This instrument was available for the present work, but several modifications were made to the constructional details, and a further description of the magnetometer is necessary.

6.3 Construction of the Magnetometer

Figure 6.1 shows a cross sectional view of the instrument body and suspension mounting in (a), and the suspended coil and specimen holder in (b). A rectangular plate of 1/2" thick brass formed a base for the instrument; on this was constructed a rectangular box of 1/4" brass sheet, the top and one end being removable and sealed with neoprene gaskets to render the system vacuum-tight. This box housed the permanent magnet which, with the torque coil, provided the basis for the counter-balancing system. This magnet was adapted from a 6" G.E.C. portable moving coil ammeter, and provided a radial field when used in conjunction with a soft iron core.

The axis of a hole in the top of the housing was aligned with the axis of the cylindrical pole-gap, and above this was mounted a bracket to support the upper suspension of the system. The inside of the brass box was lined with Mumetal sheet, to exclude stray fields from the electromagnet, thus preventing disturbance of the balancing system. A demountable plate on the side of the box carried vacuum-tight electrical lead-throughs and the pumping arm.

A three-quarter circular trough was bolted round the foot of the suspension bracket, a flange on the latter sliding in a groove underneath the trough, so that the bracket could be rotated through a small angle for adjustment of the specimen orientation. The trough was provided for damping of the suspended system, and could be filled with vacuum oil. The trough and bracket were surmounted by a glass dome, which seated on an 'O' ring, and formed an easily removable and effective vacuum jacket. The use of glass for this cover obviated the provision of a window opposite the mirror mounted on the specimen holder assembly.

The lower part of the suspended system was housed in a 31" long tube, the upper portion of which was brass and was surrounded by a headpiece for the cryostat dewar. The lower portion of the tube was of stainless steel tube, 1/2" diameter and 0.010" wall thickness. This provided good heat insulation for the specimen holder, and was demountable from the upper brass tube, providing access to the specimen holder. The stainless steel tube also carried at its end the lower suspension anchorage, which was covered by a brass cap which could be screwed up on an 'O' ring. Although the 'O' ring was held at nitrogen temperatures the system remained vacuum-tight.

The suspended part of the apparatus consisted essentially of a holder for the specimen, the counter-torque coil, and the mirror necessary for the photocell feedback system. Since the specimen had to be cooled to low temperatures it was desirable and convenient to make the specimen remote from the counter-torque coil and upper suspension. Accordingly, the specimen holder is attached to the lower end of a long 1/8" diameter, thin walled stainless steel tube. The upper end of this tube locates in the lower end block of the coil, and is locked with a grub screw.

The coil former was constructed from 1/32" brass sheet, the side members being curved to fit closely to the soft iron core of the balancing magnet, so that it was necessary to remove this core with the coil; the core was bolted on to a collar which could then be screwed to the magnet, with sufficient clearance between the core and the pole pieces for the coil, when correctly aligned, to be free to rotate through some 45° about the core. The end blocks of the coil former were removable, to permit winding of the coil, and the former was coated prior to winding with polyurethane, to act as an insulation. Further insulation was provided by a strip of P.V.C. tape wrapped around the former, and on top of this 100 turns of a double strand of No. 40 S.W.G. enamelled copper wire was wound, producing two virtually identical coils. The method of calibration rendered unnecessary a knowledge of the number of turns or the cross-sectional area. The coil leads were anchored to a small tagboard fastened above the coil, and the leads were insulated from the former by fine P.T.F.E. sleeving. The tag board also secured a copper-constantan thermocouple, which was fed through the lower end block of the coil into the 1/8" diameter stainless steel tube.

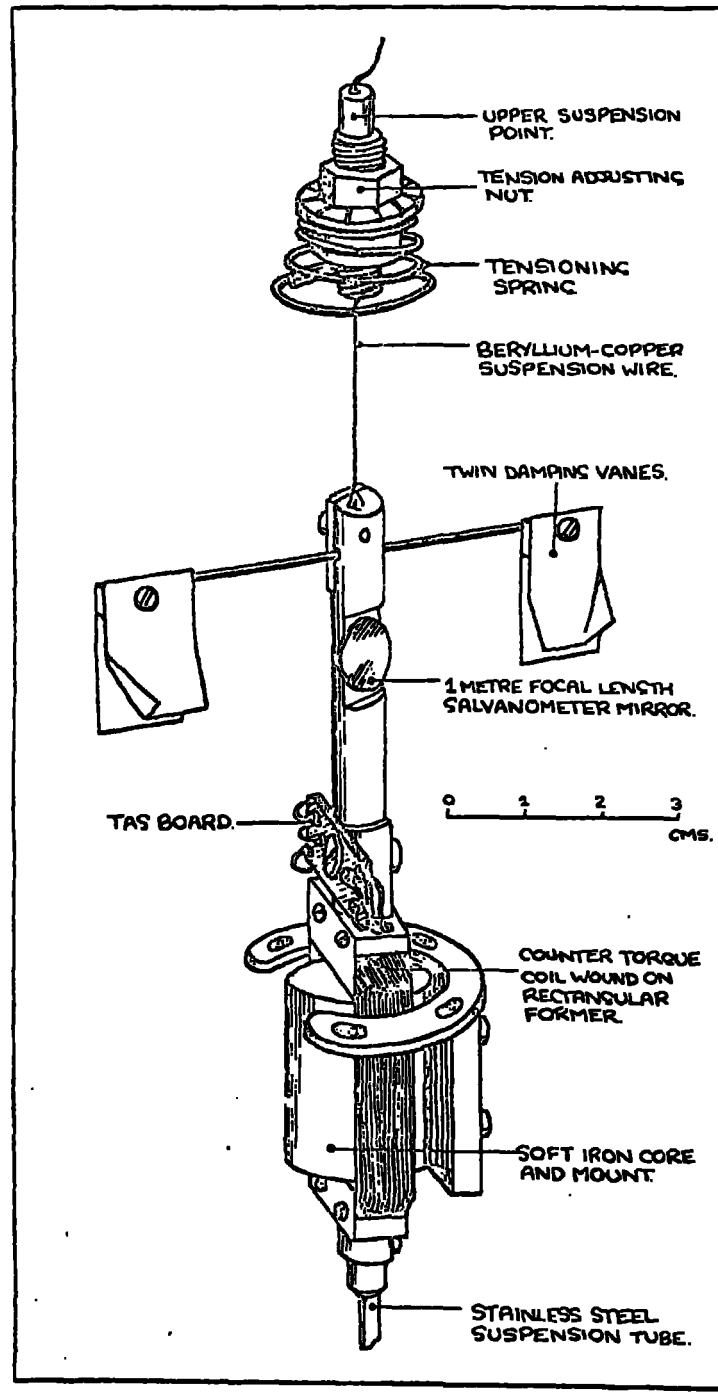

Fig. 6.2 Upper suspension and coil assembly of the torque magnetometer.

A 1/4" diameter brass rod was pushed into the upper end-block of the coil, and secured by a grub screw. On to this was attached the aluminised galvanometer mirror, 1 cm diameter and 100 cms focal length; black wax was used to secure the mirror, since it facilitated minor adjustments to the position and angle of the mirror. Above the mirror the damping vanes were mounted: these were held by one screw and could quickly be removed. The vanes were fashioned to move in the damping trough with a small clearance from the walls and floor of the trough.

The suspending ligaments were made from 0.005" diameter beryllium-copper wire. This was soldered into small holes drilled axially in the brass rods at each end of the assembly. The end of the lower suspension was simply soldered into a brass slug, which could be secured by grub screws in the anchorage provided in the outer stainless steel vacuum jacket. The upper suspension ligament was soldered into a short length of brass rod, which was machined with shoulders so that it could rotate smoothly on the end of a bored-out length of O.B.A. studding. This studding carried a nut and collar arrangement which bore on to a conically coiled spring, so that alteration of the torsion in the suspension was achieved by adjustment of the nut. The coil spring also absorbed the slight changes in the length of the assembly caused by temperature changes. The whole suspension could be rotated by twisting the uppermost brass rod, without affecting either the position of the anchorage or the tension of the suspension. This was found to be more convenient than rotation of the whole suspension bracket. The suspended assembly was centred relative to the permanent magnet and core by manual adjustment of the top suspension anchorage in a slot milled in the bracket. A system of adjusting screws as used in the original apparatus was found to be unnecessary.

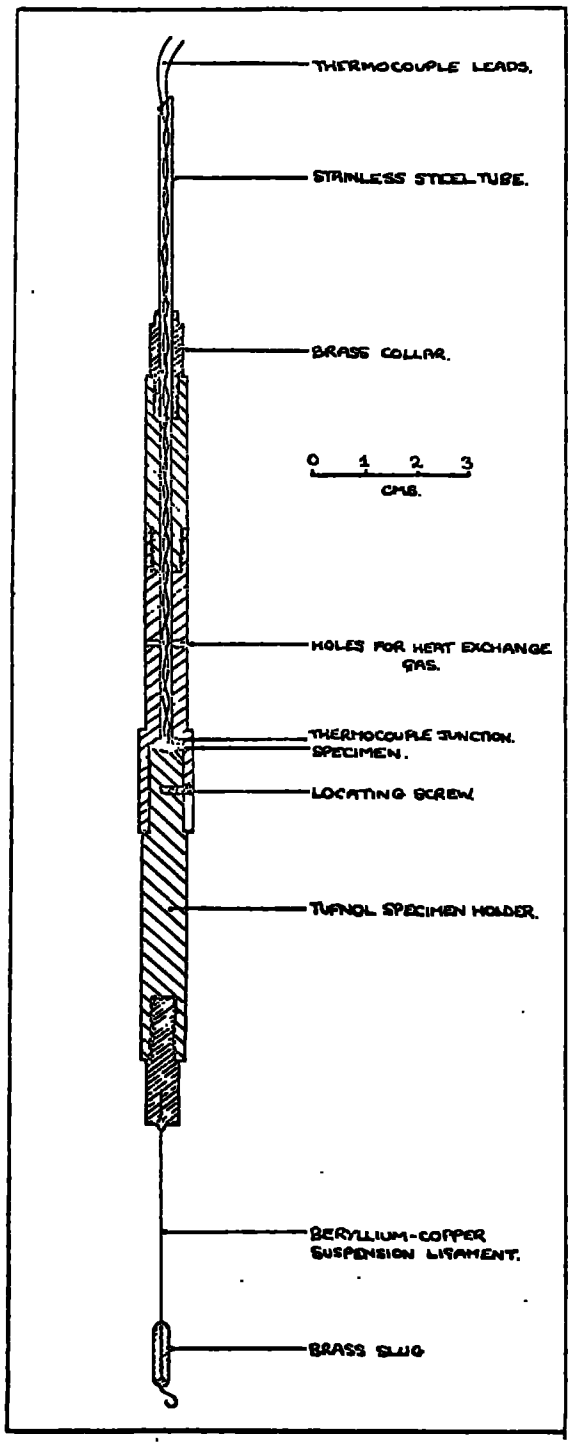

Fig. 6.3 The specimen holder.

The top section of the suspended assembly is illustrated in Figure 6.2. Connections to the coil leads were made via the tag board, the wires being coiled to lessen any torque they may have produced on the suspension, although since the instrument is null reading this torque was unlikely to vary. The thermocouple leads were treated in a similar manner, and all the leads were attached to a tag board fastened above the permanent magnet, before being taken out of the instrument through the hollow vacuum-sealed lead-throughs.

The specimen holder screwed on to a brass fitment soldered to the end of the stainless steel suspension tube. A sectional view of the holder, which was made from 3/8" diameter tufnol rod, is shown in Figure 6.3. All the material used for the suspended coil and specimen holder was non-ferromagnetic. The screw fitting top section of the holder permitted insertion of a carbon resistor for temperature measurement if necessary, while the bottom section was a push-fit into the middle section, and had a slightly dished end to accommodate the ellipsoidal specimen. A brass grub screw in the side of the specimen mount located in a groove cut in the skirt of the middle section: it was found convenient to mount each specimen on a separate bottom section, when the locating screw ensured that, when inserted, the specimen always maintained the same orientation relative to the instrument. Small holes bored through the tube allowed the circulation of a heat exchange gas, and the copper-constantan thermocouple used for temperature monitoring was threaded down the axial hole of the holder, so that the junction was in thermal contact with the specimen.

The lower suspension ligament was soldered into a brass fitting at the end of the specimen holder, the suspension being anchored into the

vacuum jacket as mentioned previously.

Roe had determined that the most successful means of attachment of the specimen to the holder was by means of 'Sellotape' adhesive tape. Since some of the original objections dealt with the difficulty of obtaining a bond at low temperatures, trials were made with resin-type adhesives. A strain gauge resin was found to be satisfactory as an adhesive at nitrogen temperatures, but its use introduced such large strains in the specimen as to change appreciably the shape of the torque curve obtained. From this point of view 'Sellotape' was found to be quite satisfactory, and this method of mounting continued to be used. The specimen was placed in the dished end of the mount, and four narrow strips of 'Sellotape' were placed diametrically across the specimen, and stuck down on to the holder. A fifth strip was then stuck circumferentially, securing the ends of the radial strips. This mounting showed no sign of allowing the specimen to twist in the holder, and appeared immune to thermal cycling.

6.4 The Automatic Balancing Equipment.

The system was first employed using the photocell amplifier constructed by Roe (79). The basic layout of the feedback mechanism followed standard practice, and is similar to that used by Pearson and Guildford (77), although the electronics differ somewhat.

A beam of light from a fixed source was reflected from a galvanometer mirror attached to the torque magnetometer, and the reflected beam was focussed onto a split photocell arrangement. The signal produced by the light beam at each photocell was amplified by a D.C. amplifier, and the difference signal applied to the balancing coil in a manner such that the coil moved back to its equilibrium position, where the reflected light

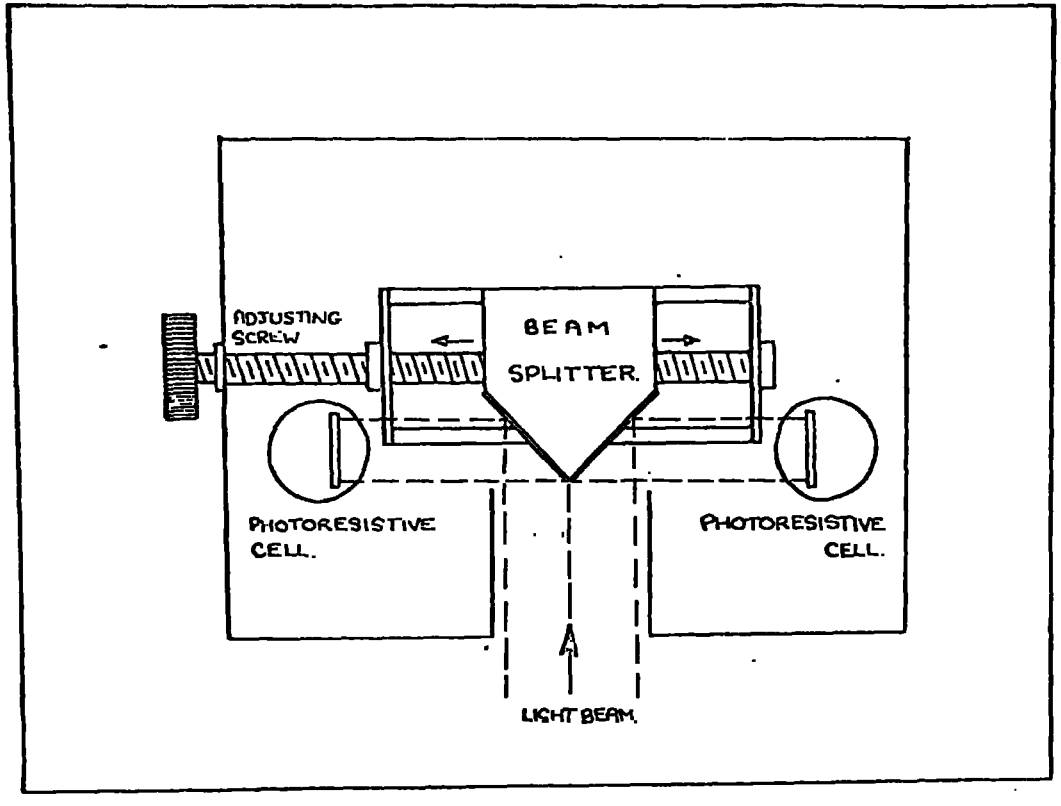

Fig. 6.4 The beam splitter.

shone equally on both photocells, giving zero difference signal A torque applied to the suspended system would then cause the reflected beam to move off the equilibrium position, and the conductance of one photocell to increase while that of the other photocell decreased. The light spot would move away from the central position until the amplified difference signal provided a torque on the coil which was just sufficient to balance the torque applied. If the torque applied was sufficiently large to move the reflected beam past the midpoint of one of the photocells (the point for maximum conductance), then the feedback mechanism was insufficient to hold such a torque.

The suspension therefore moved through half of the angle subtended by the centres of the photocells at the mirror, when the torque applied changed from the maximum torque in one direction which the servo-system could hold, to the maximum torque in the opposite direction. To reduce the effective separation of the photosensitive surfaces of the two cells a beam splitter was used, as shown in Figure 6.4. This consisted of two silvered mirrors mounted at 90° to each other, and housed in an aluminium box, the inside surfaces of which were painted matt black to cut down unwanted reflections. The light beam entered through a slot cut in the front of the box, and was split by the mirrors, which reflected the light on to the two photocells mounted on either side of the mirror holder. The position of the mirrors relative to the slot was adjustable by a screw which projected through the side of the box. The light source used was a focussable galvanometer lamp housing, with a 20 volt, 150 watt projector lamp. The beam from this was reflected by the mirror on the magnetometer, the gap in the damping trough per-

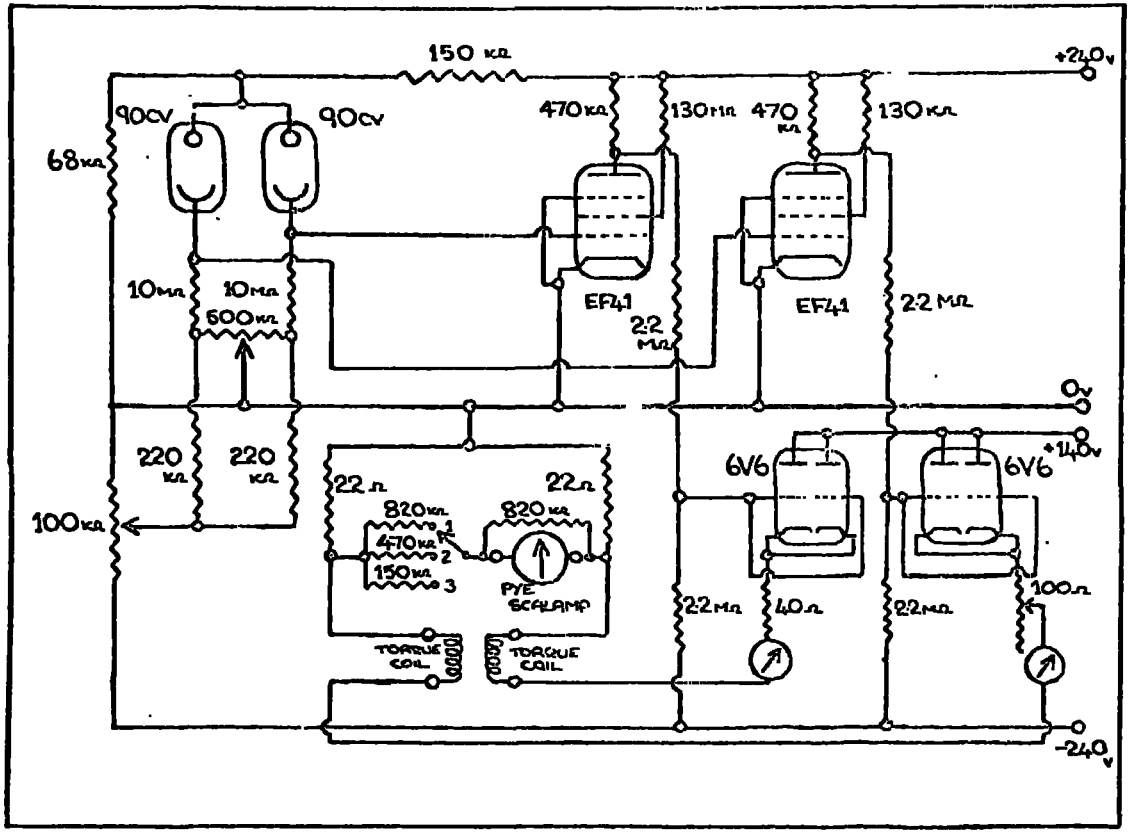

Fig. 6.5 The vacuum tube photocell amplifier.

mitting access to the mirror.

With the beam splitter the effective separation of the photo cells is approximately two centimetres: since the photocells were distant some two metres from the mirror, this corresponded to a maximum rotation of the specimen and suspended assembly through half a degree, which was better than the accuracy with which the orientation of the specimen could be determined.

A diagram of the photocell amplifier built by Roe is given in Figure 6.5. The photocells used are Mullard 90 CV, and are photo-emissive. Under equilibrium conditions the photocells receive equal illumination and are both conducting. The operating conditions for the EF 41's and 6V6's are then identical. The cathode load currents drawn by the 6V6's are therefore also identical, and it is these currents which constitute the currents through the twin coils of the balancing system. Since these two coils are connected in opposition there will be no torque applied to the coil.

If now a mechanical torque is applied to the specimen, the system will rotate and the light beam will move off the central position, so that one photocell receives more illumination than the other, and the conduction current in this photocell will increase. This drives the grid of the appropriate EF41 more positive, so that the valve current increases and the plate potential drops, making the grid potential of the 6V6 more negative. Thus the current through the balancing coil in this half of the amplifier will drop, while the reverse process causes the current in the other coil to rise. The difference in the two coil currents produces a torque which counteracts the torque

originally applied. Obviously, the inequality in illumination will only increase to the point where the torque developed by the feedback mechanism is equal to the applied torque, and the difference current produced will provide a measure of the applied torque. This difference current was monitored by a suitably calibrated Pye scalamp connected across two standard 22Ω resistors carrying the coil currents, as shown, and three switched resistors provided three current ranges.

Two controls were incorporated for zeroing purposes: the variable resistor in the cathode line of one 6V6 provided a coarse zero adjustment, while a 500 KΩ potentiometer across the cathode loads of the photocells and centre-tapped to ground provided a less sensitive zero position control. In fact only a small adjustment of either control was sufficient to overcome the servo-action of the amplifier. The bias of the EF41's could be set by adjustment of the centre tap of a 100 KΩ potentiometer strapped between earth and the -240 volt supply. This control also had a marked effect on the zero setting.

The system therefore had three adjustments, and in order to obtain maximum torque-holding the settings used were critical. The system was used to make torque measurements on a basal plane specimen of gadolinium, where the torques involved were comparatively small (of the order of 100 dyne-cms) and much trouble was experienced with drift of the zero position during the plotting of each torque curve. Later work on the available specimens indicated that the maximum torque the servo-mechanism could hold, which was approximately 1000 dyne-cms, using the 100 turn coil, would be insufficient. The figure given here is considerably smaller than the torques measured by Roe, but adjustment of the zero and bias settings failed to increase the available counter-

torque. This may have been due to ageing of the photocells and/or amplifier valves, in which case rebuilding of the amplifier may have led to an improvement.

However, the instrument is essentially a current device: it is desirable to use a low-voltage, and comparatively high current, supply with a coil formed from fewer turns of thicker wire, rather than the higher voltage, low current device described above. Hence transistor circuitry is indicated. Further, the circuit described in Figure 6.5. is inefficient in that the torque is supplied by the difference in the currents through the two coils, so that the full current-carrying capacity of the coil system is not utilised. There is no particular advantage in this arrangement, and it would be simpler to use a single coil, with an amplifier which supplies a reversible output current.

The amplifier constructed was based on a pair of Mullard ORP 94 photo conductive cells. These cadmium sulphide cells were chosen for their superior sensitivity and low impedance, which in the system used changed from 400Ω at full illumination to 18 KΩ unillluminated: the equilibrium resistance was 620Ω . The ORP 94 was also convenient because it had the same base as the 90 CV used previously, and therefore required no modification of the beam splitter: in other circumstances a double photoconductive cell unit may have been desirable, rather than two separate cells.

The circuit of the D.C. amplifier is shown in Figure 6.6. For consideration of its operation suppose that a torque is applied to the suspension; then one photo conductive cell will be illuminated more than

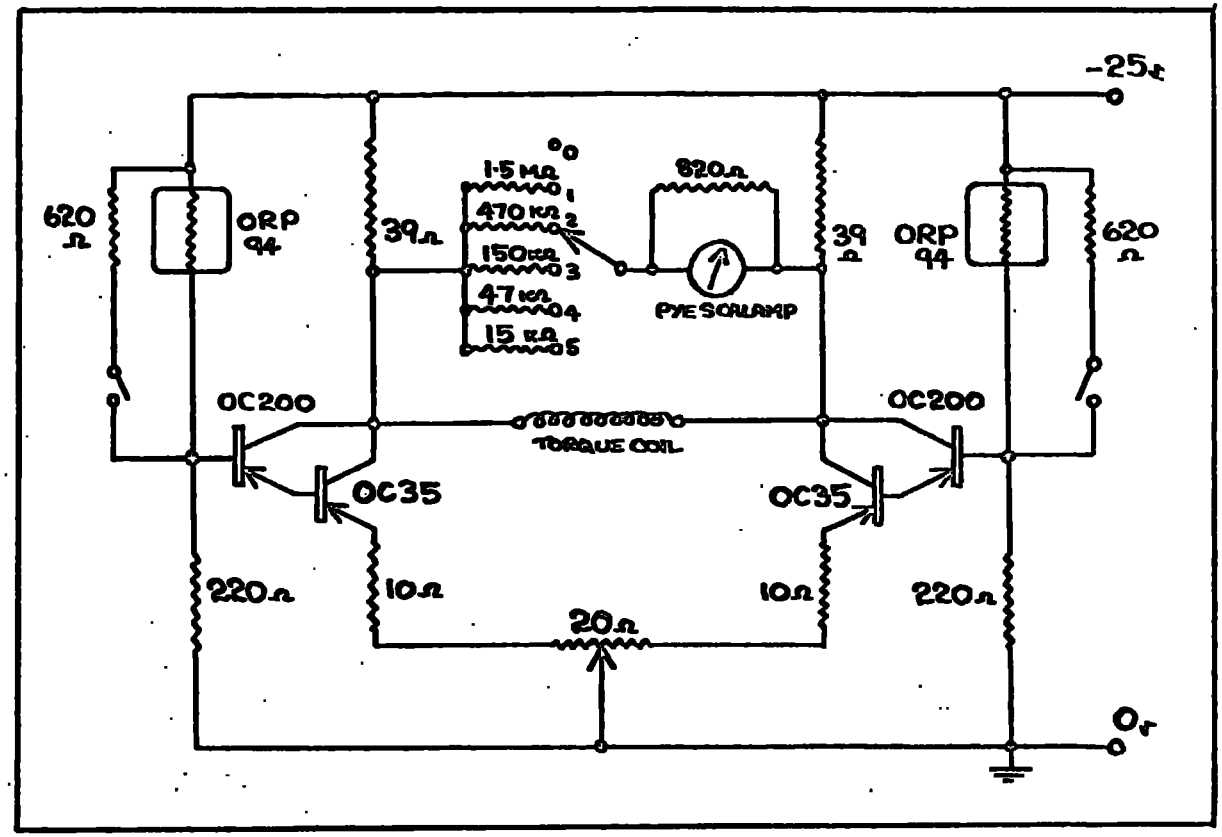

Fig. 6.6 The transistorised photocell amplifier.

the other, and its resistance will drop. This will increase the negative base voltage of the OC200, and therefore of the OC 35, which is controlled by the OC 200. The resistance of the OC 35 is accordingly decreased, and more current flows through the transistor. Consequently the potential of that end of the torque coil becomes more positive, or rather, its negative potential is decreased. The reverse process in the other half of the amplifier gives that end of the coil a higher negative potential. Thus a current will flow through the torque coil, unless there is equal illumination on both photocells. The direction of this current will depend on which photocell is most illuminated; the coil was so connected that the torque developed opposed the torque applied. The coil current was determined by a Pye Scalamp placed in parallel with the torque coil, with five switched resistances to give five current ranges, plus one open circuit position which was found to be useful for zeroing the Scalamp. The 820Ω resistance across the Scalamp ensured critical damping.

When a photoconductive cell was not illuminated it was found that its resistance was sufficiently large to cut off that half of the amplifier. This corresponded to a maximum current of approximately 300 milliamps through the torque coil, which had 150 turns wound from 30 s.w.g. enamelled copper wire, with a total resistance of 10Ω. It was considered unnecessary to incorporate zeroing devices of the type employed in the original amplifier, since it was immaterial whether zero coil current corresponded to zero applied torque or not. From the point of view of full utilisation of the counter-torque available, it was desirable that at equilibrium there was as little torque due

to the suspension as possible, and for this reason before measurements were taken the suspension was adjusted to produce an essentially zero balancing current. For the most sensitive ranges, where the small balancing current present showed as a non-zero deflection on the galvanometer, the galvanometer zero was adjusted manually. This zero tended to change with the temperature of the specimen, presumably due to a twisting of the lower suspension caused by thermal expansion or contraction. For this reason the galvanometer zero was adjusted where necessary between runs.

It was, however, found convenient to provide a control which would adjust the coil current, so rotating the coil and mirror until the reflected light beam was brought on to the photocell beam splitter. This was achieved by switching across each photocell a resistance approximately equal to the in-balance resistance of the cells, and adjusting the centre tap on the emitter resistors of the OC 35's until the light spot was central on the cells. The parallel resistors were then switched out, the servomechanism taking over to hold the system.

This system was found to be very satisfactory: zero drift with time was negligible and warm-up time, which necessitated a wait of an hour or more with the previous valve circuitry, was eliminated. The maximum torque available with the coil used was 2×10^4 dyne-cms. The limitation on the torque which can be developed in a coil is the amount of current which can be carried without resistive heating of the coil becoming serious; with the volume available for the torque coil in the magnetometer, a coil of approximately twice the number of turns used would have been possible, with no heating problem, and it would not have been difficult to modify the transistor amplifier to provide the

necessary power. However, much trouble was experienced with oscillation of the system at these high torque levels, and the torque obtained could not have been increased without a more sophisticated damping mechanism.

Although the trough was provided for oil-bath damping in the original apparatus, it was found to be unnecessary with the small torques available, a 30 microfarad capacitor across the two coils providing sufficient electrical damping, at the expense of the response time. However, in the transistorised version strong mechanical damping was necessary. To provide this the damping vanes were doubled, and ran in a viscous oil. All vacuum oils available were not sufficiently viscous to prevent oscillation. Eventually an automobile gearbox oil of viscosity S.A.E.90, Castrol 'Hypoy', was found to be adequate even when the apparatus was evacuated, the oil outgassing after a few hours under vacuum.

An inconvenience in using oil for damping was that the suspended system was no longer free enough for the coil to be centred in the permanent magnet. For this reason the vanes were made easily detachable. The presence of the oil also made the equilibrium position of the suspended assembly less definite, producing small but observable variations in the zero torque value as recorded on the galvanometer.

The -25 volt supply required by the amplifier was provided by the circuit shown in Figure 6.7. Although such a servo-system should be independent of fluctuations in its power supply voltage, it was felt that in view of the zero fluctuations observed in the previous counter-torque current it would be desirable to stabilise the supply against voltage variations. This was done by comparing the output voltage

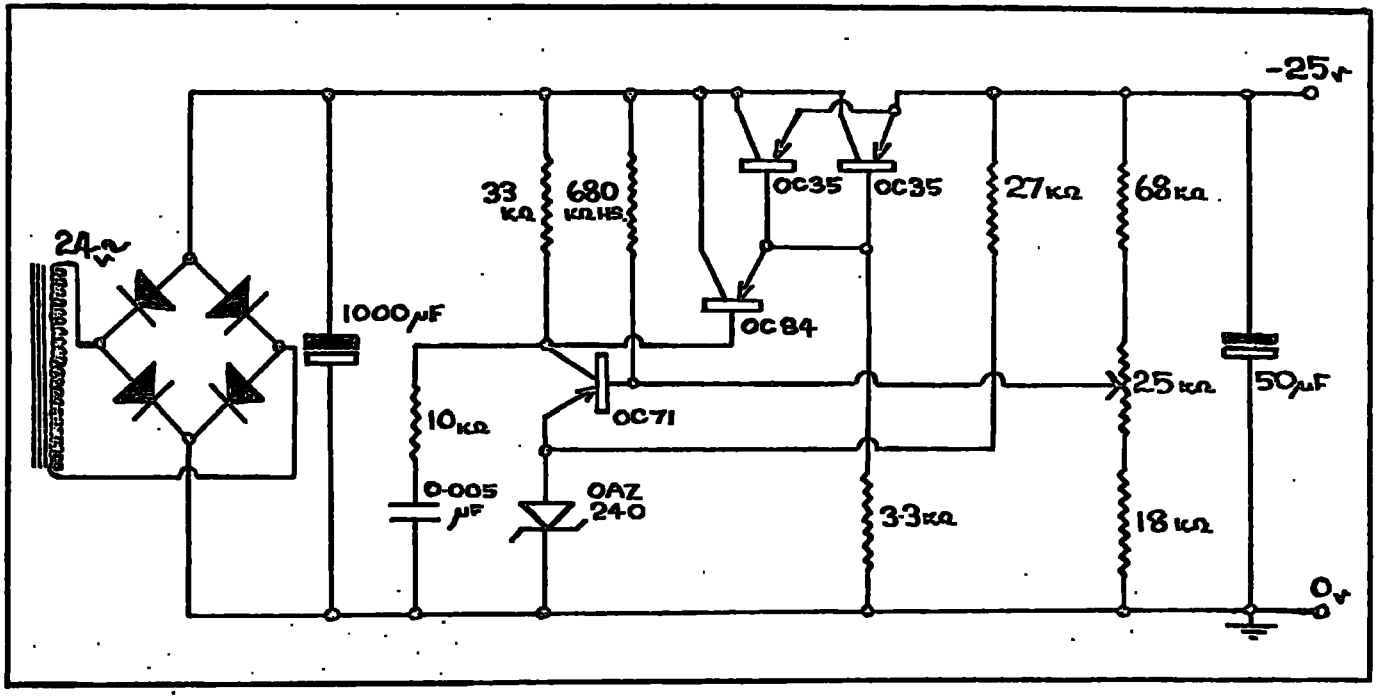

Fig. 6.7 The voltage-stabilised power supply for the transistorised photocell amplifier.

obtained from the variable voltage divider, provided by the 25Ω potentiometer, with the controlled voltage appearing across the Zener diode OAZ 240. Any increase in the tapped negative voltage will increase the current through the transistor OC71, decreasing the negative voltage of the OC84 base, and dropping the transistor current. This makes more positive the bases of the two OC35's running in parallel, increasing their resistances and thus dropping the output voltage. A decrease in the tapped voltage produces the reverse process and decreases the resistances of the OC35's, increasing the output voltage. Alteration of the setting of the 25Ω potentiometer changes the OC71 collector current and hence the resistance of the OC35's. Thus the stabilised output voltage is variable, from 18 volts to 28 volts. The output voltage varied by less than 0.1 volt for current changes from zero current to the full current drawn by the balancing system.

6.5 Temperature Control

It was required to measure the torque curves over a range of temperatures, requiring some form of control of the temperature. Because of the comparatively long period of time (about 10 minutes) involved in the plotting of a torque curve, dynamic measurement as the apparatus warmed up from nitrogen temperatures was not feasible. It was only possible to make measurements to pumped nitrogen temperatures, as there was only a single dewar available for the measurements. With a pole gap of 4.88 cms in the electromagnet, the space available for a double dewar system was rather limited, and it was not possible

to obtain dewars to fit the apparatus at the time of the experiment. An extra copper coupling unit was used to cap the 6" diameter glass dewar used, so that it could be connected to the headpiece of the magnetometer. By using a rotary vacuum pump and a one inch diameter pumping line an ultimate pressure over the nitrogen of 15 mms of mercury was obtained. This corresponded to a temperature of $55^{o}k$: at this point the nitrogen was solid, and the arrangement only permitted measurement for a space of some fifteen to twenty minutes, after which all the solid nitrogen in the dewar tail had evaporated, and the temperature commenced to rise. At this point the pressure over the nitrogen had to be increased until the nitrogen liquefied and refilled the tail, whereupon the system could be pumped again.

For temperatures above nitrogen an electrical heater system was preferred. Roe had used as a coolant nitrogen gas which had previously been passed through liquid nitrogen, following Pearson (78). Adjustment of the flow rate of the exchange gas provides a control of the temperature. However, the system had several drawbacks: long time intervals were necessary before equilibrium was reached; adjustment of the flow rate for a particular temperature was critical and not very repeatable; and lastly, the lowest temperature obtainable was some tens of degrees above that of liquid nitrogen. A heating coil of 'Kanthal' resistance wire was wound around the 1/2" diameter stainless steel tube of the vacuum jacket, at the level of the specimen. Insulation and location of the coil was achieved by the use of 'Sellotape'. The total resistance of the coil was 7Ω and the heating current was supplied from a 24 volts D.C. supply, through a rheostat. To prevent the heat from the coil being employed solely in boiling off the surrounding liquid

nitrogen, a second stainless steel tube of 3/4" diameter, with the lower end closed, was pushed over the heating element and its insulation, as shown in Figure 6.1. It was found unnecessary to pump this enclosure, the heat supplied from the heating coil producing no serious increase in the rate of boil off of the nitrogen, except at temperatures where solid carbon dioxide in methanol could better be employed as a temperature bath. At this point the bubbling of the nitrogen disturbed the lower suspension of the apparatus, and the balancing current was no longer steady. Because of this the bath of crushed solid carbon dioxide in methanol was used to provide a temperature of 197^{ok}. For temperatures above this, up to room temperature, this bath was used in conjunction with the heating coil.

The heating coil was very satisfactory: the current was calibrated against temperature for both liquid nitrogen and carbon dioxide temperature baths, and attainment of specific temperatures was found to be repeatable. The time required for thermal equilibrium to be reached varied from 15 to 30 minutes, depending on the temperature change involved. The temperature, once attained, was stable within $\pm 1^{o}K$ over the period of time necessary for the plotting of one torque curve, which was approximately ten minutes, and generally remained within these limits for the time required for a complete run using a range of magnetic fields, which involved three quarters of an hour or more.

In the case of one specimen (holmium, C axis in the plane of the disc) the use of liquid neon as a coolant was attempted to obtain temperatures well below the 55^{ok} obtained by pumping nitrogen. The capped dewar system was used, as for pumped nitrogen. Liquid neon being rather expensive, only one litre was used. A glass syphon

transferred the neon from the storage dewar to the apparatus, the storage dewar being pressurised by means of a football bladder, which, on squeezing, supplied sufficient pressure in the dewar to force the liquid neon over the transfer syphon and into the magnetometer dewar. The neon boiled off more quickly than anticipated, and could only be used for a single run. The rapid boiling of the liquid in the magnetometer dewar disturbed the readings obtained, and the experiment was not very successful.

6.6 Temperature Measurement

Throughout the temperature range used, the temperature was measured by a copper-constantan thermocouple, which was threaded down the narrow bore stainless steel support tube of the specimen holder, and had the recording junction in contact with the specimen. The leads were led from the apparatus through vacuum seal lead-throughs, so that they were unbroken. The reference junction was held under melting ice in a glass funnel, so that it remained at 0^{oc}. A Pye portable potentiometer was used to measure the e.m.f. developed by the thermo-couple, and calibration of the thermocouple in liquid nitrogen and solid carbon dioxide in methanol gave agreement with the standard tables for copper and constantan. (American Institute of Physics Handbook, 2nd Edition, McGraw-Hill (1963), 4 - 18).

6.7 The Electromagnet

The magnet for which the apparatus had originally been built was constructed by Roe and is fully described by him (79). This electromagnet was used for the present investigation.

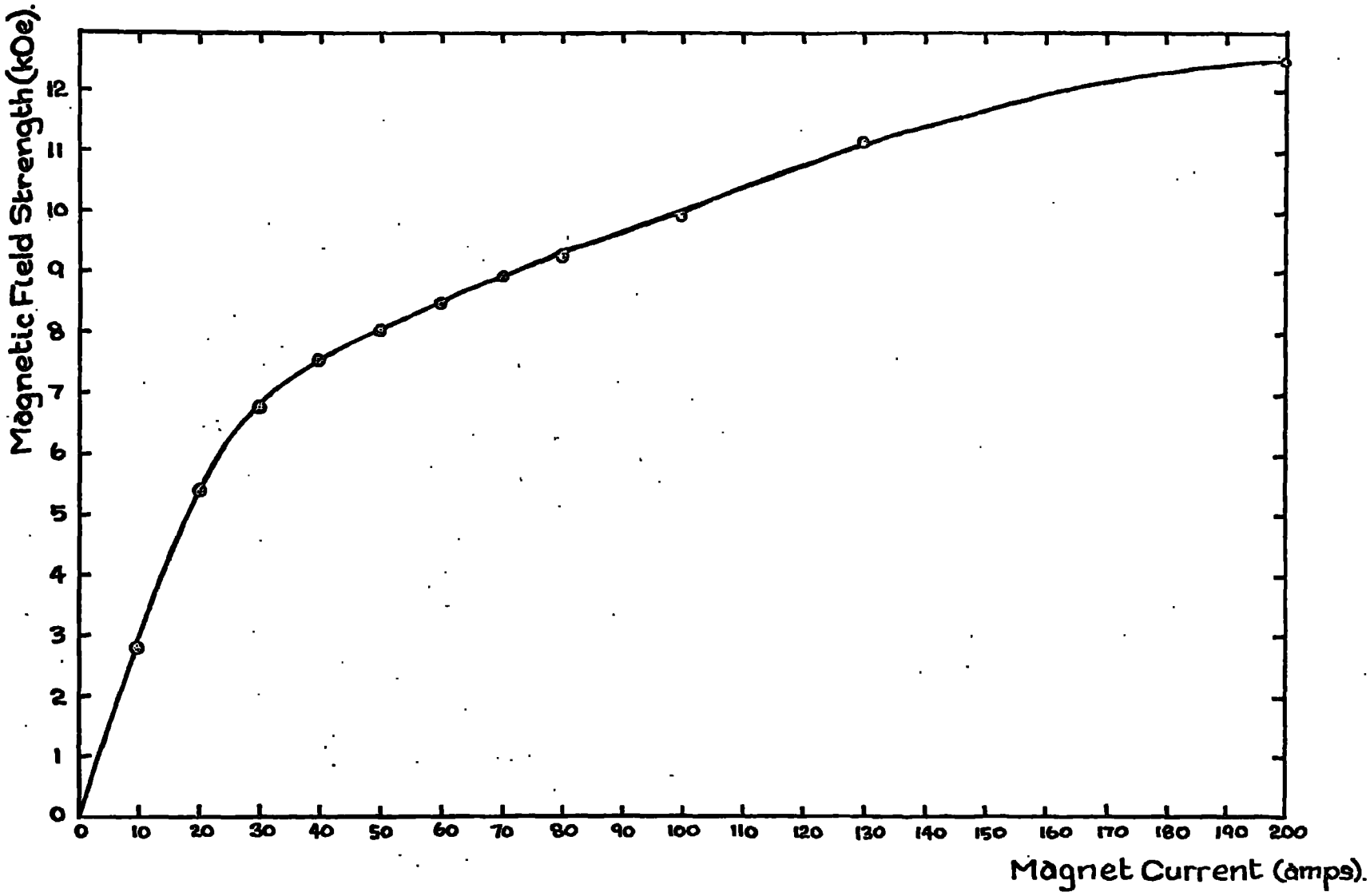

Fig. 6.8 Calibration curve for the electromagnet.

The two coil cases of the magnet each contain about 580 turns of 0.25" x 0.08" resin insulated copper strip wound about the 10 cm diameter soft iron cores in 34 layers, with 17 turns per layer. Thin Tufnol strips separate each layer, and enable the cooling water to circulate throughout the coil. The two soft iron cores also serve as cylindrical pole pieces, having a separation of 4.88 cms.

Cooling is by a closed pumping system, circulating distilled water through the magnet, and then through a multiple tube heat exchanger, where the heated water is cooled by continuously flowing mains water.

The magnet was powered by a 50 kilowatt, 200 amps D.C. Supply, provided by rectification of the mains supply. A slight ripple in the voltage output was insufficient to affect the measurements in any way.

The magnet had a resistance of just over 1Ω with the coils connected in series. At the maximum current which could be supplied, the field obtainable was 12.5 kOe. The magnet current versus field relationship was calibrated using a Grassot Fluxmeter, and the calibration curve is shown in Figure 6.8. The field was uniform to within $\pm 1/2\%$ over a volume of 3 ccs, which was more than adequate for the experiment.

The electromagnet ran on a railway track, so that it could be pushed into or out of the experimental position. The magnet could also be rotated about the vertical axis: rotation was limited to 200° because of the current cables and cooling water hoses attached to it.

6.8 Arrangement of the Apparatus

The magnetometer was supported on a rigid frame work built from "Handy Angle" girders, which bridged the magnet railway, and was bolted to the floor of the laboratory. The thick brass baseplate of the magnetometer was shimmed to make the suspended specimen holder and its support tube vertical. The position of the baseplate was adjusted on the framework until the specimen was accurately placed at the centre of the magnet gap. The baseplate was then clamped firmly to the supporting frame. The photocells and beam splitter were bolted to a rigid angle iron tower to one side of the magnet track, and some two metres distant from the magnetometer axis. To this tower the projector lamp and the D.C. amplifier and power supply were also fastened. Vibration of the projector lamp, galvanometer mirror, or the beamsplitter were found to be negligible, although a sharp knock to the magnetometer supporting frame was sufficient to cause some oscillation of the balancing current.

The specimen could be replaced by removal of the stainless steel tube supporting the bottom suspension, after first slackening the lower suspension retaining screw. This exposed the specimen holder; the lower section, on which the specimen was mounted, could be removed and replaced by an identical section holding a different specimen. The lower suspension ligament, with its brass attachment rod, was attached to the new specimen holder.

With the specimen holder so exposed, the orientation of the specimen relative to the magnetic field could be determined. A special stand for a travelling microscope was constructed, so that the

microscope could be mounted directly on a diameter of the magnet and at right angles to the field direction. This was then focussed on the specimen holder, which was oriented so that the reflected light beam fell centrally on the beam splitter, in the equilibrium position. The magnet, and hence the microscope, was then rotated until a fine scratch previously scribed on the holder was centred on the cross-hairs. At this point the Magnetic field direction was at right angles to the diameter on which this scratch lay, and the angle on the electromagnet scale at which this occurred could be related to the appropriate point on the torque curve. X-ray diffraction of the specimen, still mounted on the holder, determined the orientation of the crystal axes relative to the scratch, and hence to the torque curve. This comparison could be made to $\pm 5^{o}$, which was adequate, since in all cases investigated the easy direction coincided with a crystallographic axis, as indicated by the symmetry of the curves.

After removal and replacement of the lower suspension point, it was necessary to recentre the balance coil in the permanent magnet. The damping vanes were removed to enable the attainment of a perfectly freely suspended system, and the position of the upper suspension point adjusted until the coil and its dependent rod swung freely. The damping vanes were then replaced.

CHAPTER SEVEN

EXPERIMENTAL PROCEDURE AND ANALYSIS OF THE TORQUE CURVES

7.1 Calibration of the Torque Magnetometer

Calibration of the torque magnetometer was based on a consideration of the relationship between the torque produced and the magnetic flux through the coil. The torque produced by a coil of effective area A in a magnetic field strength H and passing a current i is given by:-

$$L = A H i \qquad 7.1$$

provided H is the component of the field in the plane of the coil. Since a radial field is used for the magnetometer, this torque will be independent of the orientation of the coil. Then the torque per unit current through the coil is:-

$$L/i = AH \qquad 7.2$$

Thus a calibration of the coil involves only a knowledge of the factor AH. If the coil is now deflected through an angle θ there will be a flux change through the coil given by:

$$\Phi = AH\theta \qquad 7.3$$

Then measurement of Φ will provide a determination of the factor AH. Experimentally the coil was connected to a Grassot Fluxmeter, of sensitivity 7.098 Maxwell-turns per cm when used in conjunction with a lamp and scale at a distance of 1 metre from the fluxmeter mirror. The magnetometer suspension was twisted away from the equilibrium position until it was hard up against a piece of plasticene. The suspension and coil were then pulled through a small deflection and allowed to swing back onto the plasticene, which prevented oscillation.

The angular movement of the coil during this process was determined by measuring the distance travelled by the light spot formed by the reflected beam on a scale placed in front of the beam splitter. At the same time the corresponding flux change through the coil, as determined by the fluxmeter deflection, was noted. The measurement was repeated many times, to give a sensitivity for the 150 turn coil used of 68.9 ± 0.3 dyne cms per milliamp.

7.2 Calibration of the Recording Galvanometer

The Pye Scalamp galvanometer used for recording the counter-torque current had a sensitivity of 0.032 micro amps/mm, and a resistance of 48Ω. The galvanometer was arranged in parallel with the coil and had a set of five resistances, each of which could be switched in series with the galvanometer, to change the sensitivity. The galvanometer was thus being used as a multirange voltmeter. Since the smallest of the switched resistances was 15 KΩ while the resistance of the counter torque coil was 10Ω , calibration could be achieved accurately by measuring the current supplied to them both from an ammeter and rheostat. This current was measured on a substandard ammeter of 150 milliamps full scale deflection, and the corresponding deflection on the Scalamp was measured as the current was systematically increased. The calibration was performed for ranges 1 and 2, for deflections to both right and left. Both calibrations were perfectly linear, and deflections to right and left gave identical calibrations. The substandard ammeter was not sufficiently sensitive for calibration of ranges 3, 4 and 5. This was achieved by comparison of the reading obtained on one range with that

obtained on the ranges above or below, with no change of current. This was repeated many times for each pair of ranges to establish the scaling factor for each pair.

The calibration gave the sensitivities for the five ranges as Range 1:48.0 ma/cm; 2:14.5 ma/cm; 3:4.71 ma/cm; 4:1.44 ma/cm, 5:0.496 ma/cm.

When used with the 150 turn coil, the torque sensitivities were: Range 1:3310 dyne cms/cm; 2:996 dyne cms/cm; 3:325 dyne cms/cm; 4:99.3 dyne cms/cm; 5:34.2 dyne cms/cm.

7.3 Plotting the Torque Curve

The upper suspension was adjusted until the reflected beam fell on the centre of the beam splitter. The position of the beam splitter could then be adjusted slightly to produce zero balancing current. The glass dome was then replaced and the system evacuated. This produced some outgassing of the damping oil, particularly if the oil had been removed from the trough and replaced. During this outgassing it was found convenient to switch on the automatic balancing system, for if the suspension was not held in the equilibrium position, the violent bubbling of the oil in some cases moved the suspension point slightly, causing the coil to catch on the permanent magnet assembly. Outgassing ceased after a few hours, whereafter, provided no further disassembly of the magnetometer was performed, future runs could be made without an outgassing period.

The magnetometer dewar was filled with the appropriate coolant, and the heater current adjusted to provide the required temperature.

If the temperature required was critical (as, for example, when working at the Néel point)further adjustment of the heater current was generally necessary to provide a final change of the temperature over a few degrees to the required value.

When the specimen thermocouple indicated that the temperature was steady, the electromagnet was switched on, the current being adjusted to give the required field setting as obtained from the field calibration curve.

To record a complete torque curve the magnet was then rotated in steps of 10° for the C axis specimens, where the torque curves were of the 2θ type, and in steps of 5° for the basal plane specimens, where the torque curves had a more rapid angular dependence. At each orientation of the field, the counter torque current as indicated by the Scalamp was recorded, and the torque curve could then be plotted in terms of magnet orientation and Scalamp deflection.

7.4 Analysis of the Torque Curves

From the symmetry of the rare earth crystals, all the torque curves must have at least two fold symmetry. Thus determination of a torque curve for rotation of the applied magnetic field through 180° is sufficient. The relationship between torque and the anisotropy constants was discussed in Chapter Five. If the direction of the magnetisation in the crystal is specified by the angle θ, the polar angle from the C axis, and the angle ϕ, the azimuthal angle in the basal plane measured from the a axis, then the torque developed is given by equations 5.4 and 5.5. Provided the experimental torque curve has precisely this ideal shape, a knowledge of the value of a few points on

the curve is sufficient to determine all the constants. However, it is obviously better to analyse the whole curve for the constants and determine the best fit, when the significance of any deviations from the predicted shape may be considered. Such deviations may arise from the presence of shape anisotropy, or mis-orientation of the specimen, for example. It is convenient to make a computer analysis of the curve.

For the C axis anisotropy as indicated in 5.4 it appears to be sufficient to analyse for the sin 2θ, sin 4θ and sin 6θ components. For the basal plane anisotropy, as in 5.5, we expect only a term in 6ϕ. In the work of Corner, Roe and Taylor (69) allowance was made during analysis for the fact that the magnetisation would tend to lie between the direction of the applied field and the easy axis if the applied field strength were insufficiently great, while the angle θ is taken as the direction of the applied field. This produced a distortion of the apparent torque curve so plotted, in which the torque maxima were moved towards the hard directions. In the cases where such a distortion was observed in this work, the extent of the distortion was found to be highly strain dependent, and application of the above correction was hardly justified. For the C axis anisotropy measurements with the metals in the ferromagnetic state the distortion was very marked because the fields applied were insufficient to pull the magnetisation appreciably out of the easy direction. This effect was investigated, and again the correction could not be used effectively.

In the case of the basal plane anisotropy measurements, the constant K_4 is in all cases much smaller than the constant K_1. Thus any misorientation of the specimen produces a component of K_1, (and K_2 and K_3 if present) in the basal plane torque curve, giving rise to terms in

2ϕ and 4ϕ as well as in 6ϕ. If the axis of the specimen normal to the major cross-section is not accurately parallel to the axis of the magnetometer, or if the sample has not a perfect cylindrical symmetry, then there will be an additional torque due to variation of the shape anisotropy energy with the angle ϕ giving primarily terms in 2ϕ. Further, since the anisotropy constant K_3 is a coefficient of terms in 6θ it might be expected to contribute to the 6ϕ component. The analysis for this situation has been carried out by Darby and Taylor (73) and involves defining the direction of magnetisation relative to the crystallographic axes, rather than the axes of symmetry of the specimen. The analysis shows that if the angle between the crystallographic C axis and the axis of rotational symmetry of the specimen, θ_c is small, then the coefficient of the sin 6ϕ term is unaffected by the mis-orientation; the contribution of the constants K_1, K_2 and K_3 gives rise to a term in sin 2ϕ as:

$$L(\phi) = \theta_c^2(K_1+2K_2+3K_3)\sin 2\phi + 6K_4\sin 6\phi \qquad 7.4$$

This expression was used as a basis for the basal plane torque curve analysis, and a curve fit was obtained which was satisfactory. The angle θ_c was found to be small ($\lesssim 5^\circ$) in all cases, as determined by X-ray orientation of the specimen on the specimen holder. Since the sin 6ϕ component is only affected by K_3 in the order θ_c^2 the amplitude of the hexagonal component may be equated to $6K_4$: in the C axis determinations no. K_3 component was observable, in any case.

7.5 Computer Analysis

There were two types of torque curve to analyse: that for the

C axis specimens, where it was required to determine the amplitudes of the 2θ, 4θ and 6θ components, and that for the basal plane specimens, where it was required to determine only the 2ϕ and 6ϕ components.

The analysis used was of the Fourier type, using the fact that

$$\int_0^{\pi} \sin(m\theta)\sin(n\theta)d\theta = 0 \text{ if } m \neq n,\ \pi/2 \text{ if } m=n \qquad 7.5$$

for m, n integers.

Thus to determine the sixfold component in a mixture of twofold, fourfold, or any other components in θ each point on the torque curve was multiplied by the appropriate value of $\sin 6\theta$ and the curve integrated numerically. The resultant integration for all components except the sixfold term was then zero, while the value obtained for the total integration from 0 to π was $\pi/2$x the amplitude of the hexagonal component.

The integration was carried out using Filon's numerical quadrature formula (see, for example, 80). This states that if the integral $\int_b^a f(x)\sin(mx)dx$ is divided into $2k$ parts, each of length h, on the x axis, then

$$\int_b^a f(x)\sin(mx)dx \triangleq h\{\alpha[f(a)\cos(ma)-f(b)\cos(mb)] + \beta S_\beta + \gamma S_\gamma\} \qquad 7.6$$

where $S_\beta = -[f(a)\sin(ma)+f(b)\sin(mb)] + 2\sum_{j=0}^{k} f(a+2hj)\sin([a+2hj]m)$,

and $S_\gamma = \sum_{j=1}^{k} f(a+h(2j-1))\sin[(a+h(2j-1))m]$,

$$\alpha = \frac{1}{\theta} + \frac{\sin 2\theta}{2\theta^2} - \frac{2\sin^2\theta}{\theta^3}, \qquad \beta = \frac{1+\cos 2\theta}{\theta^2} - \frac{\sin 2\theta}{\theta^3},$$

$$\gamma = 4(\sin\theta/\theta^3 - \cos\theta/\theta^2), \quad \text{where } \theta = mh.$$

The factors α, β and γ can be expressed as a power series in θ, and for small θ, where powers of θ^2 or greater are ignored, the formula reduces to an application of Simpson's rule. The only condition for validity of the formula is that $f(x)$ must be such that $\int_b^a f(x)dx$ can be evaluated using Simpson's rule. This is the case here.

The integration was performed over 180°, and the starting angle.

a, was chosen such that the function was zero (ie zero torque) at x = o or 180°. The interval h was either 5° or 10°, depending on the interval at which the torque measurements were taken. The integration was done using an Elliott 803 computer, the programming being done in Algol 60 on a five hole punched tape system.

For convenience the numerical integration using Filon's equations was turned into a procedure in several parameters, since the same programme could then be called upon for analysis for any of the anisotropy constants. The parameters involved were the number of torque values read in from the curve, an array of these values, the initial value of x (where x now corresponds to θ or ϕ in the torque equations) determined by the condition that f(x) shall be zero at x = o or π for the particular component required, and lastly, the order of the component required (2, 4 or 6).

The anisotropy constants were then calculated: for the c-axis anisotropy, using equation 5.4:-

$$K_1+K_2+15K_3'/16 = -\frac{2}{\pi} \times \text{Filon's Procedure(2nd order)} \qquad 7.7$$

where $K_3' = K_3+K_4\cos 6\phi$,

$$\tfrac{1}{2}K_2+\tfrac{3}{4}K_3' = -\frac{2}{\pi} \times \text{Filon's(4th order)},$$

and $$3K_3'/16 = -\frac{2}{\pi} \times \text{Filon's(6th order)}.$$

For the basal plane anisotropy, using equation 7.4:-

$$6K_4 = \frac{2}{\pi} \times \text{Filon's(6th order)}, \qquad 7.8$$

and $$\theta_c^2(K_1+2K_2+3K_3') = \frac{2}{\pi} \times \text{Filon's(2nd order)}.$$

The programme used also provided a print out of the torque curves calculated using the values of the anisotropy constants obtained by analysis, so that the fitted curves could be compared with the experimental curves. This was particularly useful for those basal plane torque curves where there was an appreciable contribution from the $\theta_c^2(K_1 + 2K_2 + 3K_3)$ term.

The fit obtained (e.g. see Figure 8.1) was in all cases found to be satisfactory, indicating that the treatment of Darby and Taylor was adequate. In the case of the holmium basal plane sample, it was also necessary to analyse for a twelve fold component, to obtain a satisfactory fit.

It was also found convenient to have the programme calculate the 'error' in the curve fitting, in the form of the sum of the squares of the differences between the experimental torque values and those calculated using the constants obtained from the computer analysis. Although this had no meaning as far as the errors on the values obtained for the anisotropy constants were concerned, it was a useful indication of the reliability of the different analyses, and would also indicate any large errors made in the punching of the data, of which there was a substantial quantity. Furthermore, the programme was made to change the value of the anisotropy constant in steps of a few percent about the obtained value, and recalculate the error. This indicated the sensitivity of the analysis for the constant: the error was generally a minimum at the value obtained, or at most for values of the anisotropy constant not more than 4% away from the obtained value.

One of the parameters required by the Filon's procedure was the initial value of x. In cases where one component dominated in the torque curve, the point where the curve crossed the axis could be taken as the origin for x. However, in curves where there were several components of the same order of magnitude, the resultant torque was not necessarily zero at x=o. An approximate value for the position of the zero could be obtained by inspection. A range of values about this point was then used for a trial set of analyses for the anisotropy constant

required, and the errors so calculated plotted to determine the value of the origin which produced a minimum error in the fit.

This method of analysis is reasonably quick and simple: any component can be analysed for provided the position of the origin is fairly well defined. There are more complicated methods of analysis which will determine a large number of components without a knowledge of the origin for each component. However, such methods require a large amount of computer time. The analysis used in all cases gave a satisfactory fit to the experimental data, except in those cases where the curve could not be expected to conform to a simple trigonometrical series, because of the presence of domains, or modification of the anisotropy by strain, etc. Any description of these curves in terms of coefficients of a trigonometrical series is likely to be complicated, and will in any case be meaningless, since the symmetry supplied by the crystal lattice has been modified.

7.6 Accuracy of the Anisotropy Determinations

It is difficult to assign uncertainties to the values of the anisotropy constants. Individual torque measurements could be made with an accuracy of ±2% but the method of analysis of the curves provides no means of evaluating the error involved. The results of changing the values obtained for the anisotropy constants suggest that the probable error is less than 2%. The temperature was known to within $\pm 1^{\circ}K$. However, the presence of rotational hysteresis in the curves tended to produce two values for the constants, for rotation of the applied field in opposite directions, which differ by rather more than would be suggested by these

figures. When the hysteresis was very large, generally at low field strengths and where the torques obtained were very small, the difference was as much as 10%, and in a few cases even more. Similarly, the presence of strain in the specimen could change the anisotropy constants by 10%. The occurrence of such large discrepancies is indicated in the results. For the other determinations, the error in the values of the anisotropy constants should be appreciably less than this.

CHAPTER EIGHT

RESULTS AND DISCUSSION

8.1 The Measurements

Torque measurements have been made in the temperature range from 55 ^{ok} to room temperature on the single crystal specimens available, and the resultant curves have been analysed to give values of the appropriate anisotropy constants. The specimens investigated were as follows:-

(i) Gadolinium ellipsoid, basal plane contained in the plane of the ellipsoid.

(ii) Terbium ellipsoid, with the C axis and an a axis in the plane of the ellipsoid. Terbium disc, with the C axis and an a axis in the plane of the disc.

(iii) Terbium ellipsoid, with the basal plane in the plane of the ellipsoid. Terbium disc, with the basal plane in the plane of the disc.

(iv) Dysprosium ellipsoid, with the C axis and an a axis in the plane of the ellipsoid.

(v) Dysprosium ellipsoid, with the basal plane in the plane of the ellipsoid. Dysprosium disc, with the basal plane in the plane of the disc.

(vi) Holmium ellipsoid with the C axis and an a axis in the plane of the ellipsoid (two specimens).

(vii) Holmium ellipsoid with the basal plane in the plane of the ellipsoid.

In addition, an erbium ellipsoid, whose plane contained the basal plane of the crystal, gave no observable signal at temperatures down to 55^{ok}, and

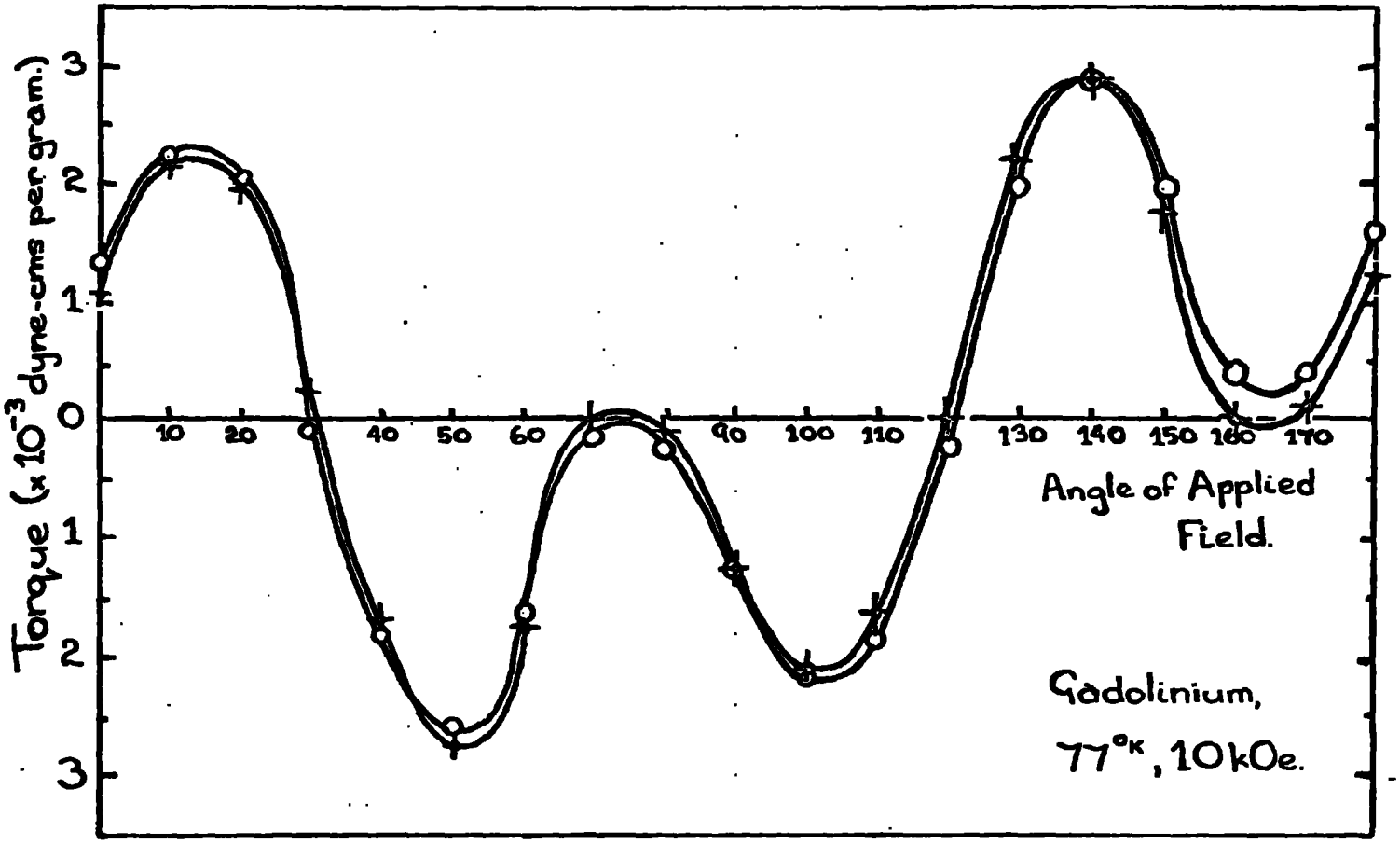

Fig. 8.1 Torque curve (circles) for the gadolinium basal plane specimen at 77°K, in an applied magnetic field strength of 10 kOe. The crosses are points calculated from the computer analysis of the torque curve.

applied magnetic field strengths of 12.5 kOe. At such temperatures the critical field value is of the order of 16 kOe, according to Flippen (81) and the system would be in the antiferromagnetic state, where any basal plane anisotropy might be expected to be small.

Results obtained on the various rare earth metals will be treated in order of increasing atomic number of the metals.

8.2 Gadolinium Basal Plane Anisotropy

Values obtained for the anisotropy constant $\mathcal{K}_4$ for gadolinium have already been published, both from measurements on the crystal used here (73) and also from measurements by C. D. Graham (74). The repeated measurements on the sample used here are of some interest because the measurements have been extended to slightly lower temperatures, and also because a more sensitive computer analysis has shown that the basal plane anisotropy persists to somewhat higher temperatures than was previously indicated.

A typical torque curve obtained for the gadolinium basal plane specimen is shown in Figure 8.1. It can be seen that appreciably large components in 2ϕ, and possibly 4ϕ, appear in the curve, as well as the 6ϕ term expected from the basal plane anisotropy. The computer analysis determined the contribution of the 6ϕ component and the summed contribution of the 2ϕ and 4ϕ components. These computed values were then used to plot a torque curve for comparison with the experimental curve. This computer fit is shown in Figure 8.1, and can be seen to be in satisfactory agreement with the experimental plot.

The resulting $\mathcal{K}_4$ values are plotted against temperature in

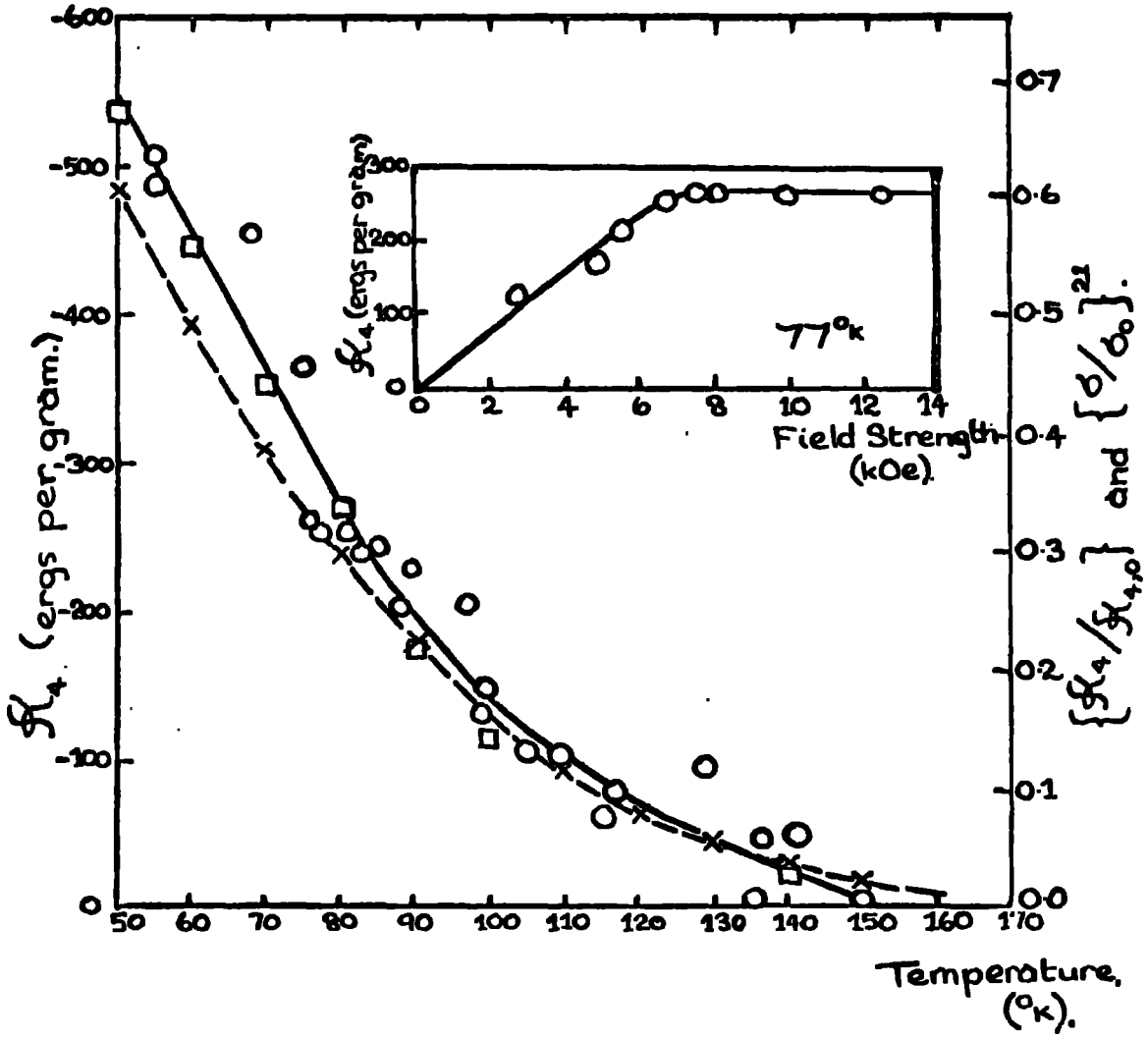

Fig. 8.2 Temperature variation of the anisotropy constant $\mathcal{K}_4$ for gadolinium. Open circles correspond to values obtained by the author, squares to values obtained by Graham (74). Crosses indicate the temperature variation of $\{\sigma/\sigma_0\}^{21}$. Inset shows approach to saturation of the apparent anisotropy constant $\mathcal{K}_4$.

Figure 8.2. It should be noted that most of the torque curves involved were obtained on the original torque magnetometer, where zero drift was a problem, and this accounts for the relatively large scatter of the points. However, the $\mathcal{K}_4$ values were checked using the transistorised magnetometer and found to be consistent. The $\mathcal{K}_4$ value approaches zero near 150^{ok}, in agreement with the results of Graham, while earlier investigations using this crystal suggested a disappearance of $\mathcal{K}_4$ at approximately 130^{ok}. The larger $\mathcal{K}_4$ values obtained at lower temperatures confirmed the earlier measurements.

The values obtained by Graham are indicated in Figure 8.2 by the squares, and are in satisfactory agreement with the values obtained here.

The inset diagram shows the approach to saturation of the $\mathcal{K}_4$ values. At all temperatures saturation was reached at approximately 8kOe, which is a slightly lower field strength than that indicated by Graham as necessary for saturation. Graham's crystal was cylindrical in shape, and therefore the field may not have been as homogeneous as in the case of an ellipsoid.

X-ray orientation of the specimen showed that the easy direction is the $\langle 11\bar{2}0 \rangle$ or a axis, corresponding to a negative value for $\mathcal{K}_4$ and in agreement with Graham. The basal plane anisotropy is at all times small compared with that between the C axis and the basal plane. $\mathcal{K}_4$ is less than 1% of the corresponding value of $\mathcal{K}_1$.

Figure 8.2 also compares the temperature variation of $\mathcal{K}_4/\mathcal{K}_{4.0}$ with that of $(\sigma/\sigma_0)^{21}$, using a value of - 800 ergs per gram for $\mathcal{K}_{4.0}$, the anisotropy constant at 0^{ok}, and values for σ/σ_0 given by Graham. It can be seen that the two curves are in approximate agreement. Since the

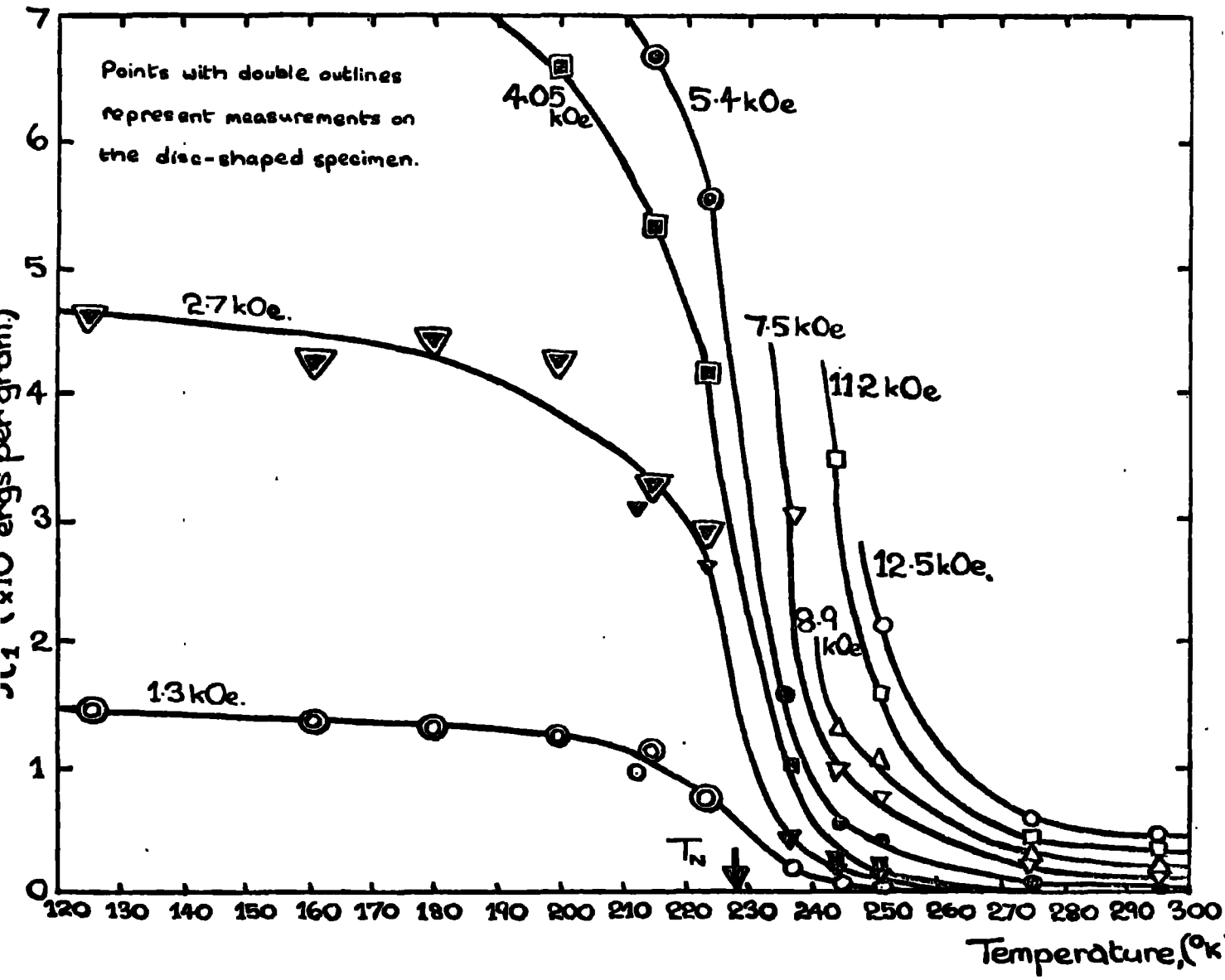

Fig. 8.3 Variation of $\mathcal{L}_1$ for terbium with temperature for various applied magnetic field strengths.

value of σ/σ_0 at 150^{ok} is 0.83 Zener's theory might be expected to be valid in the temperature range investigated.

8.3 Terbium - C Axis anisotropy

The maximum magnetic field available was 12.5kOe, while magnetisation measurements on terbium by Hegland, Legvold and Spedding (17) indicate that at such fields the magnetisation along the C axis is only 10% of the saturation value. Because of this it is to be expected that when terbium is ferromagnetic, the spins will not move very far out of the basal plane on application of such a comparatively small field along the C axis, and that any torque curve measured in the ferromagnetic region will not therefore give a true indication of the anisotropy constants of the crystal. When such measurements were made, it also became apparent that the torques developed by the system were at least an order of magnitude larger than the maximum compensating torque (20,000 dyne-cms) which the magnetometer could supply. At temperatures below the Curie point, the system was not able to hold the specimen in the null position at applied field strengths greater than about 3kOe. Consequently, the only useful measurements which could be made were in the paramagnetic region.

The torque curves obtained were all of a simple $\sin 2\theta$ type, so that the only anisotropy constant required is K_1. The signs of the torques were such as to indicate an easy direction in the basal plane of the crystal, which was orientated by X-ray diffraction techniques. The K_1 values obtained are plotted against temperature for various applied fields in Figure 8.3. It can be seen that the anisotropy is becoming very large some ten degrees above the Néel point for the higher

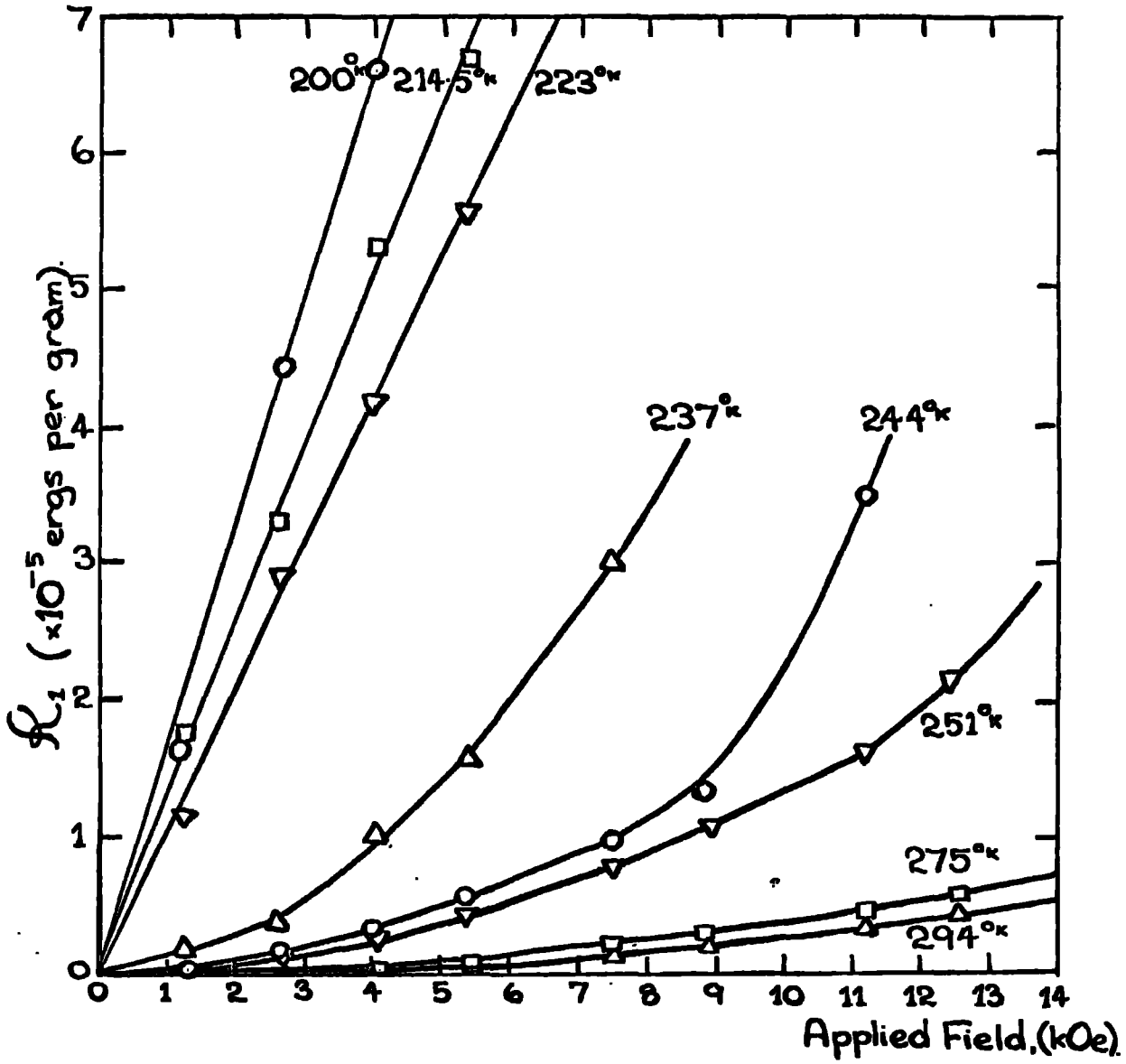

Fig. 8.4 Dependence of $\mathcal{K}_1$ for terbium on applied magnetic field strength at various temperatures.

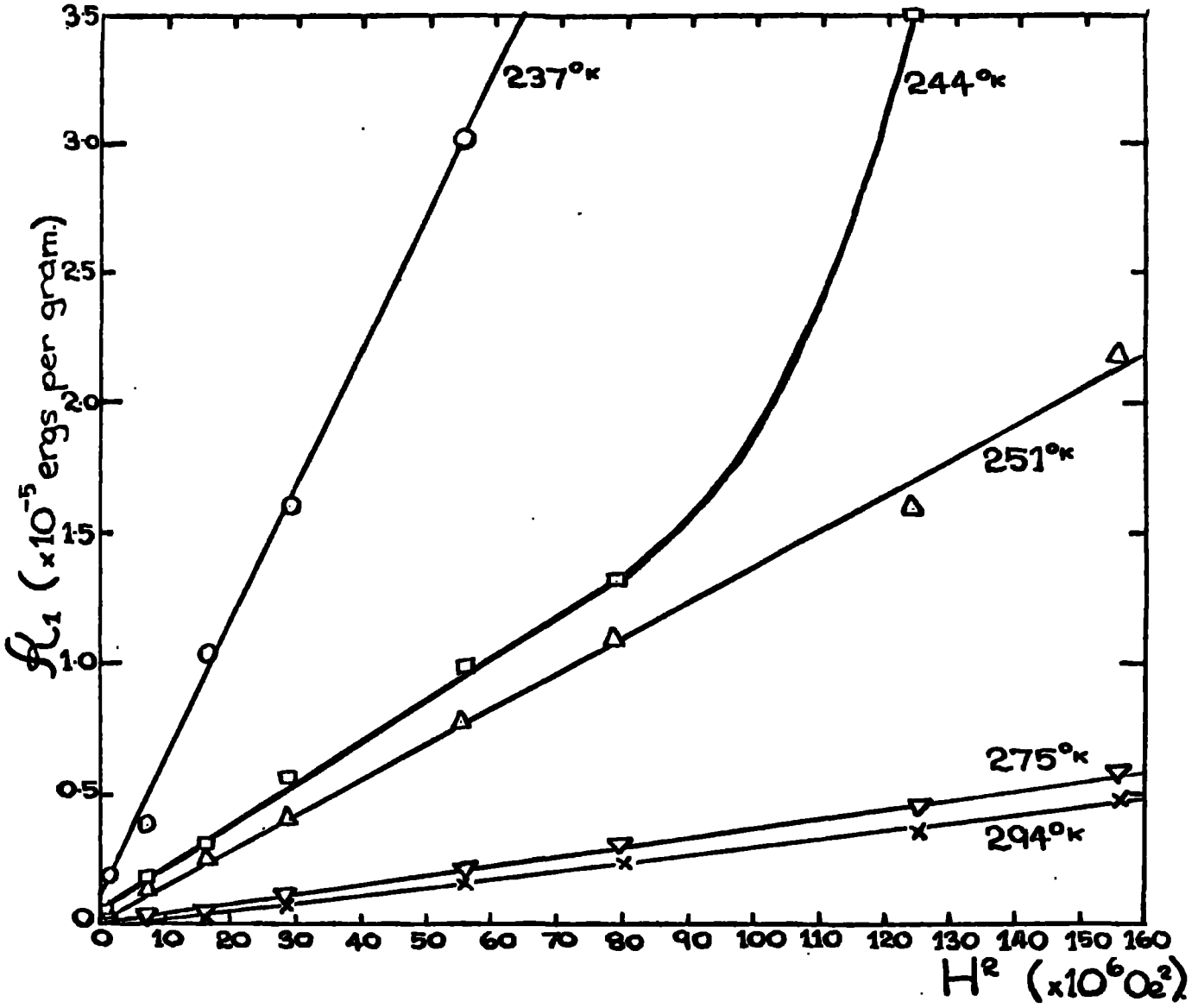

Fig. 8.5 $\mathcal{A}_1$ versus H^2 for terbium above the Néel point.

field values. Below the Néel temperature the torque values obtained were larger than the maximum torque measurable by the magnetometer, except for fields below about 3kOe. For such fields the amplitude of the torque curve varied little with decrease in temperature, so there would appear to be little increase in magnetisation with decrease in temperature at low field values, where all magnetisation must lie in the basal plane. It therefore seems likely that domains exist at fields up to 3kOe. The dependence of the $\mathcal{K}_1$ values on the applied magnetic field strength is shown in Figure 8.4, where several isotherms are plotted. Callen and Callen (52) predict that in the paramagnetic range the anisotropy constant $\mathcal{K}_1$ (or, more properly, K_2, the equivalent coefficient in the expression for the anisotropy energy in spherical harmonics) will be proportional to the square of the magnetisation, $M^2(T,H)$. Hence it follows that:

$$K_2 \propto (\chi H)^2 \propto \frac{H^2}{(T-\theta)^2} \qquad 8.1$$

The dependence on H^2 is demonstrated in Figure 8.5. Here the plot for 244^{ok} curves upwards sharply at higher fields, but this is not seen in the 237^{ok} values, and cannot be taken as evidence of any change in the magnetic ordering, as a small temperature change during the measurement would, at this temperature, have a large effect on the slope of the curve. For the temperature dependence the choice of θ is not obvious. In all one-ion theories $M(T,H)$ defines the distribution of the spins, and is assumed isotropic. In the paramagnetic region M is certainly not isotropic, and although the $1/\chi$ versus T plot is linear and has the same gradient whether the magnetisation lies in the basal plane or along the C-axis the intercept on the temperature axis differs. Where the easy

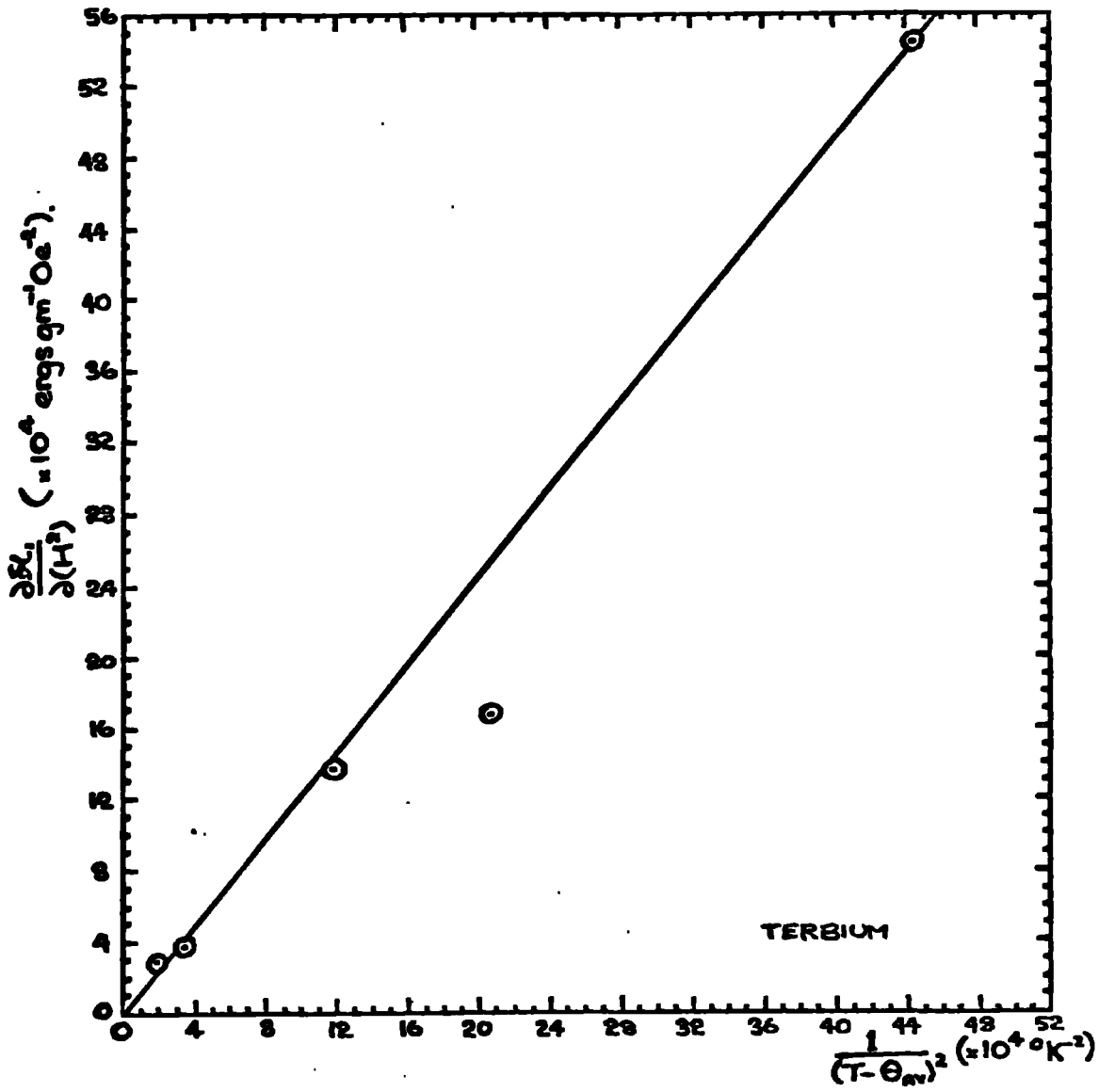

Fig. 8.6 Plot of $\frac{\partial \mathcal{K}_1}{\partial (H^2)}$ versus $\frac{1}{(T-\theta_{av})^2}$ for terbium in the para-

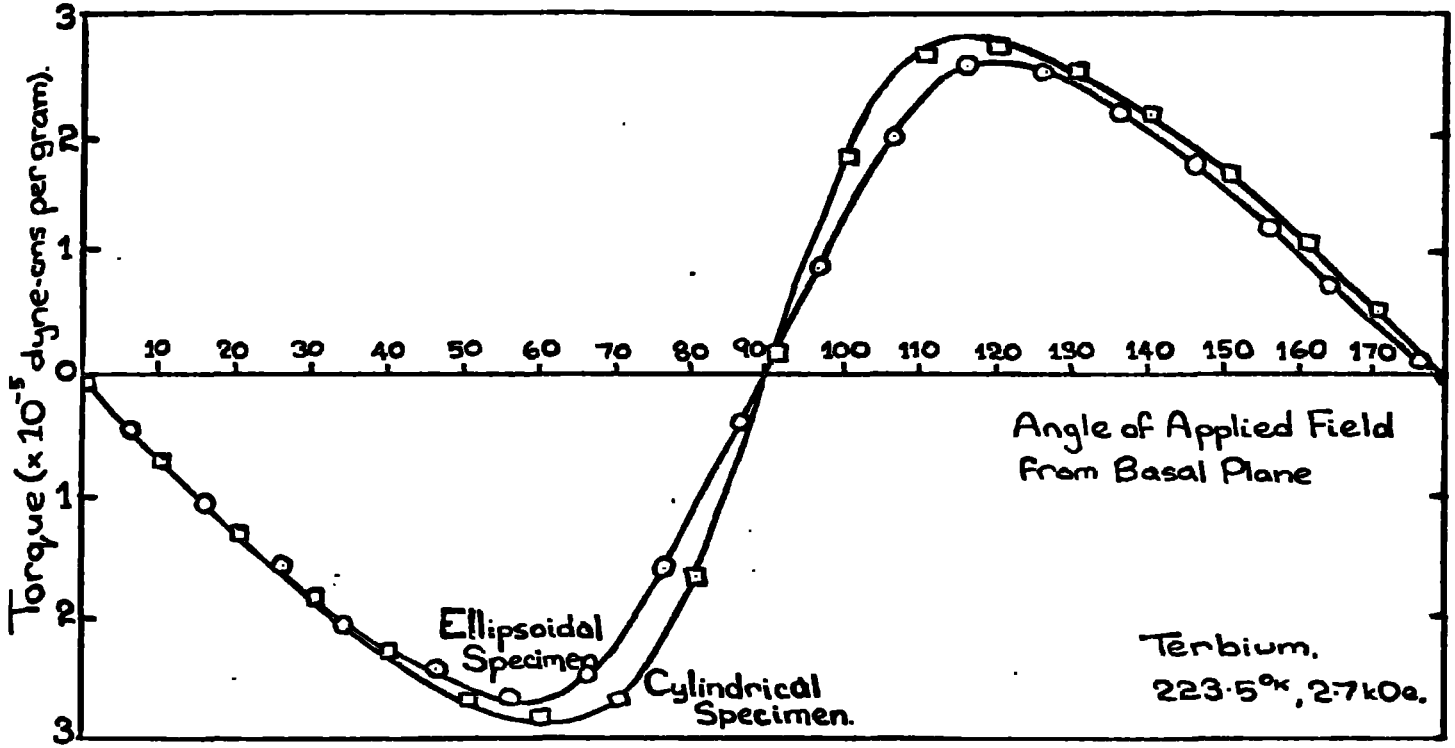

Fig. 8.7 Typical torque curve for ferromagnetic terbium, showing the deviation from a true sinusoidal curve.

direction lies in the basal plane, the paramagnetic Curie temperature θ_b is higher than that for the C axis θ_c. Consequently, it seems reasonable to take for the value of θ in equation 8.1 the average value for the paramagnetic Curie temperatures $(\theta_b+\theta_c)/2 = \theta_{av}$.

The dependence of the gradient of the $\mathcal{K}_1$ versus H^2 lines on $(T-\theta_{av})^{-2}$ is plotted in Figure 8.6, using a value for θ_{av} of 222^{ok}, obtained from Koehler (37). From the few points available the plot appears sufficiently linear: it is to be noted that the point which lies well off the line corresponds to the values obtained at 244^{ok}, which were in any case suspect.

A typical torque curve is shown in Figure 8.7. It will be noted that the curve is not a true sinusoid, but is distorted so that the maximum torque occurs closer to the C axis than the basal plane. This distortion was only found in the ferromagnetic measurements, the paramagnetic torque curves being perfectly sinusoidal. Two terbium C axis specimens were available, one being ellipsoidal, and the other a thin disc of approximately half the mass of the ellipsoidal specimen, enabling measurements to be taken to slightly lower temperatures. A torque curve at 223.5^{ok} in an applied field of 2.7 kOe is shown for each specimen in Figure 8.7, where the distortion is more marked for the cylindrical specimen than for the ellipsoid. It is of interest to consider the causes of this distortion.

In the ferromagnetic region the magnetic fields in which torques could be measured were small enough to justify the assumption that the spins remain in the basal plane for any orientation of the applied field. This situation is shown in Figure 8.8.

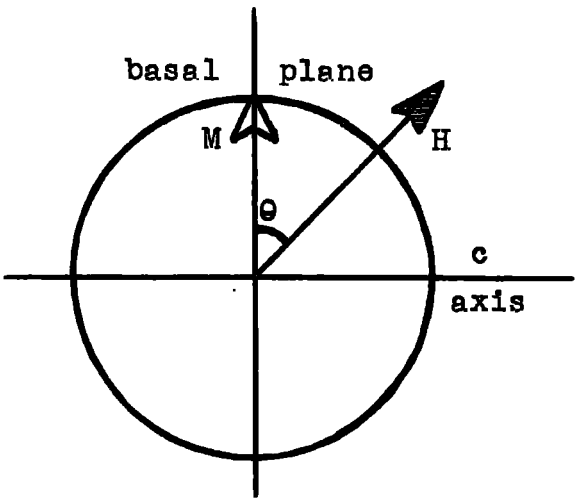

Fig. 8.8

As the applied field direction is rotated from the basal plane towards the C axis there will be some component of the field, $H\cos\theta$, remaining in the basal plane and maintaining the magnetisation in its original direction. The torque will be:

$$L(\theta) = MH\sin\theta \qquad 8.2$$

This expression increases to a maximum of MH at $\theta = 90^{\circ}$, and as the field sweeps across the C axis the magnetisation in the basal plane will suddenly flip to the reverse basal plane direction. Consequently, the torque will change discontinuously from a maximum value in one direction to a maximum value in the opposite direction.

However, when the field component in the basal plane is sufficiently small, the system will consist of domains whose magnetisation will lie in the basal plane along each of the easy directions. The results of Hegland, Legvold and Spedding indicate that the easy direction is the b axis, so that it is to be expected that some domain pattern will exist in which the magnetisation in the various domains will lie along both positive and negative directions for each of the three b axes. As the field in the basal plane is increased those domains with

magnetisation in the field direction are energetically favourable and grow at the expense of the other domains, and the magnetisation in the easy direction is not now constant. For very low field strengths the magnetisation is a function of the field component in the basal plane, and we can rewrite equation 8.2 as

$$L(\theta) \propto (H\cos\theta)H\sin\theta \qquad 8.3$$

$$\text{or} \quad L(\theta) \propto \sin 2\theta \qquad 8.4$$

Then at low field strengths the torque curve tends to the $\sin 2\theta$ type, as is observed. For somewhat higher fields the basal plane component of the applied field is only sufficiently small for the existence of domains when the direction of the applied field is near to the C axis. Thus as the field direction nears the C axis the magnetisation in the basal plane direction reduces, and the discontinuity in the $\sin\theta$ curve is smoothed out. As the field strength is increased the change in sign of the torque at the C axis will become more abrupt, as observed.

If we assume that all the magnetisation lies in the basal plane and that the torque is completely defined by $MH\sin\theta$ then the magnetisation data supplied by Hegland, Legvold and Spedding may be used to predict torque curves. Interpolation of the isothermal magnetisation curves will determine the value of the magnetisation M present in the basal plane direction for the appropriate value of the component of the applied field in this direction, the component gradually decreasing as the field is rotated away from the basal plane and into the C axis direction.

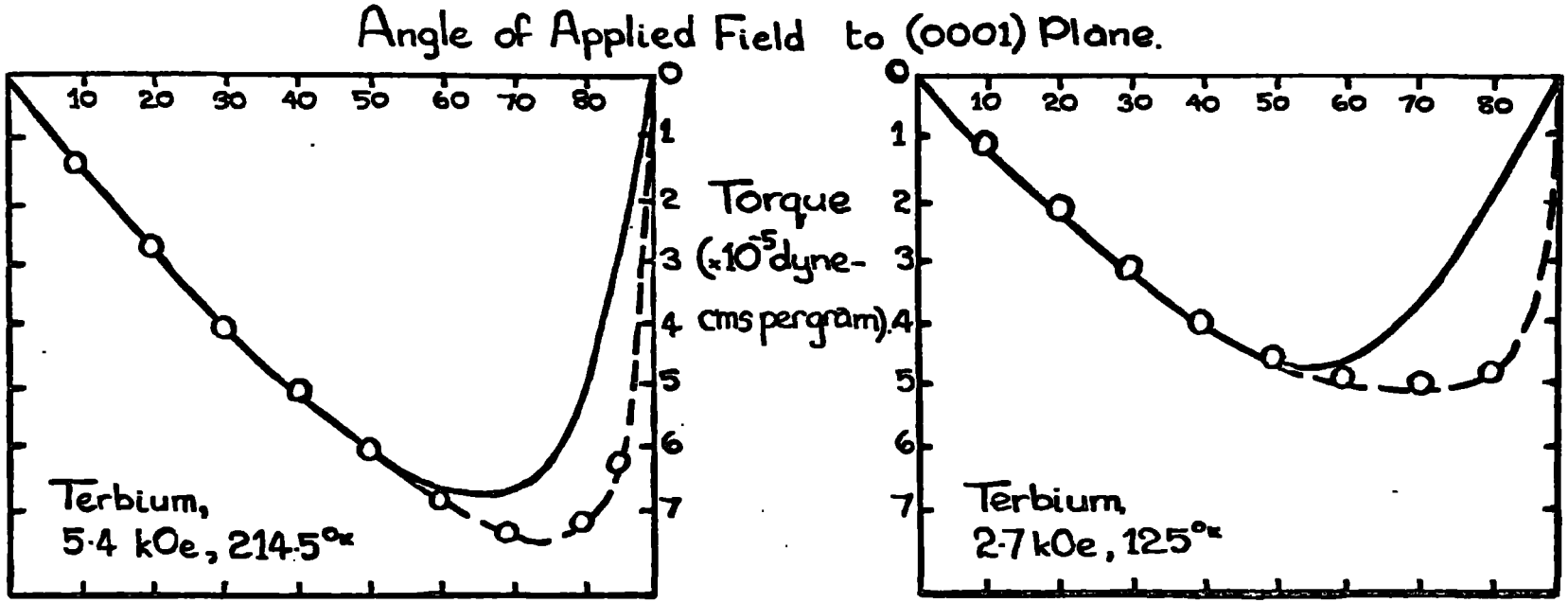

Fig. 8.9 Comparison of experimental torque curves (rings) for the c-axis terbium specimen with curves (solid line) calculated on the basis of magnetisation measurements by Hegland et al (17), assuming that the magnetisation is confined to the basal plane.

This value for the magnetisation can then be used in equation 8.2 to calculate the torque for a range of orientations of the applied field. The torque curves thus obtained for 214.5^{ok} and 5.4kOe, and 125^{ok} and 2.7 kOe, are shown in Figure 8.9 where they are compared with the experimental curves obtained for the cylindrical crystal. The agreement at angles close to the basal plane is remarkably good. At larger angles the experimental curves are closer to a $\sin 2\theta$ function than the calculated curves. Curves obtained for the ellipsoidal specimen indicate an even greater deviation from this prediction, but the precise pattern of domains existing in the crystal must depend to a large extent on the shape of the sample.

The Néel point of terbium is 227.7^{ok}, as determined by the neutron diffraction studies of Koehler et al (82) and the ferromagnetic Curie point is 220^{ok}. The critical field at the Néel point is only 200 Oe, and anisotropy observations must be made at applied field strengths smaller than this if the antiferromagnetic region is to be investigated. The torques developed at such fields were too small for useful measurement, although they appeared to be of the $\sin 2\theta$ type.

In order to investigate the shape of the ferromagnetic torque curve at higher fields than could be used with the automatic torque magnetometer, a simple torsion wire balance was set up, using a rotatable torque head and a short length of beryllium copper wire. As the magnetic field was rotated about the specimen the torque head was rotated manually to bring the specimen back to the zero displacement position. The torque curves obtained were similar both in shape and

magnitude to those reported for the dysprosium specimen (Figure 8.21) showing the behaviour predicted above, whereby as the applied field was increased the initial $\sin 2\theta$ type curve becomes more and more distorted, the maximum moving towards the C axis. At fields above 6kOe the torque reached a maximum value some 15° from the c axis, and at angles of the applied field closer to the C axis the system became unstable, the specimen flipping from the maximum torque position in one direction to that in the other direction. At 12kOe a maximum torque of 2×10^7 dyne cms/gram was developed at 77^{ok}. The specimen was still far from saturation at this field, and such a torque cannot be taken as an indication of the anisotropy, which must be considerably larger than that given by such torque values.

8.4 Terbium: Basal Plane Anisotropy

Torque curves were obtained for the ellipsoidal terbium basal plane specimen from 55^{ok} to 220^{ok}, for applied magnet field strengths up to 12.5kOe. The torque curves were found to be of the $\sin 6\phi$ type, components in 2ϕ and 4ϕ being comparatively small except at the higher temperatures. At temperatures below 100^{ok} the torques developed became too large at maximum field for the servomechanism of the torque magnetometer to hold them. A disc-shape specimen of approximately half the mass of the ellipsoid was available and enabled torque measurements to be made down to 55^{ok} at field strengths of 12.5 kOe. At temperatures above 220^{ok} no hexagonal component was observable, only a 2ϕ component from the C axis anisotropy remaining. Thus the basal plane anisotropy is only observable in the ferromagnetic region.

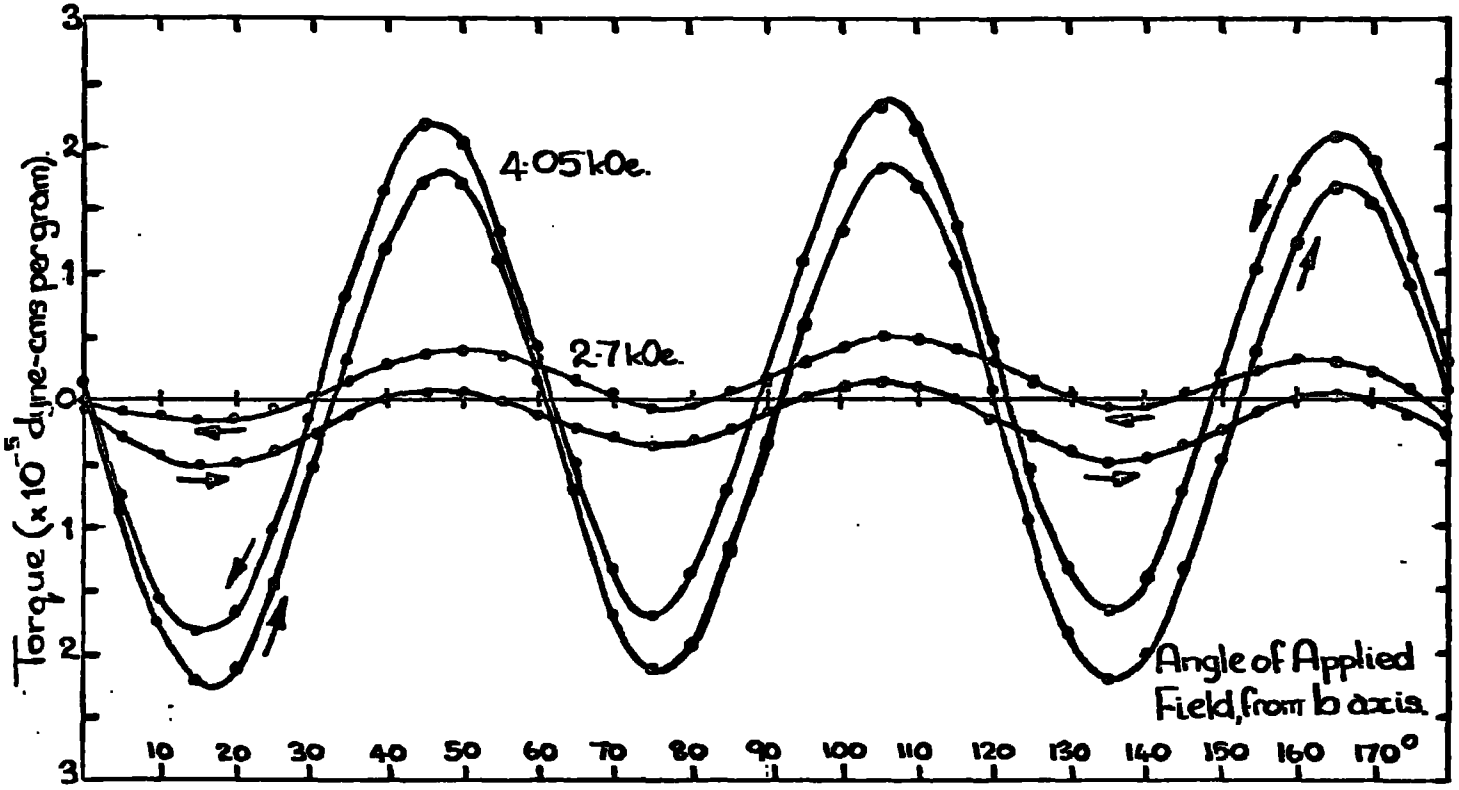

Fig. 8.10 Low field torque curves for the terbium basal plane specimen, showing rotational hysteresis. Temperature is 77°K.

Considerable rotational hysteresis was observed, and this became troublesome at low field strengths, computer analysis for the 6ϕ component producing values for the torque curves for opposite directions of field rotation which differed by up to 50% at the lowest field strengths used. If the two torque curves obtained for field rotation in opposite directions were averaged, then analysis of the average plot gave a $\mathcal{K}_4$ value which agreed with that obtained by averaging the separate $\mathcal{K}_4$ values obtained from the individual curves; this latter value is taken for the $\mathcal{K}_4$ value here. However, since domains exist at these low field values, the meaning of the anisotropy constant obtained is problematical.

Low field torque curves for the ellipsoidal specimen at 96^{ok} are shown in Figure 8.10 in which the rotational hysteresis can be seen. This hysteresis persists to the highest fields used, although at 12.5kOe the difference between the curves is less than 5% at the maxima. Thus hysteresis is appreciable at field strengths above technical saturation, where all magnetisation processes should be reversible. It is possible that the rotational hysteresis is due to domains existing in low field regions on the edges of the specimen, and if this is the case the disc shaped specimen, in which the field will be less homogeneous, would be expected to show a greater degree of hysteresis, as is found to be the case.

At temperatures below 110^{ok} the torque curves began to deviate noticeably from a sin 6ϕ form, the torque maxima becoming closer to the hard direction. This was more marked in the disc shaped specimen than in the ellipsoid. The distortion was affected to a large degree by

the way in which the crystal was mounted on the specimen holder, and it was found that in the cases where the deviation from a $\sin 6\phi$ curve was large, the amount of rotational hysteresis present was also large. A preliminary method used to mount the specimen was by a resin adhesive of the type used for strain gauges, and this produced such a large distortion of the torque curve as to produce what was almost a saw-tooth trace, again with a large amount of hysteresis. A specimen mounting using 'Sellotape' adhesive acetate tape was eventually found to be the most satisfactory, in that the torque curves obtained were reproducible, and showed a minimum of deviation from the sinusoidal, together with the smallest amount of rotational hysteresis. The very thin disc shaped crystal, when mounted on a dished specimen holder intended for the ellipsoidal specimens, also gave a very distorted torque curve, the distortion decreasing when the crystal was attached to a flat specimen holder. It therefore appears that any strain present in the specimen will greatly increase the deviation of the torque curve from the sinusoidal form, and is therefore presumably distorting the crystalline anisotropy energy by broadening the energy minima and sharpening the energy maxima. Since the presence of strain will change the lattice parameters slightly, it is to be expected that the anisotropy energy surface will be affected, and the symmetry of the lattice, and hence of the torque curve, presumably lowered. It seems possible that a strain free crystal would have a perfectly sinusoidal energy surface in the basal plane at all temperatures, and that this distortion produced in the lower temperature measurements represents a straining of the

crystal during thermal contraction. If this is so, then the disc shaped crystal, which had a thickness of only 0.24 mms, would be expected to show a greater degree of distortion in the torque curve than the more substantial ellipsoid. This was observed for all three disc shaped specimens (terbium C axis, terbium basal plane, and dysprosium basal plane).

The result of this deviation from the sinusoidal is that the computer analysis for the 6ϕ component produced a somewhat lower value for $\mathcal{K}_4$ than would be obtained by consideration of the overall amplitude of the torque curve. Since it became apparent when the effect on the torque curve of the specimen mounting was being investigated that the more the specimen was strained the greater would be the overall amplitude of the distorted torque curve, it is better to use the result of the 6ϕ analysis for the $\mathcal{K}_4$ value, rather than the torque curve amplitude.

The rotational hysteresis is also strain dependent, and if this hysteresis is purely a domain property the presence of strain, which will impede the movement of domain walls, can be expected to affect the hysteresis. Another possible effect of large strains, in producing dislocations in the crystal lattice, will be to cause local discontinuities in the anisotropy energy surface. Since there will be an angular distribution of the individual spins about the mean magnetisation direction due to thermal perturbations, and this spread might cover many dislocation produced anomalies in the energy surface, rotation of the applied field might produce a differently shaped distribution for one direction of rotation than for the other. Such a mechanism could produce rotational

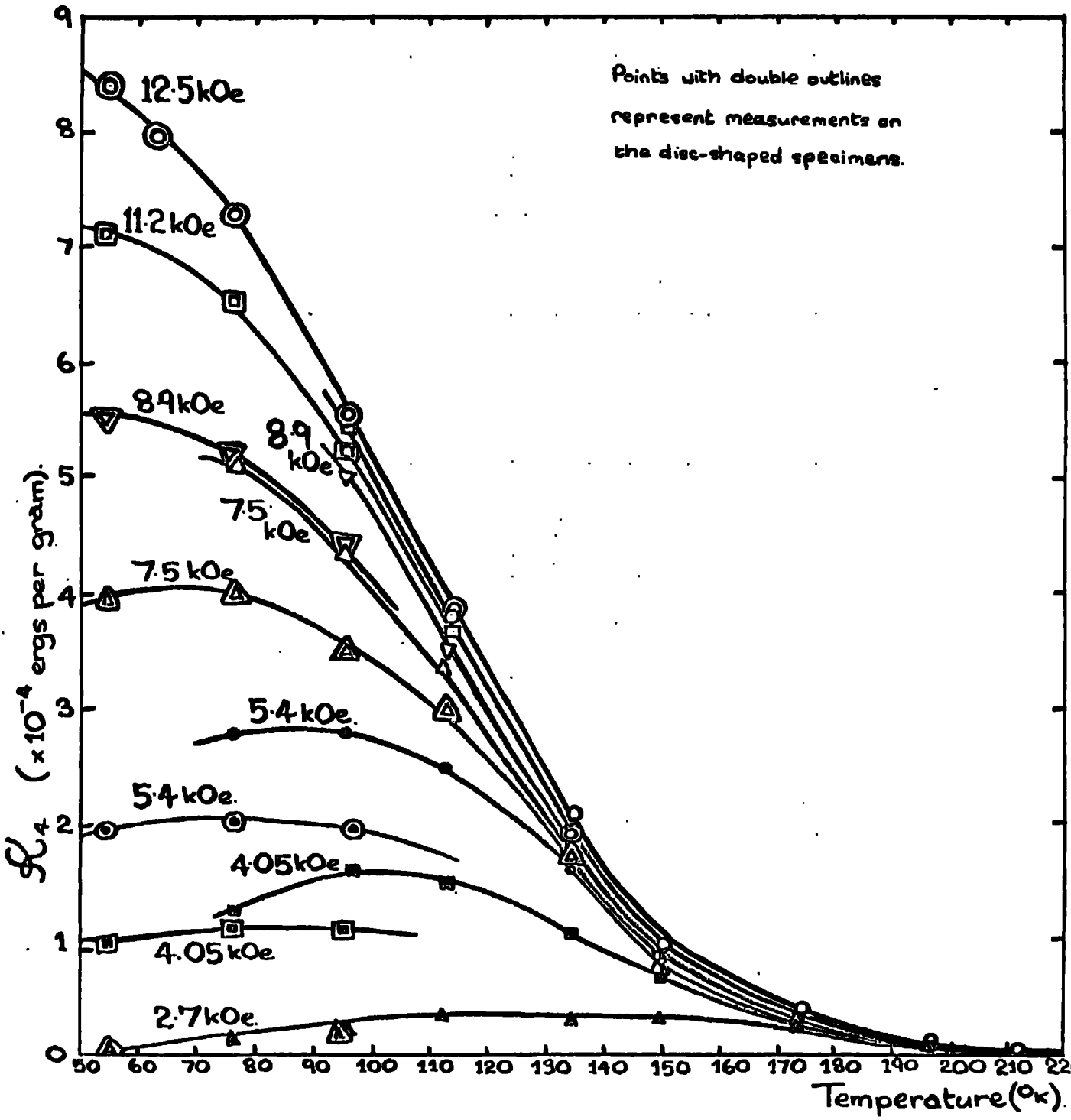

Fig. 8.11 Temperature dependence of $\mathcal{K}_4$ for terbium at various values of the applied field strength.

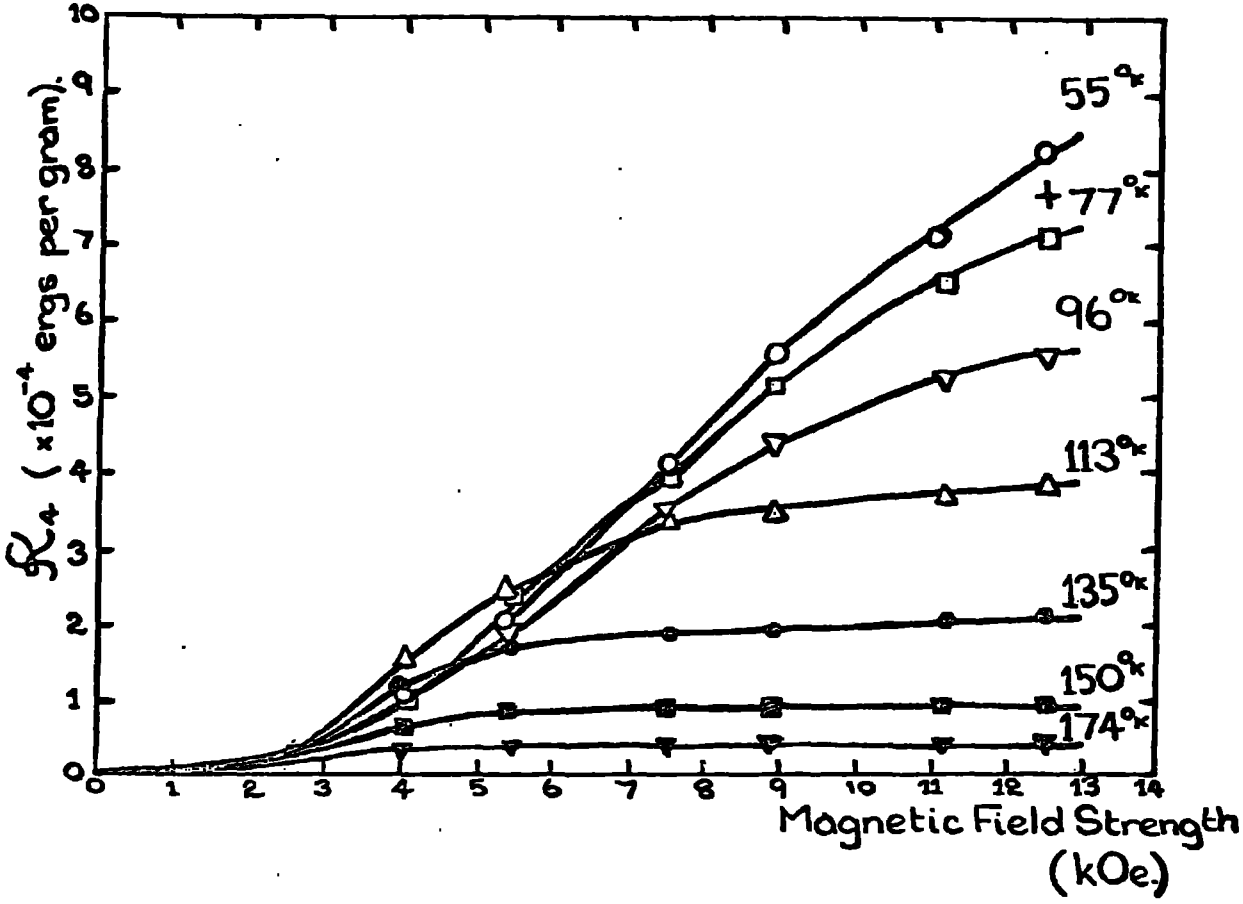

Fig. 8.12 Variation with applied magnetic field strength of $\mathcal{R}_4$ values for terbium, at various temperatures.

hysteresis at field strengths beyond the domain region.

X-ray orientation of the specimen showed that the easy direction lay in the b axis, in agreement with the magnetisation measurements of Hegland, Legvold and Spedding (17), and corresponding to a positive value for $\mathcal{K}_4$. Variation of $\mathcal{K}_4$ with temperature at various values of the applied field is shown in Figure 8.11. Isothermal variation of $\mathcal{K}_4$ with applied field strength is shown in Figure 8.12. From this it can be seen that at temperatures below 100^{ok} saturation of the $\mathcal{K}_4$ value has not been reached at 12.5kOe, although the magnetisation saturates at 3kOe. Generally, the value of $\mathcal{K}_4$ increases with decreasing temperature. However, at low field strengths the anisotropy constant appears to reach a maximum and then decrease as the temperature is further decreased. At this point rotational hysteresis is large, and there is some deviation from a purely sinusoidal curve. The latter phenomenon is not the reason for the decrease in $\mathcal{K}_4$ with decreasing temperature: the decrease is observed whether the value for $\mathcal{K}_4$ is derived by computer analysis or from the torque curve amplitude.

The distortion of the torque curve increases with increasing strength of the applied field, which may indicate strains produced by magnetostrictive effects. At field strengths low enough for the existence of domains, the torque curves become sinusoidal. The difference between the computer analysis value for $\mathcal{K}_4$ and that obtained from the torque curve amplitude is nowhere more than 10%, while the anisotropy constants obtained from the ellipsoidal and disc-shaped specimens differ by more than this, particularly at low field strengths. Since the field in the disc-shaped specimen will be less homogeneous than that in the ellipsoid,

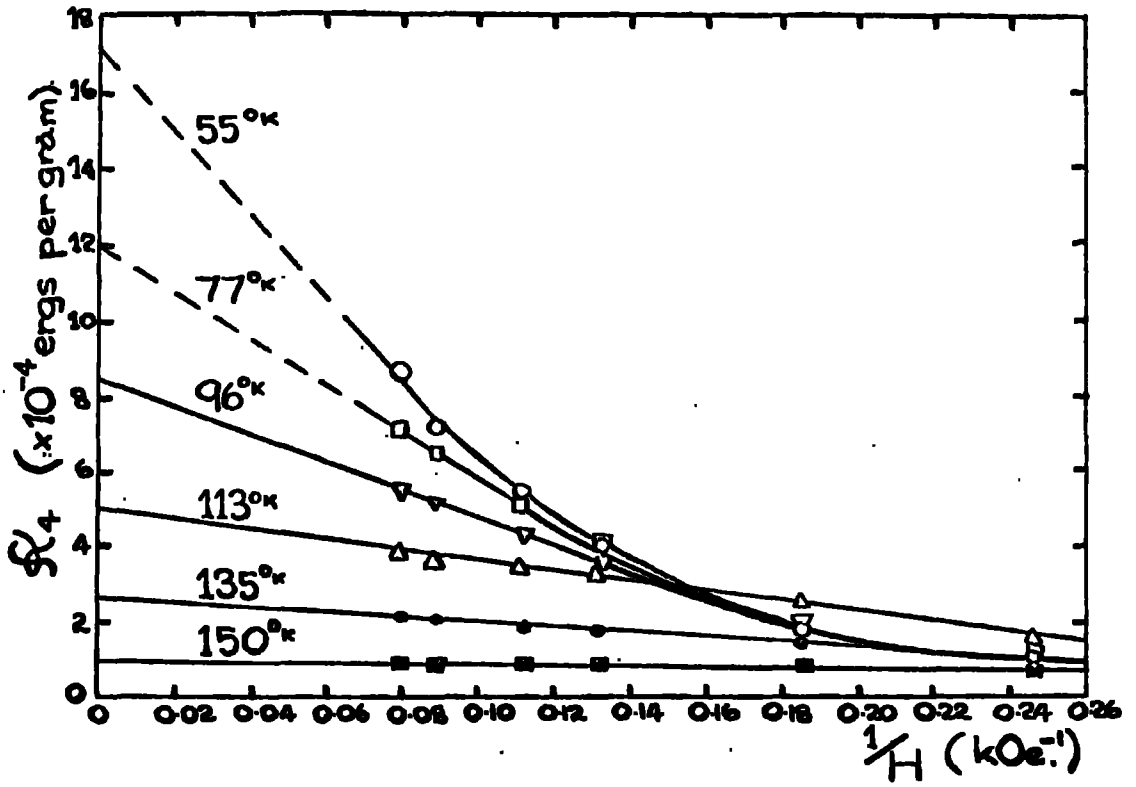

Fig. 8.13 Plot of $\mathcal{K}_4$ versus $1/H$ for terbium.

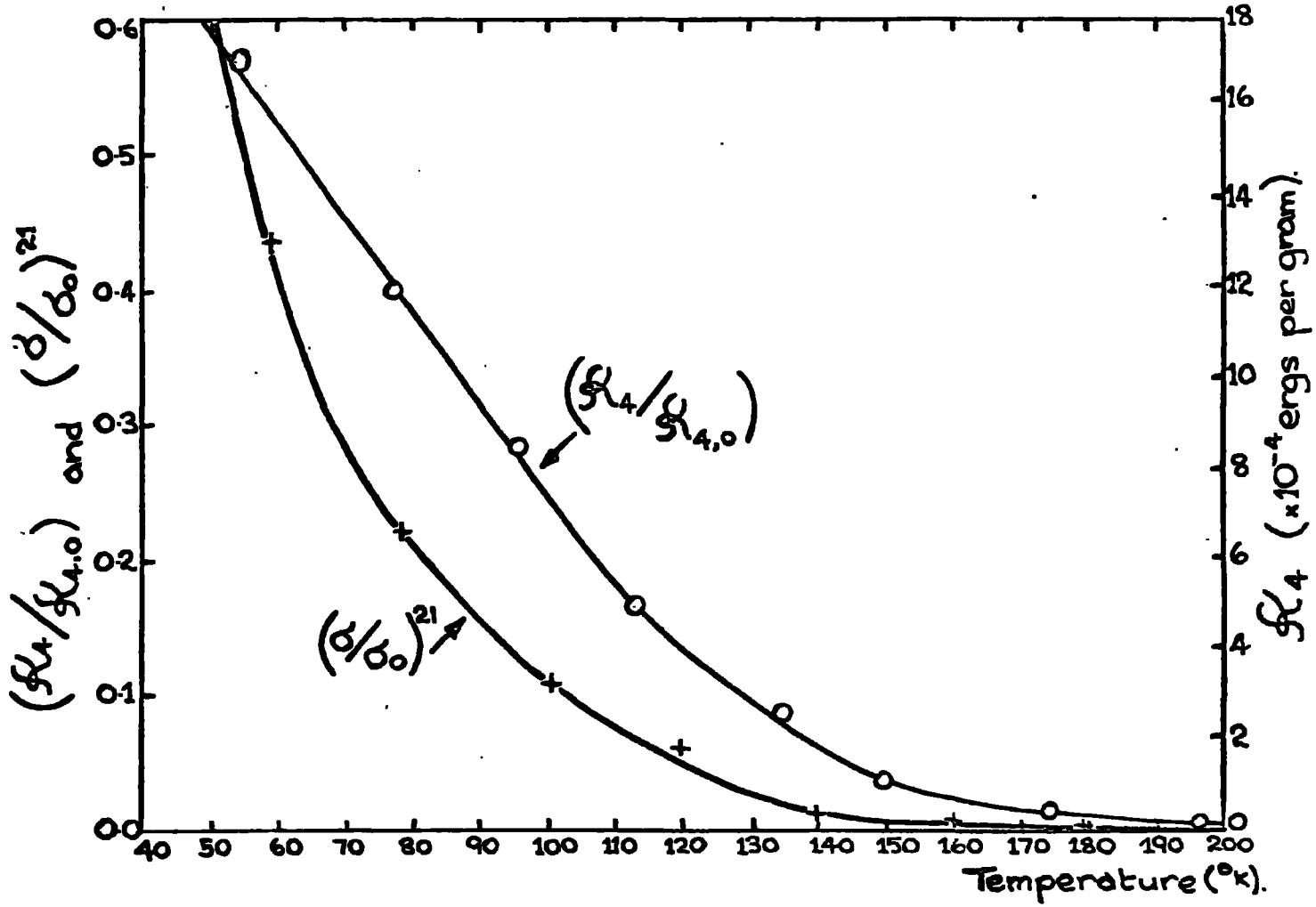

Fig. 8.14 Temperature dependence of anisotropy constant $\mathcal{K}_4$ for terbium, and comparison with the variation of $\{\sigma/\sigma_0\}^{21}$. Assumed value for $\mathcal{K}_4$ at 0°K is 3×10^5 ergs/gram.

the effective mass of the disc will be less than the true mass and will lead to a measured $\mathcal{K}_4$ value lower than is actually the case. The disc-shaped specimen was also a poor crystal, there being a spread in the grain orientation of some 7° and this again will reduce the measured value of $\mathcal{K}_4$.

The obtained $\mathcal{K}_4$ values are plotted against the reciprocal of applied field strength in Figure 8.13, in order to obtain the infinite field value of the anisotropy constant. The extrapolation was very inprecise for the 55^{ok} and 77^{ok} measurements, since at the maximum available field strength saturation was only beginning at these temperatures. The $\mathcal{K}_4$ values at infinite field so obtained are plotted against temperature in Figure 8.14. In order to compare this temperature variation with the predictions of Zener's theory it is necessary to know the saturation value of $\mathcal{K}_4$ at 0^{ok}, whereas the lowest temperature available for experimental measurements was 55^{ok}. Hence extrapolation to 0^{ok} cannot be done with confidence. The value so obtained, 3×10^5 ergs per gram, is likely to be a maximum value, since if the variation of $\mathcal{K}_4$ follows that of the anisotropy in gadolinium as found by Graham (74), there will be a tendency to saturation at low temperatures.

Figure 8.14 compares the temperature variations of $\{\mathcal{K}_4/\mathcal{K}_{4.0}\}$ and $(\sigma/\sigma_0)^{21}$ using values for the magnetisation obtained by Hegland et al. The agreement is poor, and cannot be improved by another choice of the $\mathcal{K}_{4.0}$ value. Callen and Callen (52) have shown that Zener's theory should hold for temperatures where

$$1 - I/I_{sat} < 0.7 \qquad 8.5$$

This would be true for temperatures less than 174^{ok} but in this case it appears that the temperature dependence is somewhat gentler than Zener's theory predicts. Zener's theory makes no allowance for changes of lattice parameters with either temperature or magnetic field strength, and in view of the large magnetostriction exhibited by terbium (83) some modification may well be required.

The basal plane anisotropy for terbium is some 400 times larger than that for gadolinium, a ratio which appears to be true in order of magnitude for the $\mathcal{K}_1$ value also.

8.5 Dysprosium: C axis Anisotropy

The Néel temperature for the paramagnetic to antiferromagnetic transition in dysprosium is 178.5^{ok}, and the antiferromagnetic to ferromagnetic transition occurs at 85^{ok}. Furthermore Flippen (81) gives the critical field near the Néel point as 12 kOe. Thus although measurements of anisotropy were not possible in the ferromagnetic region because of the low field strengths available and the torque limit of the magnetometer, it was possible to make anisotropy measurements in the anti-ferromagnetic region, as well as paramagnetic measurements.

For the specimen in the paramagnetic region the torque curves obtained were of the $\sin 2\theta$ type, as was observed for terbium. Throughout this paramagnetic region the anisotropy constant $\mathcal{K}_1$ determined for dysprosium is very much smaller than the constant for terbium. The room temperature value for dysprosium is 4.6×10^3 ergs per gram, while terbium gives a $\mathcal{K}_1$ value of 4.8×10^4 ergs per gram at fields of 12.5 kOe. In the ferromagnetic region, below 85^{ok}, the torque curves obtained are also of the $\sin 2\theta$ type, although here the

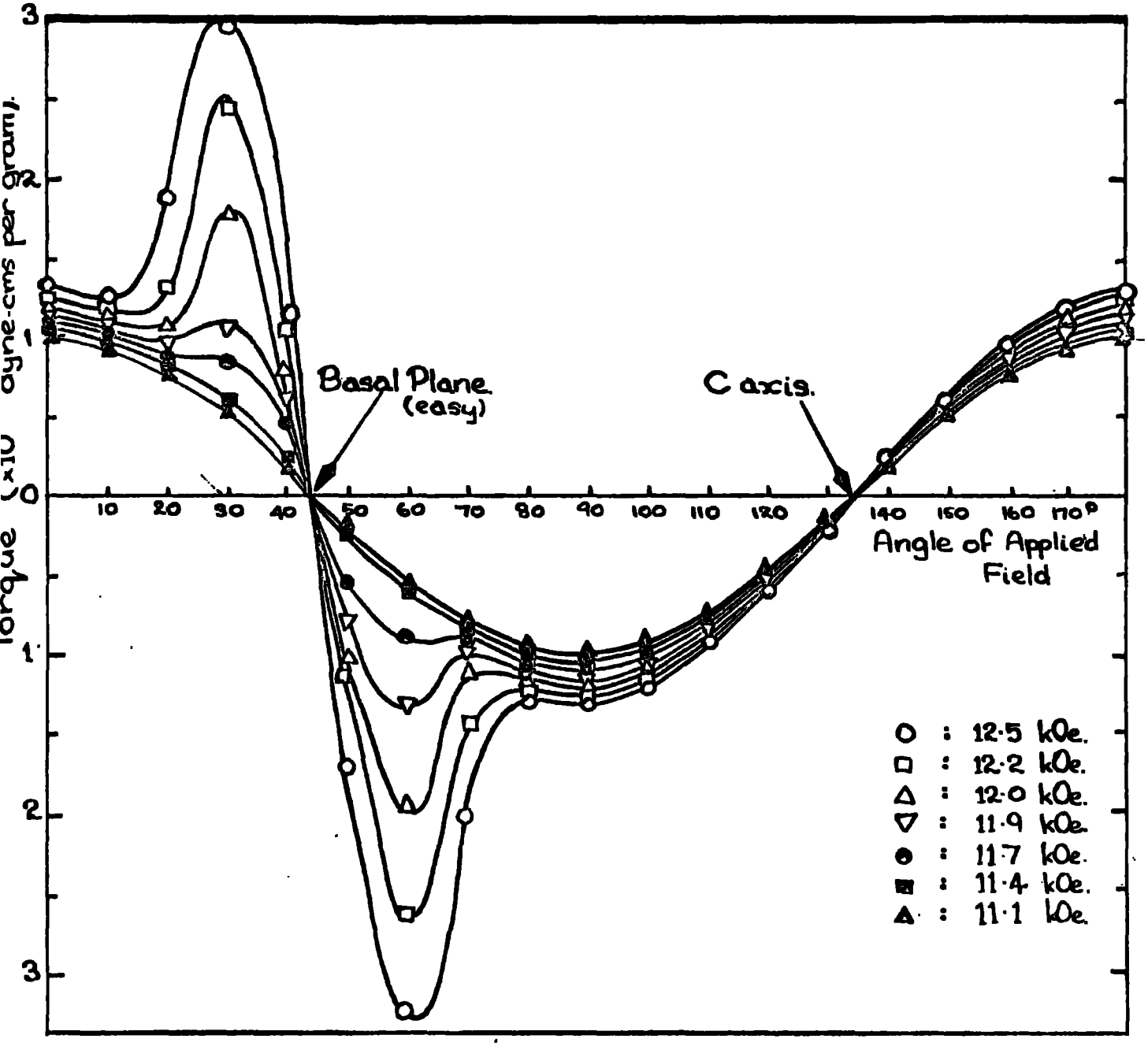

Fig. 8.15 Torque curves obtained for the dysprosium c-axis specimen at 158°K in various applied field strengths, showing the development of ferromagnetism as the applied field direction crosses the basal plane.

measurements could only be made at field strengths below 3kOe because of the large torques produced. X-ray orientation of the sample showed that the easy direction lay in the basal plane, in agreement with the neutron diffraction studies of Koehler-et al (82).

For the antiferromagnetic region, 85^{ok} to 178.5^{ok}, the shape of the torque curve obtained depended on the strength of the applied magnetic field. A typical set of curves is shown in Figure 8.15 for a temperature of 158^{ok} and a range of applied field strengths from 11.1 kOe to 12.5 kOe. When the applied field strength is below a certain critical value the torque curve is of a simple $\sin 2\theta$ type, similar to the curves obtained in the paramagnetic region. When the field strength is further increased large values of the torque begin to develop on both sides of the basal plane direction, the angular extent of these two torque maxima increasing as the applied field is increased. The cause of these large torque values is, of course, the onset of ferromagnetism, occurring whenever the component of the applied field in the basal plane exceeds the critical field. Since the basal plane is the easy direction for magnetisation the torque occurring when the applied field exceeds the critical field and lies in the basal plane will be zero. As the field is rotated out of the basal plane direction the torques produced correspond to part of that ferromagnetic torque curve appropriate to temperature and applied field strength, that is to say a $\sin 2\theta$ curve of large torque amplitude. As the field is rotated further from the basal plane direction the component of the field in the basal plane will drop below the critical value, and the system becomes antiferromagnetic once more, the torques decreasing at this point to the

value appropriate to the antiferromagnetic torque curve. It is to be noticed that there is no very rapid change from high to low torque values at this point, as might be expected for a sudden transition from ferromagnetism to antiferromagnetism. It is possible that field inhomogeneities in the crystal cause the transition to take place in different volumes of the crystal over a range of field strengths.

Since the component of the applied field, H, in the basal plane is $H\cos\alpha$ if α is the angle between the basal plane and the applied field direction, ferromagnetism will exist while

$$H\cos\alpha > H_c \qquad 8.6$$

where H_c is the value of the critical field at the temperature of the specimen. Thus the ferromagnetism will be observed to disappear, i.e. the torque curve will revert to the small amplitude $\sin 2\theta$ curve appropriate to antiferromagnetism when the applied field is at an angle α to the basal plane given by

$$\alpha = \cos^{-1}(H_c/H) \qquad 8.7$$

Thus the critical field value can be obtained from the set of torque curves by determining the maximum value of the applied magnetic field strength which will produce an undistorted $\sin 2\theta$ curve; it is to be expected also that the cosine of the maximum angle of the applied field to the basal plane direction at which ferromagnetism still exists will vary as the ratio of the critical field to the applied field. In general this is true, although the angle α tends to be a few degrees larger than predicted by equation 8. 7. In Figure 8.15 it can be seen that the critical field is approximately 11.5 kOe at 158^{ok}.

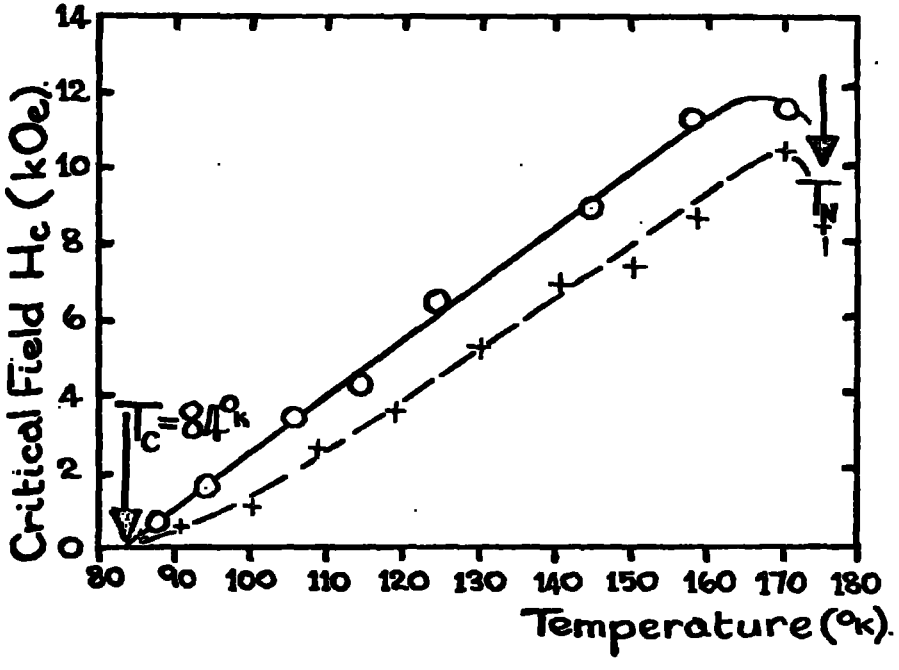

Fig. 8.16 Temperature dependence of the basal plane critical field for dysprosium. Crosses indicate values given by Flippen (81).

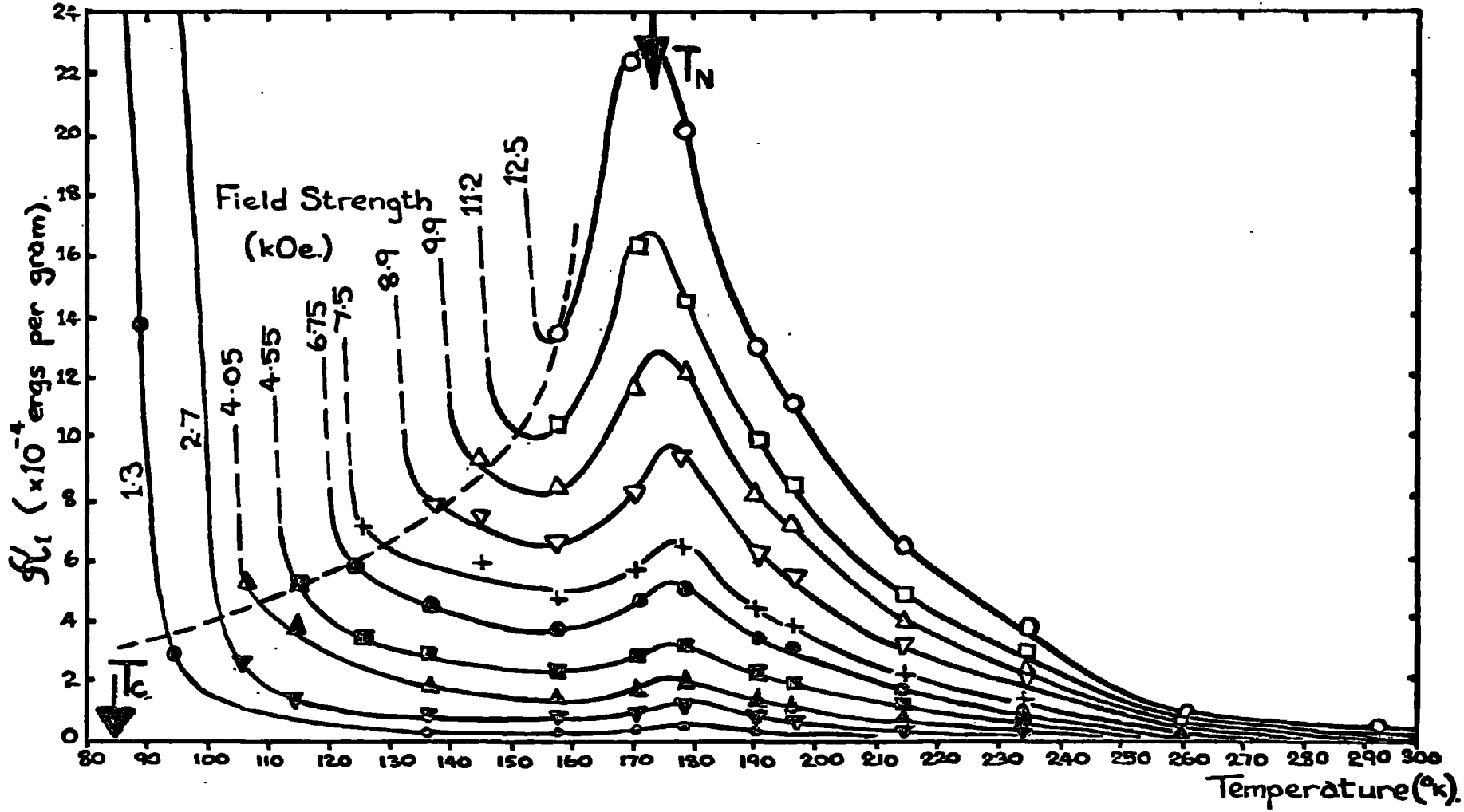

Fig. 8.17 Temperature dependence of χ_1 for dysprosium at various applied field strengths, in the paramagnetic and antiferromagnetic regions.

From these results the value of the critical field throughout the antiferromagnetic temperature range could be determined. The values obtained increase from zero at an indicated Curie temperature of 84^{ok}, to 11.8 kOe at approximately 167^{ok}, as shown in Figure 8.16. This agrees reasonably well with the values given by Flippen (81).

The torque curves obtained for the dysprosium C axis crystal indicated no detectable rotational hysteresis, as was the case for the ellipsoidal terbium C axis specimen. Rotational hysteresis was only troublesome in the basal plane measurements. In the case of the disc-shaped terbium C axis specimen, rotational hysteresis was present, but it has been pointed out previously that the hysteresis is to some extent a function of mechanical strain in the crystal.

In the antiferromagnetic region, where the applied field was greater than the critical field the K_1 values were obtained from the amplitude of the antiferromagnetic section of the torque curve, since the curves were accurately sinusoidal in this region. Figure 8.17 shows the variation of the K_1 values with temperature for various applied field strengths. In the paramagnetic region the anisotropy constant increases with decreasing temperature to reach a maximum at the Néel point. In the antiferromagnetic region K_1 decreases with decreasing temperature until the magnitude of the applied magnetic field exceeds the critical field value at that temperature, whereupon the system is driven ferromagnetic and very large torques are produced. These large torque values exist only while the applied field is at a relatively small angle to the basal plane, and hence it is not possible to estimate K_1 in the ferromagnetic region. For applied field strengths well above the

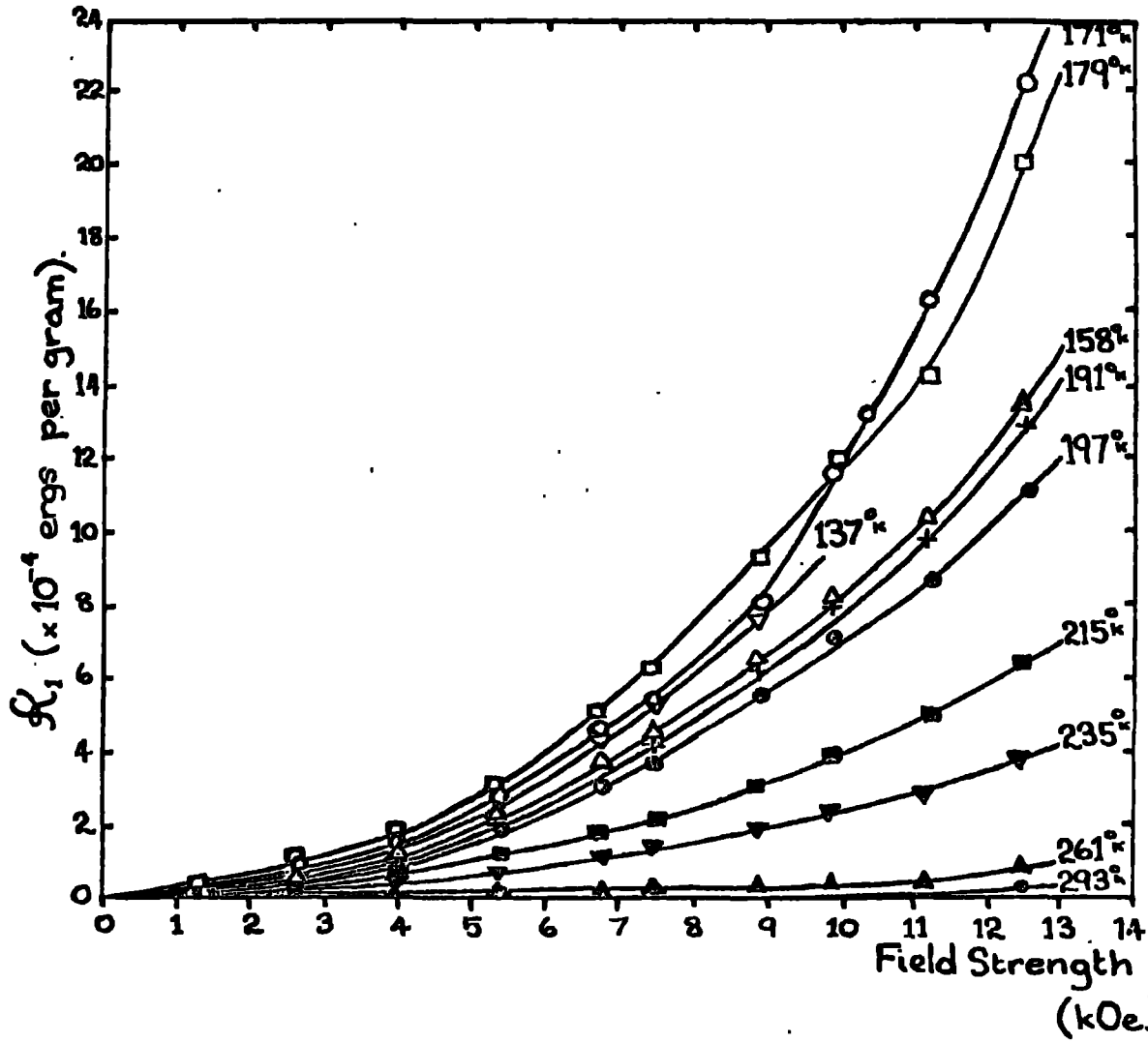

Fig. 8.18 Variation of $\mathcal{K}_1$ for dysprosium with applied magnetic field strength, at various temperatures.

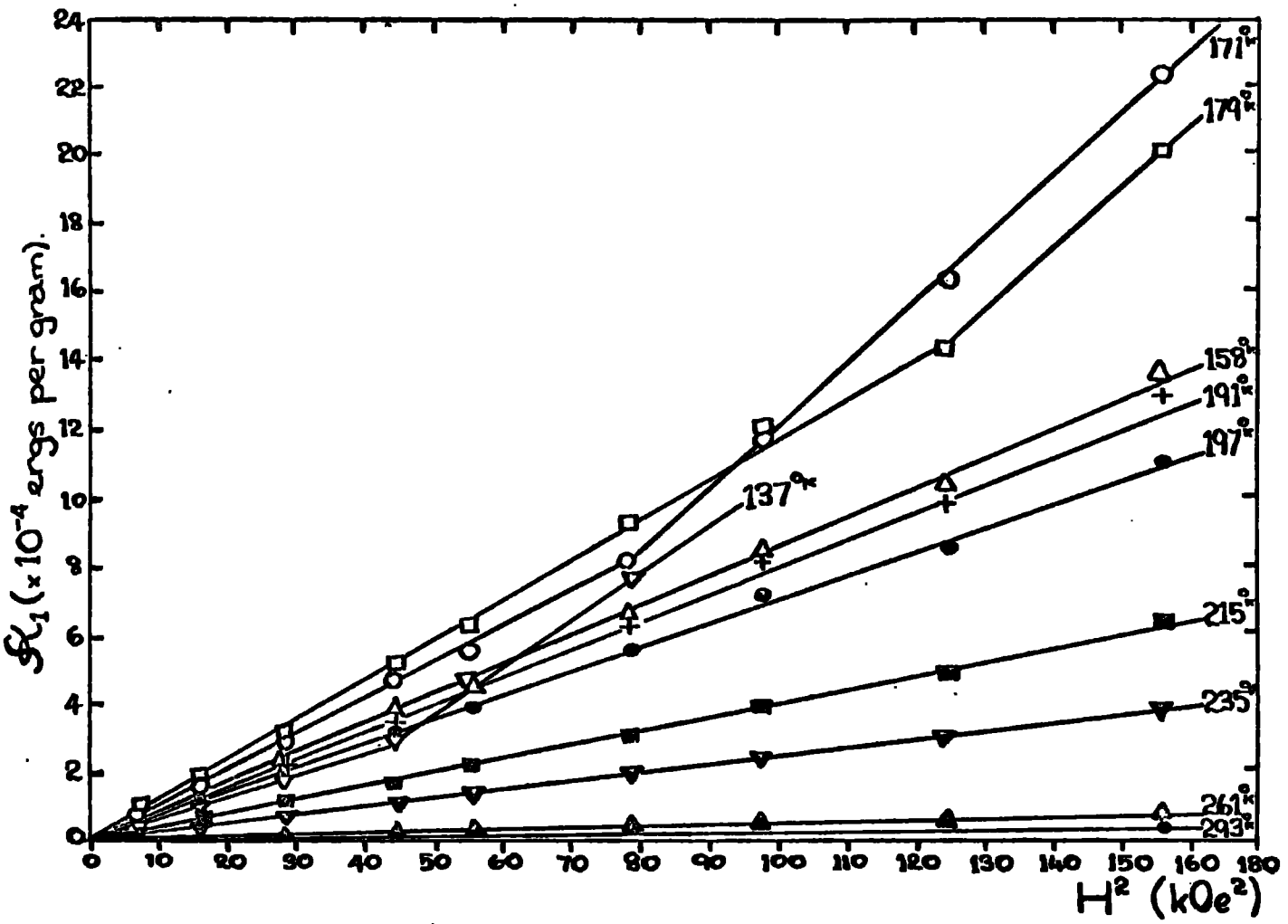

Fig. 8.19 Plot of $\mathcal{K}_1$ versus H^2 for dysprosium above the Néel temperature.

critical field the torques obtained are too large to be measurable with the magnetometer.

The position of the maxima in the $\mathcal{K}_1$ versus temperature curves at the Néel point was field dependent, moving to lower temperatures as the field strength is increased. This field dependence of the Néel point has been found to exist in all the rare earth metals which exhibit antiferromagnetism (17, 23, 24, 28, 30). Extrapolation of the positions of the maxima to zero applied field agrees well with a Néel temperature of 178.5^{ok} (23).

The $\mathcal{K}_1$ values are plotted against applied field strength for various temperatures in Figure 8.18 and against the square of the field strength in Figure 8.19. It can be seen that in general there is a linear dependence of $\mathcal{K}_1$ on H^2. This is true for both the paramagnetic and the antiferromagnetic region, indicating that in the antiferromagnetic region, where a spiral spin structure exists, the effect of an applied field is to produce a magnetisation which is directly proportional to the field, as in the more normal two-sublattice type of antiferromagnetism. For the two temperatures close to the Néel point, 171^{ok} and 179^{ok}, there is an abrupt change of slope at higher fields. At these temperatures $\mathcal{K}_1$ is changing rapidly with temperature, and the gradient change may be due to a small temperature change during the measurements, rather than a field induced change in the magnetic ordering. The gradient change for the 137^{ok} plot may well indicate a change in the ordering at field strengths below the critical field: certainly the amplitudes of the antiferromagnetic torque curves are increasing rapidly at values of the applied field just below the

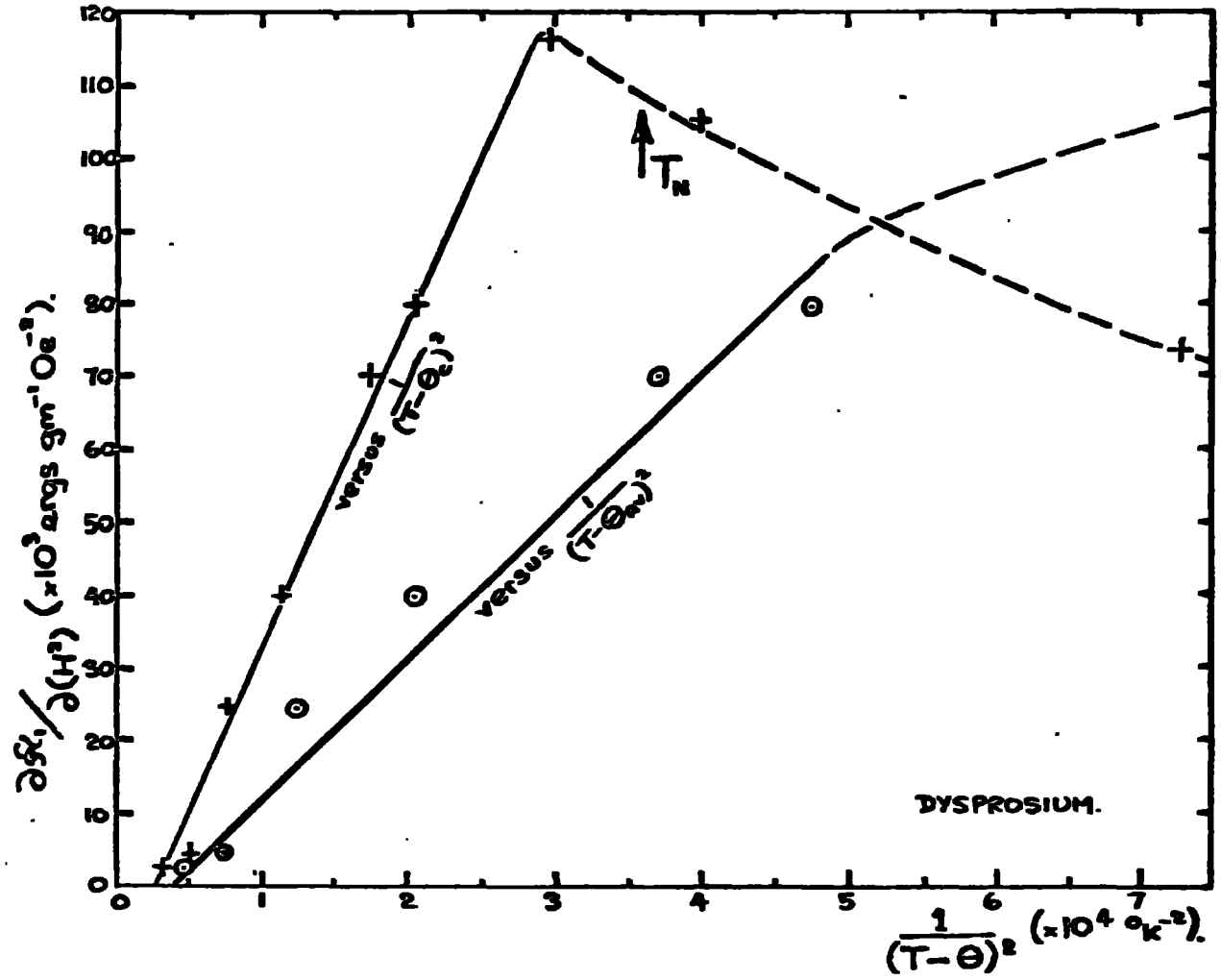

Fig. 8.20 Plot of $\frac{\partial \mathcal{L}_1}{\partial (H^2)}$ versus $\frac{1}{(T-\Theta)^2}$ for dysprosium in the paramagnetic region.

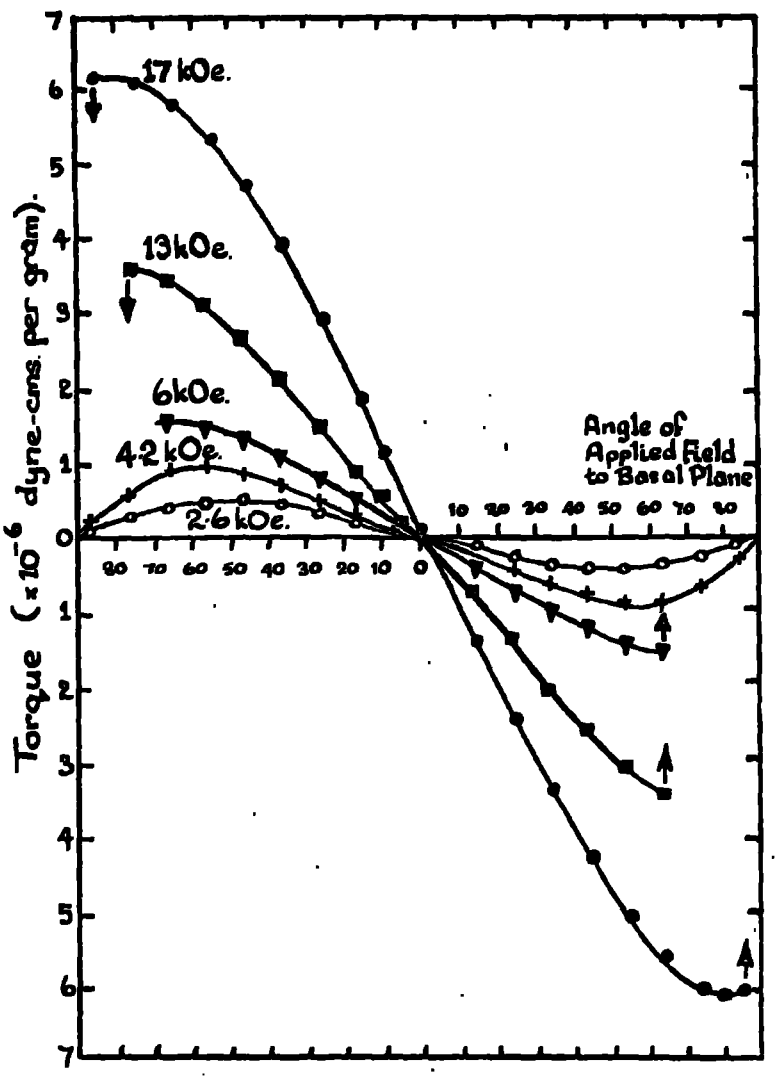

Fig. 8.21 Torque curves obtained for the dysprosium c-axis specimen in the ferromagnetic state, using the simple torsion-wire balance. Curves were all recorded at 77°K.

critical field. As for terbium the temperature dependence of $\frac{\partial \mathcal{L}_1}{\partial (H^2)}$ was considered from the viewpoint of a $\frac{1}{(T-\theta)^2}$ dependence. The plot against $\frac{1}{(T-\theta_{av})^2}$, $\theta_{av} = 145^{ok}$ (37), is shown in Figure 8.20, but there is a marked departure from linearity some 15^{ok} above the Néel point. The function was plotted against $\frac{1}{(T-\theta_c)^2}$, $\theta_c = 121^{ok}$, and this is seen to be not only more linear than the previous plot, but there is also no deviation from linearity until the temperature falls below the Néel point.

In order to investigate the field dependence of the ferromagnetic torque curves for dysprosium, a simple torsion wire balance was used, as described for terbium. The torque curves so obtained at 77^{ok} are shown in Figure 8.21. The mechanism for this change from a $\sin 2\theta$ type curve to a $\sin\theta$ form has already been discussed for terbium. It can be seen that for small values of the applied magnetic field the curve is a symmetrical $\sin 2\theta$ function, but that as the field is increased the curve becomes more nearly a $\sin\theta$ expression with a discontinuity at the C axis. For the 6kOe torque curves, and at higher fields, the system became unstable near the C axis, the specimen suddenly twisting through an angle of nearly 180° to the opposite maximum torque position as the angle of the applied field to the C axis decreased. In the field region where this instability existed, the point of instability grew closer to the C axis as the field was increased. The curve for 17 kOe had a definite maximum in the torque values just before the system became unstable, and it is to be expected that as the field is further increased the curve will approach a $\sin 2\theta$ function once more, as the spins are pulled

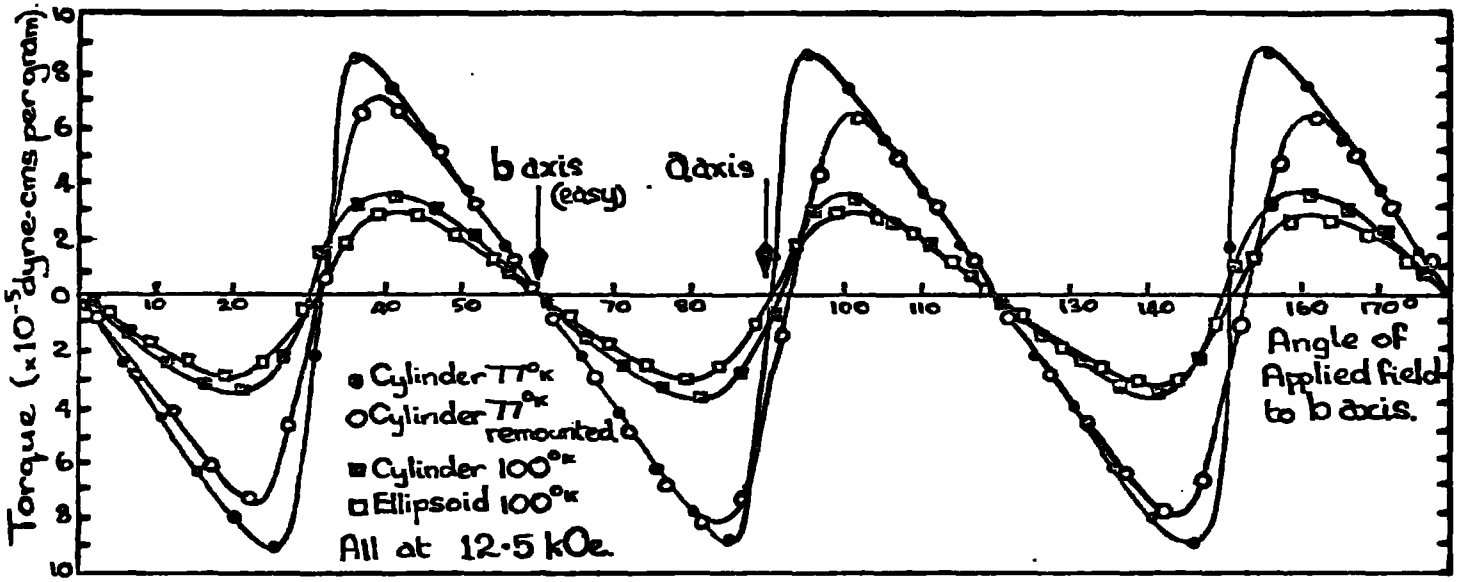

Fig. 8.22 Typical torque curves for the cylindrical and ellipsoidal basal plane specimens of dysprosium, showing the asymmetry.

further from the basal plane and are able to sample the crystal anisotropy. The magnitudes of the torques developed were very similar to those observed for terbium: the maximum torque at 17kOe was 6 x 10^7 dyne cms per gram.

8.6 Dysprosium: Basal Plane Anisotropy

The torque curves produced by the ellipsoidal dysprosium specimen with the basal plane in the plane of the ellipsoid were measured for applied field strengths up to 12.5^{ok}, and for temperatures above 55^{ok}. No basal plane component of the anisotropy was observable above 160^{ok}, and in all cases the observed basal contribution was hexagonal. At temperatures below 100^{ok} the torques became very large, and the torque curves were asymmetric, the maxima of the $\sin 6\phi$ curve moving away from the easy direction, which X-ray orientation of the crystal showed to be the b axis.

Because at the lowest temperatures the high field torques were beyond the range of the magnetometer, a second disc-shaped specimen of approximately half the mass of the ellipsoidal specimen was used. This specimen had a hollow on the circumference, and some shape anisotropy was to be expected. The asymmetry in the torque curves shown by this disc shaped specimen was greater than that shown by the ellipsoidal specimen, and was very dependent on the strain produced in the crystal by the mounting, as discussed for terbium. Typical torque curves are given for both the dysprosium specimens in Figure 8.22.

Changes of sign in the anisotropy constant K_4 were discovered for high field measurements at temperatures above 135^{ok}, and for low

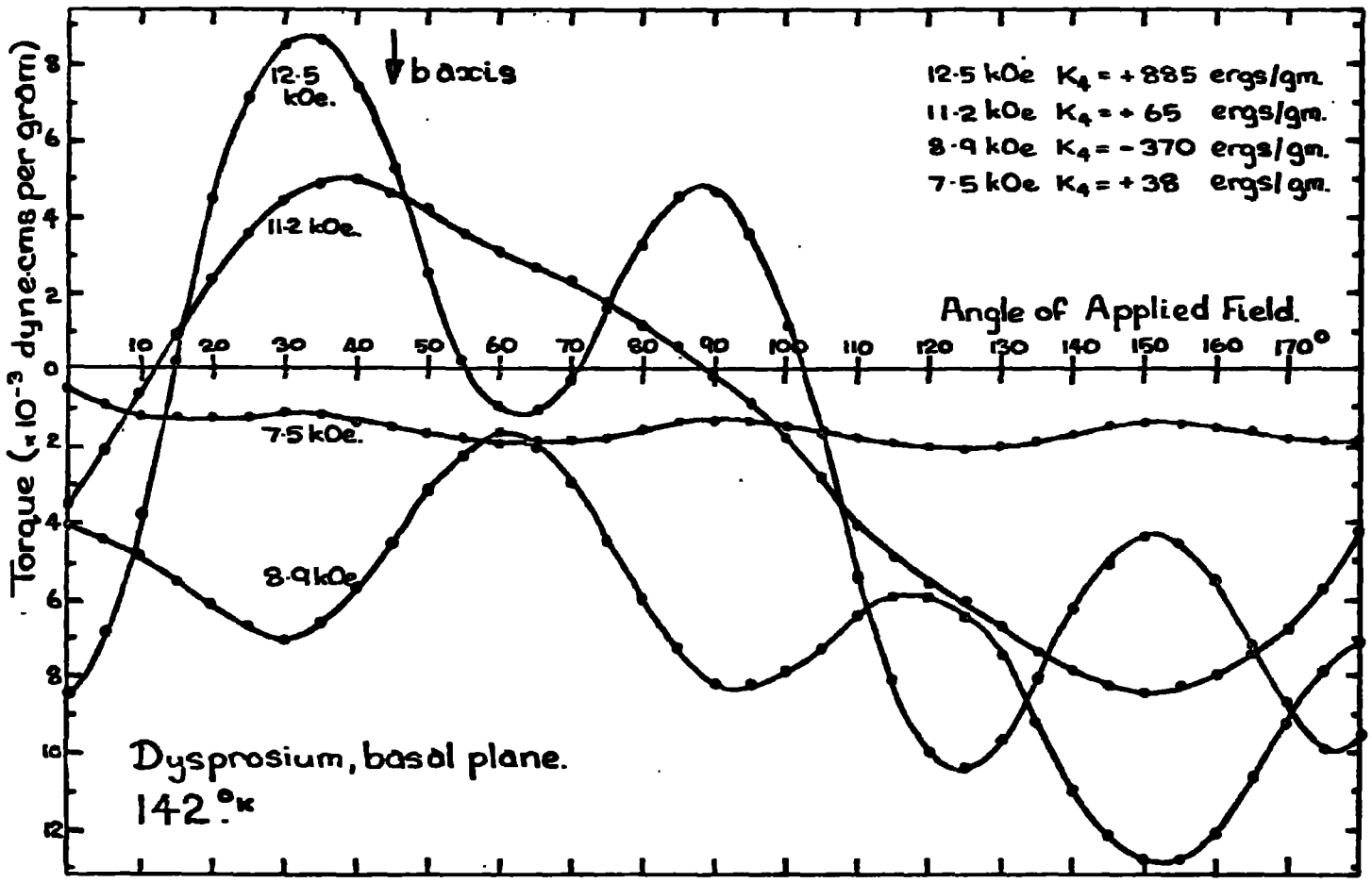

Fig. 8.23 Torque curves for the basal plane dysprosium specimen at 142°K for various applied field strengths, showing the changes in sign of K_4.

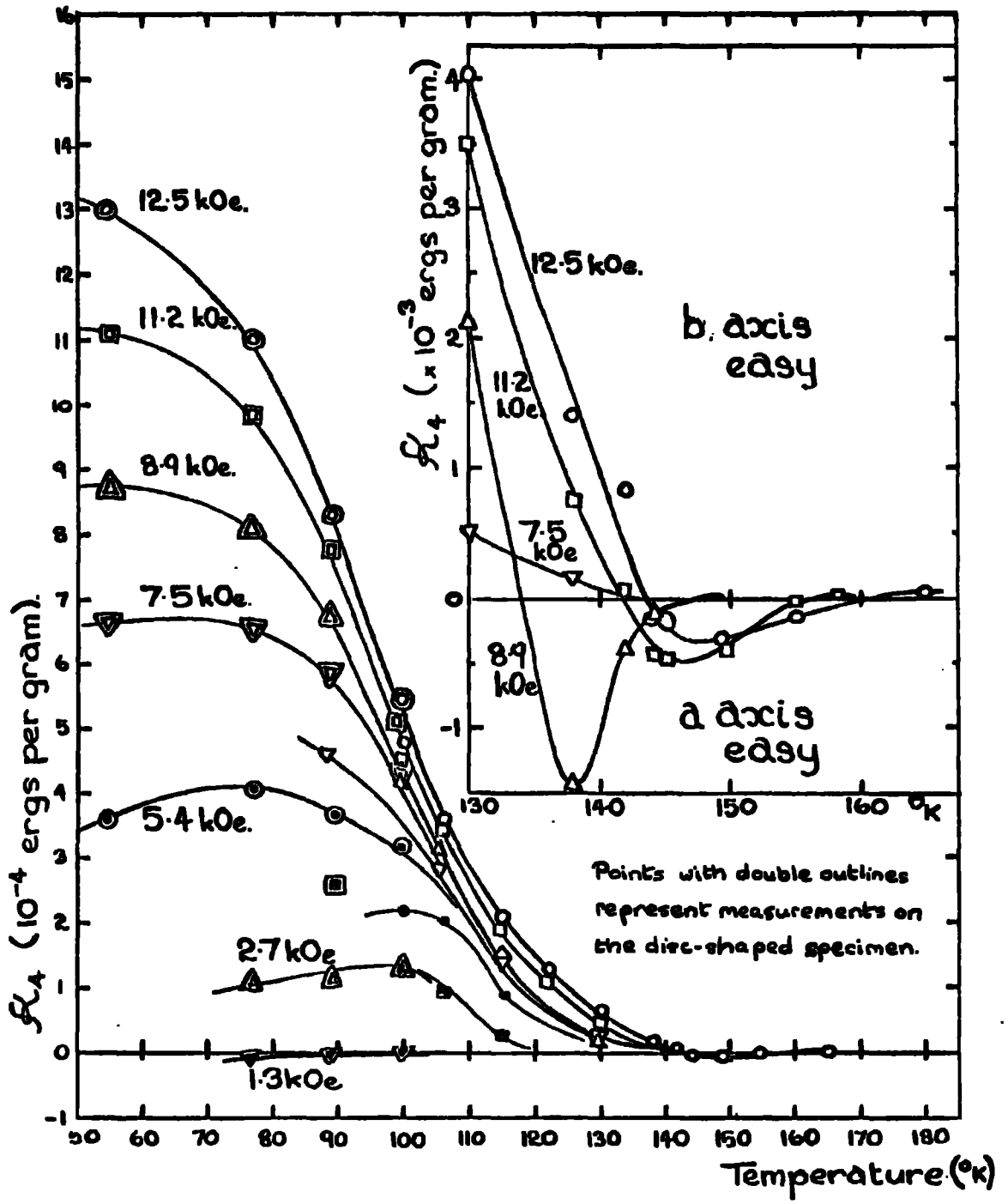

Fig. 8.24 Temperature dependence of $\mathcal{K}_4$ for dysprosium, at various applied field strengths. Inset shows the changes in easy direction which occurred at the higher temperatures.

field measurements below 100^{ok}. The higher temperature reversals were very field dependent, and occurred at field strengths just above the critical value. At applied field strengths below the critical field no hexagonal component was observed, although a $\sin 2\phi$ component with a large degree of rotational hysteresis was present. At these temperatures, as the field is decreased, the value of K_4 is at first positive (b axis easy) and then goes through zero to become negative (a axis easy). At this reversal the observable anisotropy is small, and, as the field decreases further, quickly vanishes, the system becoming antiferromagnetic as the critical field value is reached. In two cases, the measurements for 149^{ok} and 142^{ok} at applied fields of 8.9 kOe and 7.5 kOe respectively, the torque curve was observed to undergo a second reversal, the b axis becoming easy once again, although the anisotropy was extremely small here. The set of torque curves for 142^{ok} is shown in Figure 8.23. The curve for 12.5 kOe corresponds to a positive value of K_4 whereas at 11.2 kOe there is very little hexagonal component compared with the $\sin 2\phi$ term, although analysis indicates the K_4 value is still positive. The curve for 8.9 kOe shows that K_4 is reversed in sign, the a axis being easy, while at 7.5 kOe the K_4 value is again positive, but small. For fields below 7.5 kOe, no hexagonal component was observable.

The value of the anisotropy constant K_4 is plotted as a function of temperature for various values of the applied field in Figure 8.24, the inset showing the reversals in K_4 which occurred at small values of the anisotropy constant. It can be seen that here again there is considerable discrepancy between the anisotropy constants

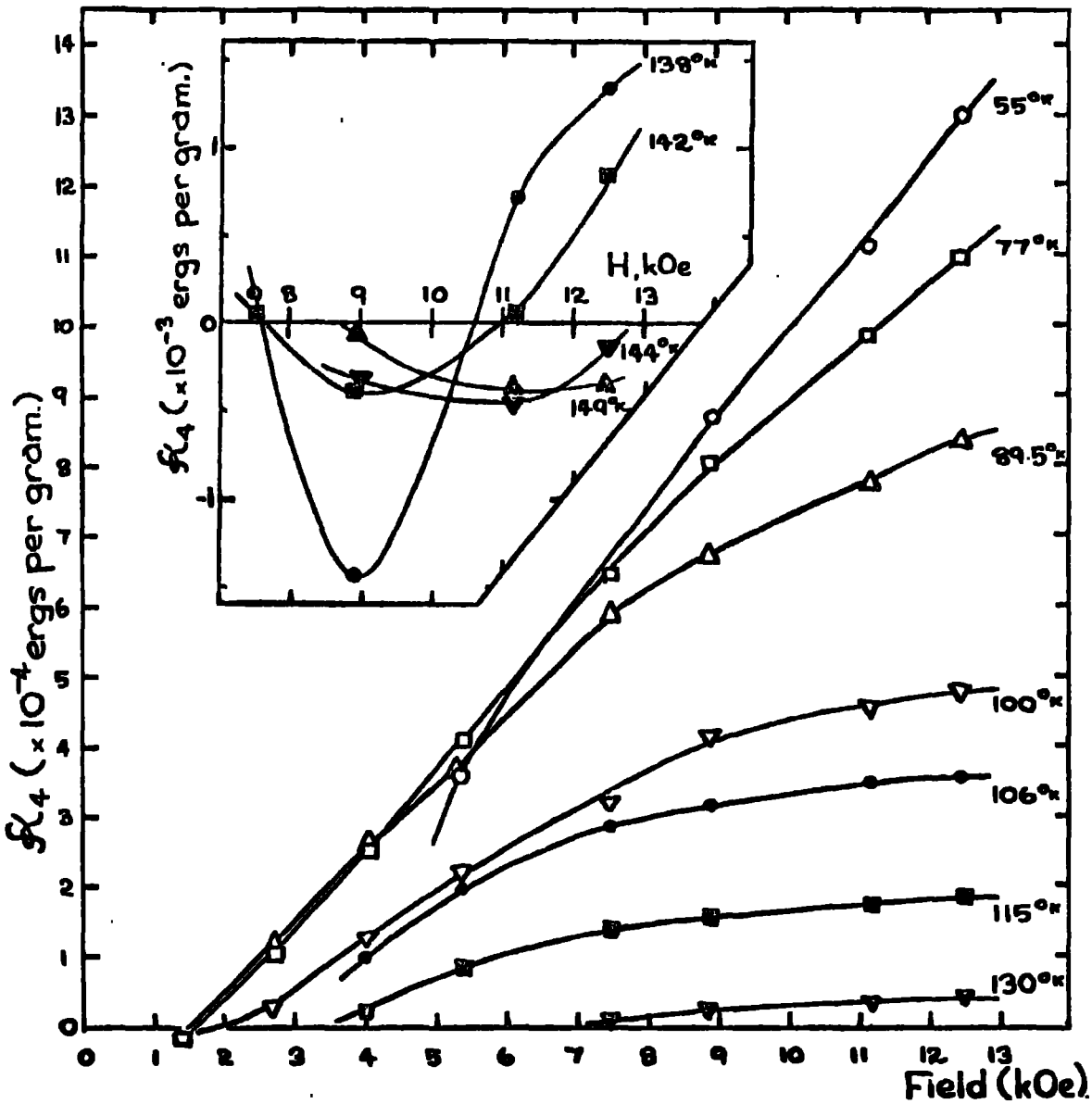

Fig. 8.25 Variation of $\mathcal{K}_4$ for dysprosium with applied field strength. Inset shows the easy axis changes which take place at higher temperatures.

obtained for the ellipsoidal and the disc-shaped specimens. Unlike the result for terbium, however, $\mathcal{K}_4$ here is larger for the disc-shaped specimen. The reason for this is not understood.

At the lower temperatures reversal occurs only at fields below approximately 1.5 kOe and does not appear to be very field dependent. As the field is increased from zero the easy direction is at first the a axis ($\mathcal{K}_4$ negative), changing to the b axis ($\mathcal{K}_4$ positive) as the field increases.

The field dependence of $\mathcal{K}_4$ is shown in Figure 8.25, the inset showing the changes in easy direction at the higher temperatures. It can be seen that the anisotropy constant is far from saturation at the lower temperatures.

A survey of the magnetisation measurements of Jew and Legvold (21) as tabled in their report, indicated that the easy direction (i.e. the axis showing maximum magnetisation) in the basal plane changes from the a axis to the b axis as a function of temperature and applied field strength. However, their results predict that for temperatures below 100^{ok} the easy direction should be the a axis for a large range of the applied field strength: for example, at 90^{ok} the change in easy direction from a axis to b axis does not take place until a field of 12 kOe is applied. An easy axis change from b to a with increasing field is also indicated at very low field strengths. Although the higher temperature $\mathcal{K}_4$ reversals observed here agree approximately with those predicted from the measurements of Jew and Legvold, there is no agreement at the lower temperatures. Both of the dysprosium single crystals showed an easy direction in the b axis for most of the range of field strengths used, and measurements on the two specimens gave agreement over

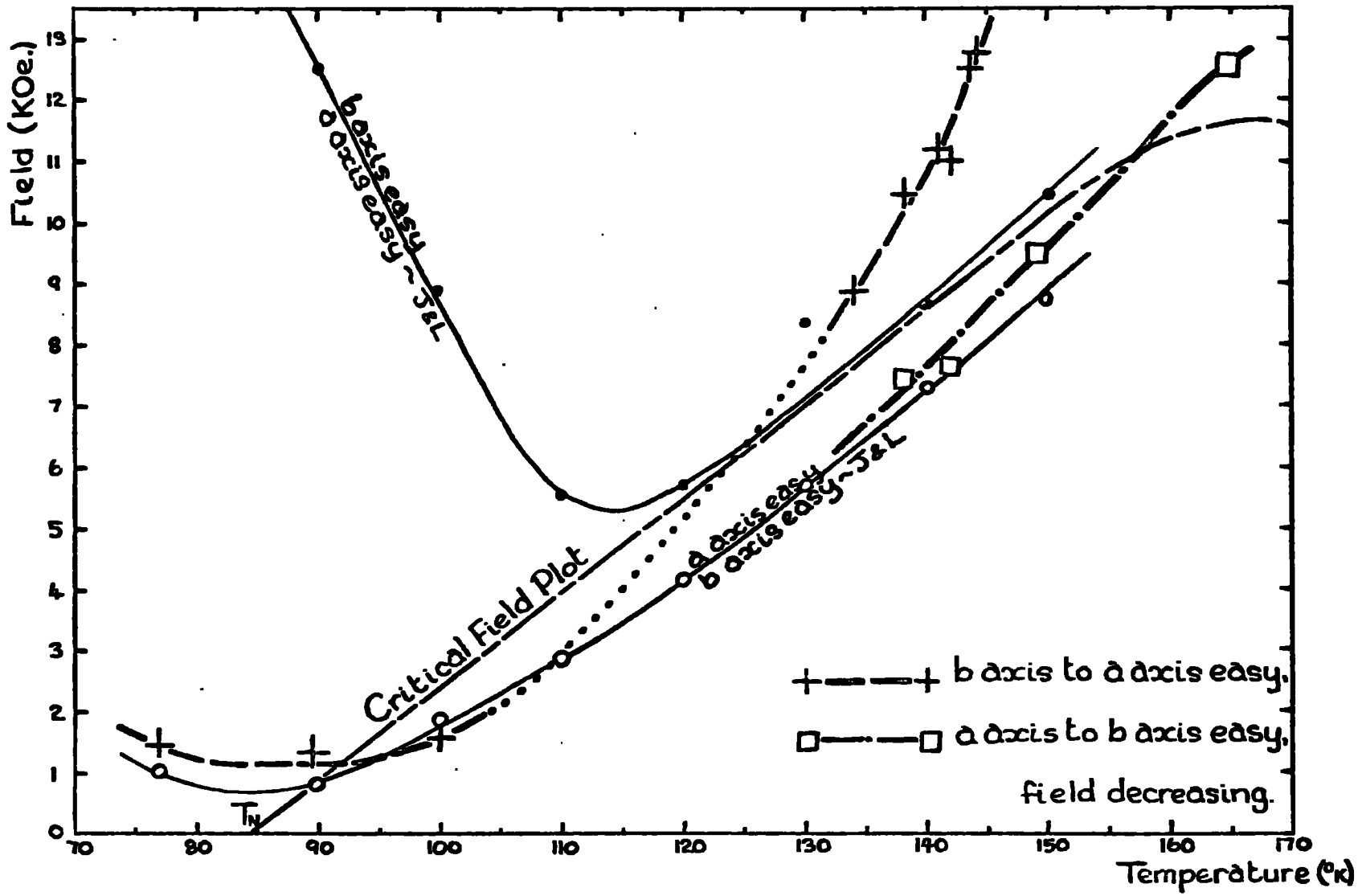

Fig. 8.26 Field and temperature dependence of the changes in easy direction which take place in the basal plane of dysprosium. Dots and open circles indicate the field and temperature values at the easy axis changeovers as determined from the magnetisation measurements of Jew and Legvold (21). Also shown is the temperature dependence of the critical field.

the position of the easy direction changes. These results indicate that a plot of the value of the applied field at the transition versus temperature is a steadily decreasing function of field with temperature, and not a function which passes through a minimum and then increases, as predicted on the basis of the measurements of Jew and Legvold. This comparison is made in Figure 8.26. It is perhaps of interest to note, however, that the temperature-field position of the knee on the K_4 versus field plot in Figure 8.25 lies close to the line of the low temperature, high field a axis easy to b axis easy transition found in Jew and Legvold's measurements. Thus this transition, although not found in the torque measurements, occurs after the initial, fairly rapid, rise in magnetisation, just as do the other transitions, which occur after the rise in magnetisation at the critical field value. That there should be such a large disagreement between the two sets of measurements is rather surprising. The transition, presumably, must be very sensitive to the values of the lattice parameters, and it would be interesting to investigate the effect of strain on the transition points.

Any comparison of the temperature dependence of K_4 with Zener's theory is likely to be unprofitable, because of the comparatively small temperature range over which the anisotropy has been investigated, and because of the lack of saturation of the anisotropy constant at the maximum field strengths available. The same objection which was broached in the case of terbium, on the grounds of the large magnetostriction, is also valid here (84,85). The function $(\sigma/\sigma_o)^{21}$ becomes 0.01 at 110^{ok}, so that it seems probable that $\left[K_4/K_{4.2}\right]$ will fall off somewhat less rapidly, as was observed for terbium. Also the Zener theory cannot

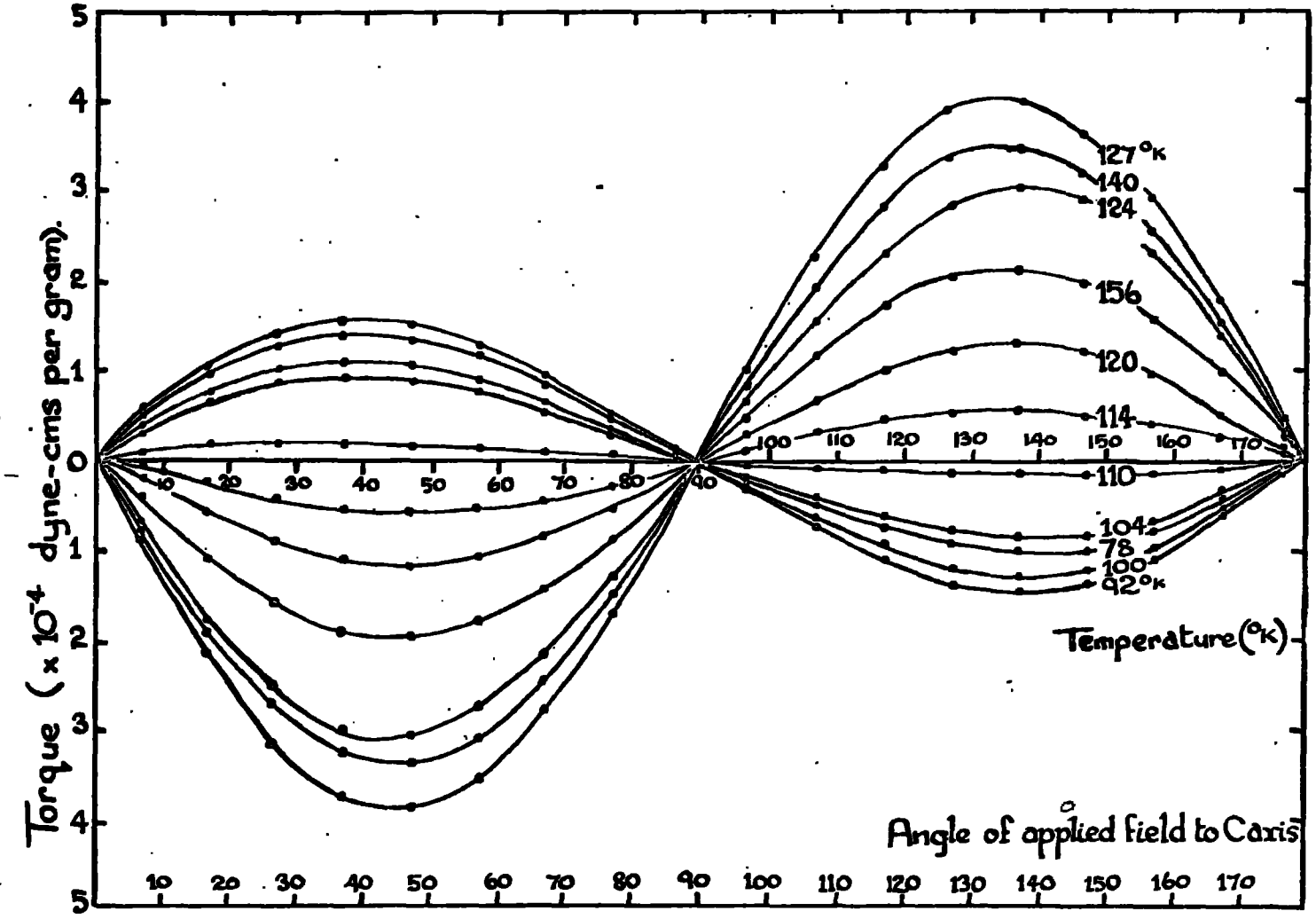

Fig. 8.27 Torque curves obtained for the c-axis specimen of holmium in an applied magnetic field strength of 12.5 kOe, in the paramagnetic and antiferromagnetic regions.

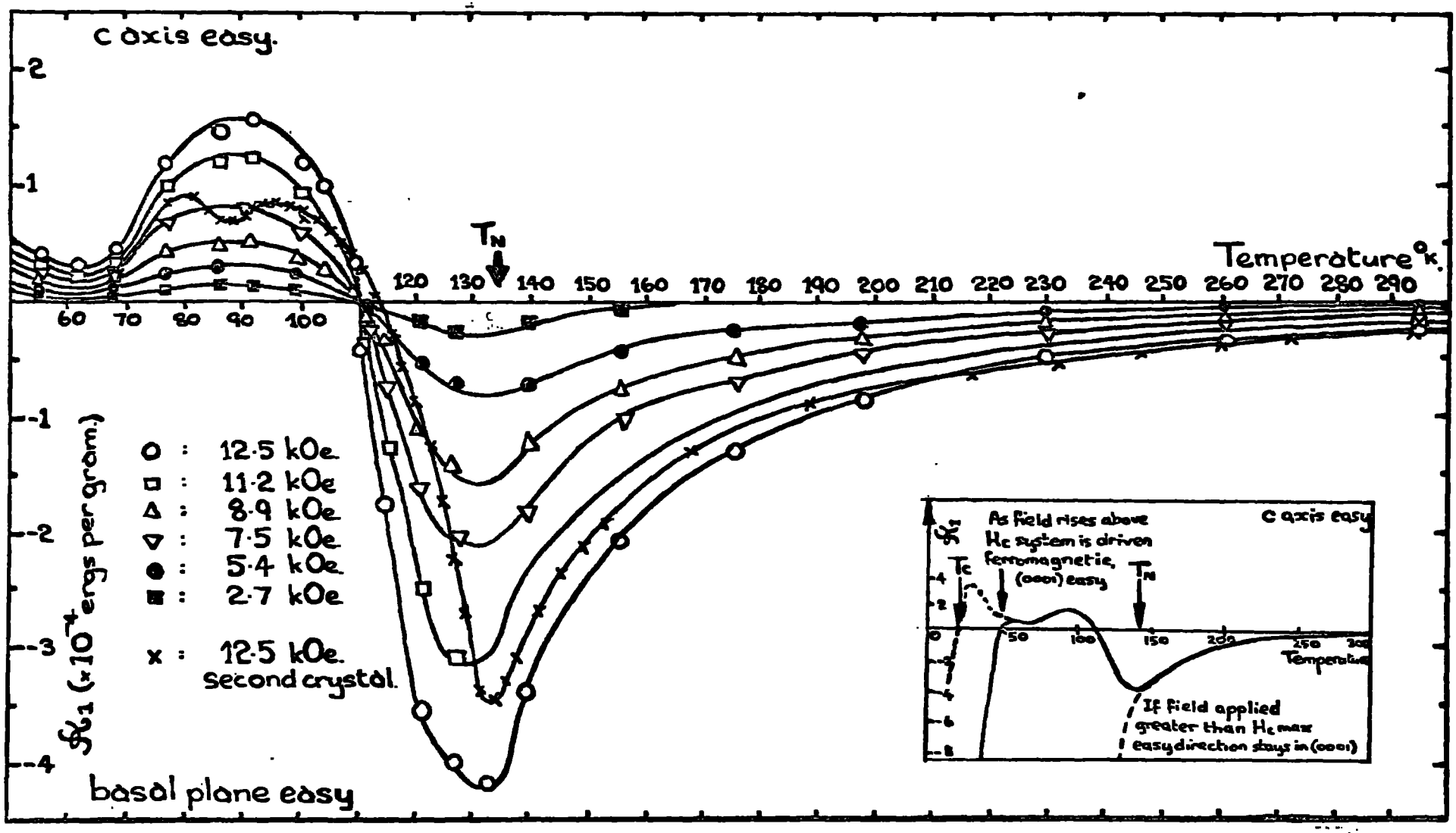

Fig. 8.28 Temperature dependence of $\mathcal{K}_1$ for holmium at various applied field strengths, showing the change in easy direction from basal plane to c-axis. Inset shows suggested behaviour of the anisotropy in the antiferromagnetic region.

account for reversals in the sign of K_4, although K_4 is very small when this occurs.

8.7 Holmium: C axis anisotropy

Holmium shows a paramagnetic to antiferromagnetic transition at a Néel temperature of 132^{ok}. A transition to ferromagnetism occurs at a temperature of 20^{ok} in zero applied field, and the maximum critical field is 26 kOe (81). Thus only the paramagnetic and antiferromagnetic regions could be investigated.

The torque curves obtained were in all cases of the sin2θ type, with no asymmetry and very little rotational hysteresis. In the paramagnetic range X-ray orientation of the specimen showed that the easy direction was in the basal plane, but at 110^{ok} the torque curves inverted and the easy direction lay in the C axis. This behaviour of the torque curves is shown in Figure 8.27.

The temperature variation of the K_1 values for various applied field strengths is plotted in Figure 8.28. In the paramagnetic region the anisotropy increases with decreasing temperature, reaching a maximum at the Néel point, this maximum moving to slightly lower temperatures as the field increases, but agreeing well with a Néel temperature of 132^{ok}, as determined by Hegland, Legvold and Spedding (17).

Below the Néel point the K_1 values decrease rapidly, K_1 becoming positive (C axis easy) below 110^{ok}, the torque curves remaining purely sinusoidal. The temperature at which reversal occurs is not field dependent. At lower temperatures the anisotropy constant becomes maximum at 90^{ok}, decreases to a minimum at 63^{ok} and is rising slightly at 55^{ok}.

A second ellipsoidal crystal was available for measurement, but the specimen had a crystallite spread of some 10°. The anisotropy values

obtained for this crystal were accordingly rather lower than for the single crystal specimen: also this specimen showed a reversal in sign of the anisotropy constant at a temperature some 3° higher than for the first crystal, and there was also a further minimum in the anisotropy constant values at 87^{ok}. Thus although the temperature variation of the anisotropy constant is in general the same for the two specimens, there is some discrepancy in the details.

Because of this anisotropy reversal, the behaviour of the crystal in the ferromagnetic region was of great interest. As there was only a single dewar available for the apparatus measurements at helium temperature were not possible, and liquid neon was considered as a possible alternative. One litre of neon was transferred to the magnetometer dewar and the torque curve at 12.5 kOe measured. Because the neon boiled off rather more quickly than anticipated only one run was possible, and during this run the neon level was at the level of the sample, resulting in an equilibrium temperature of 33^{ok}. The results obtained during the run were sufficient to show that the system became ferromagnetic at applied fields greater than 6 kOe, and that for an applied field strength of 5.4 kOe the torque curve was of the $\sin 2\theta$ type, giving a value for K_1 of approximately 3.2×10^4 ergs per gram. The antiferromagnetic anisotropy constant is therefore rising sharply below 50^{ok}. The easy direction is still the C axis. For applied field strengths greater than 6 kOe, ferromagnetism developed when the field direction was close to the basal plane direction, in a similar manner to the onset of ferromagnetism observed in the dysprosium C axis specimen. Thus in the ferromagnetic crystal the easy direction is again

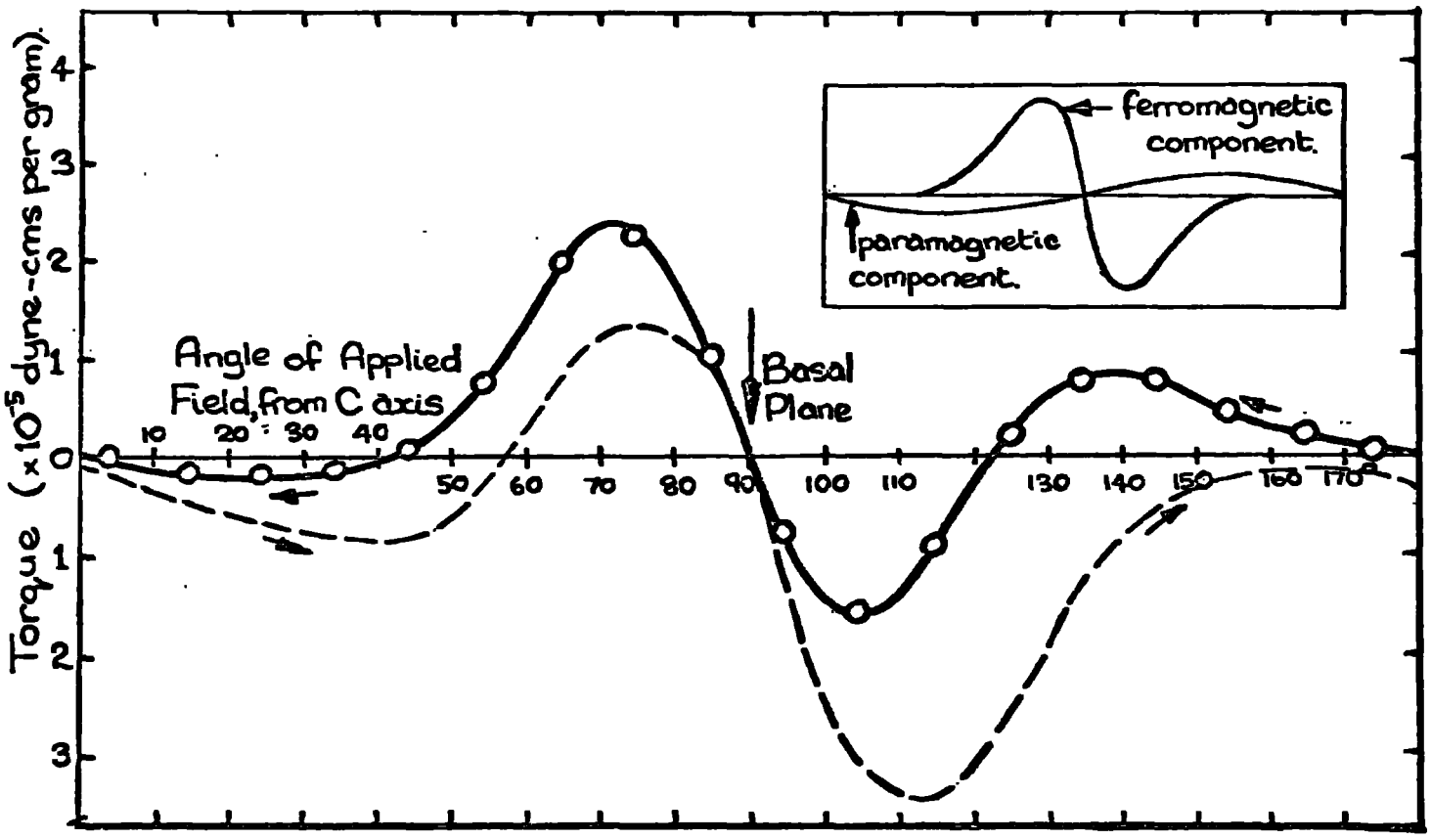

Fig. 8.29 Torque curve obtained for c-axis specimen of holmium at 55°K, where the applied field strength of 12.5 kOe is sufficiently large to drive the specimen ferromagnetic as the field direction crosses the basal plane. Inset shows the suggested composition of the curve, and the change in easy axis.

in the basal plane, as indicated also by the directions of the torques produced. Further runs at neon temperatures were not practicable because of the cost involved.

However, it was discovered that if the maximum field strength available (12.5 kOe) was applied to the specimen at a temperature of 55°k, which was the lowest temperature obtainable by pumping on nitrogen, the critical field value was exceeded and ferromagnetism developed when the applied field direction was close to the basal plane direction. When this happened, the easy direction changed from the C axis to the basal plane. The torque curve obtained is shown in Figure 8.29 and, inset, the suggested composition of the curve. It was found that at these low temperatures there was a large amount of rotational hysteresis present, as is indicated by the broken curve in the diagram.

Thus it would appear that the easy direction for magnetisation in holmium is in the basal plane in the paramagnetic and ferromagnetic region, but along the C axis in the antiferromagnetic region. The first of these observations agrees with magnetisation measurements by Strandburg, Legvold and Spedding (24), and with neutron diffraction studies by Koehler et al (37). An easy direction along the C axis in the antiferromagnetic region would not conflict with the magnetisation measurements, since in this region there is no appreciable difference between the magnetisation produced by magnetic fields along the C axis, or in the basal plane, indicating that the anisotropy is not large in this region. Inspection of the magnetisation curves shows that at 30°k and an applied field of 5 kOe, which is below the critical field value at this

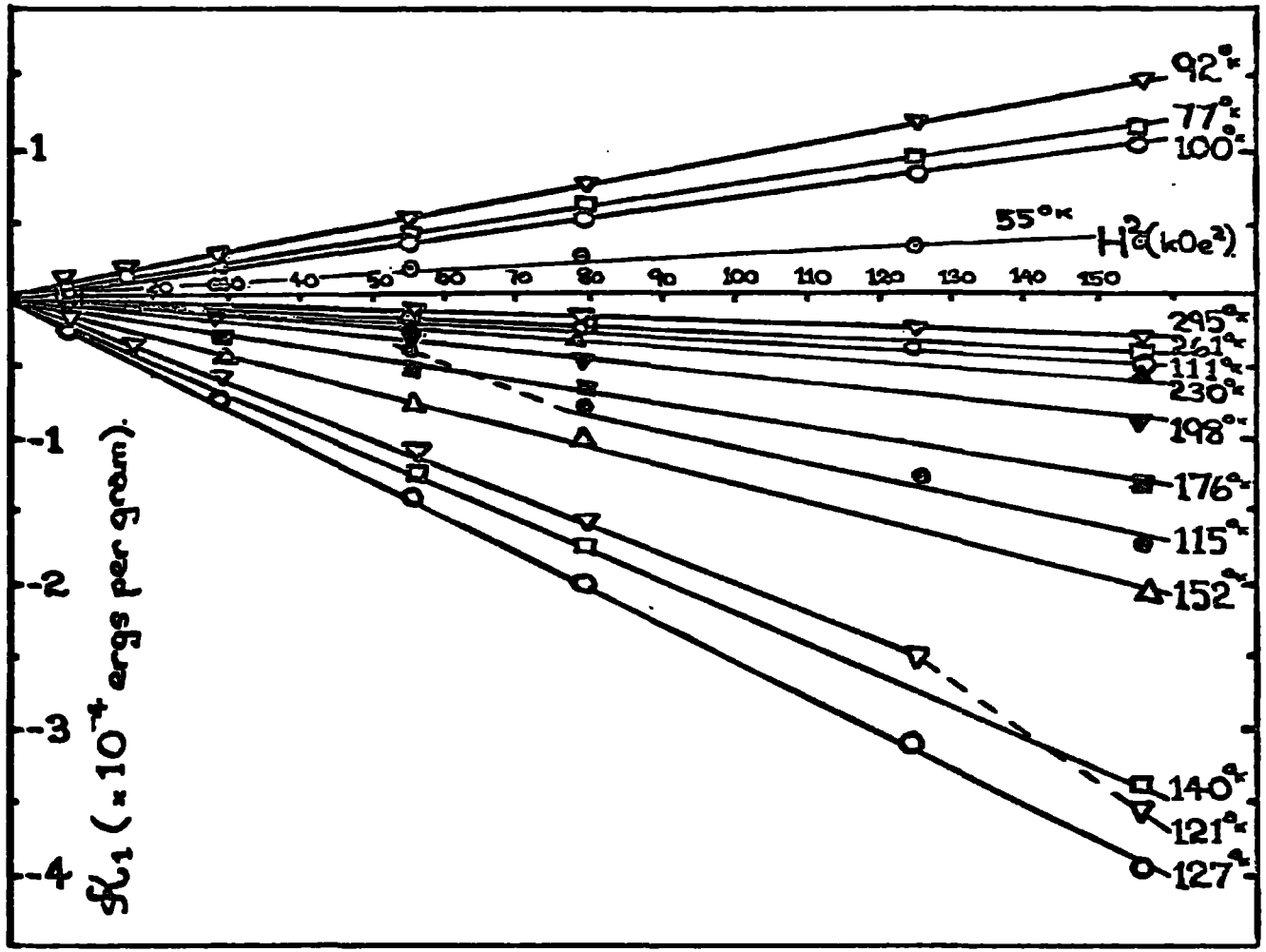

Fig. 8.30 Plot of $\mathcal{K}_1$ versus H^2 for holmium.

temperature, the magnetisation produced in the basal plane is approximately 15 e.m.u. per gram, whereas that produced in the C axis direction is 35 e.m.u. per gram. This would indicate the C axis is the easy direction at this temperature, and that the anisotropy is much bigger than at nitrogen temperatures.

However, the neutron diffraction studies of Koehler et al have indicated a simple spiral structure for the antiferromagnetism, with all the spins lying in the basal plane. Below the Curie point a small ferromagnetic C axis component was observed, but not at higher temperatures. This cannot be the case if the easy direction is the C axis, as suggested by the torque measurements. Some C axis component must exist, and, further, for a given applied field strength the magnetisation produced along the C axis must be larger than that produced in the basal plane. Figure 8.30 shows that the antiferromagnetic ϕ_1 values vary as H^2, so that the C axis component is either paramagnetic or antiferromagnetically ordered. If the component is antiferromagnetic it will vary in some periodic manner along the C axis, otherwise it must be completely disordered in zero field. If ordering does exist, then it is possible that the arrangement is similar to that found in erbium and thulium where an antiphase domain system exists along the C axis, as shown in Figure 1.4 (f). In this case it is not unreasonable to suppose that a magnetic field applied along the C axis will produce a larger magnetisation in this type of spin arrangement than will be produced by the application of the same field in the plane of the spiral spin configuration in the basal plane, since in the former case all the spins are in the line of the field and distortion of the periodicity will produce a growth of the favourably oriented 'domains', whereas in the latter case the field

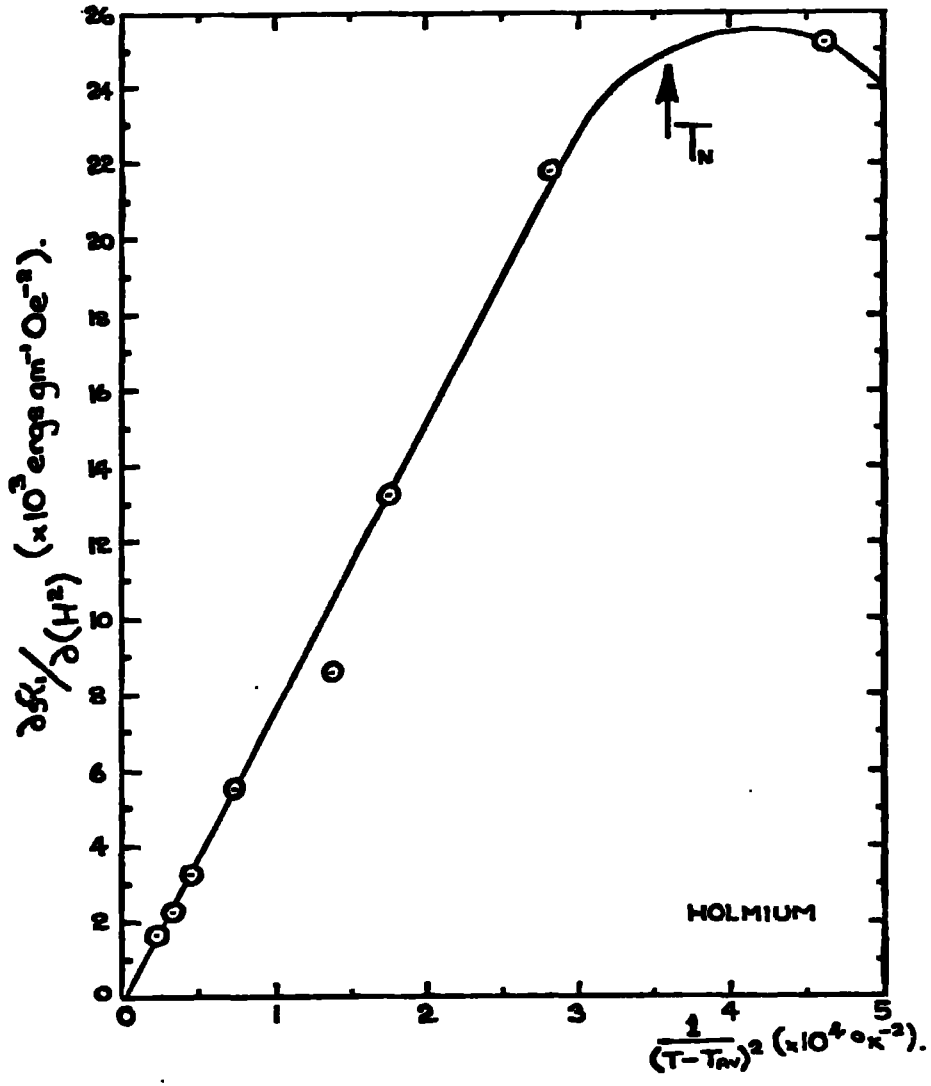

Fig. 8.31 Plot of $\frac{\partial \mathcal{K}_1}{\partial (H^2)}$ versus $\frac{1}{(T-T_{AV})^2}$ for holmium in the paramagnetic region.

merely produces a slight distortion of the spiral.

Although the studies of Koehler et al were in zero applied field, it is difficult to understand why the existence of such a C axis component was not observed, unless the phenomenon is field induced.

Figure 8.31 shows the linearity of $\frac{\partial \chi_1}{\partial (H^2)}$ with $\frac{1}{(T-\theta_{av})^2}$, θ_{av}= 80.5°K(37). As for dysprosium, linearity is observed only until the Néel point is reached, the plot curving over below this temperature.

The critical field at 55°k appeared to be 11 kOe, and a measurement at 63°k showed that a field strength of 12.5 kOe was just sufficient to induce ferromagnetism. These values are slightly lower than the critical field values determined by Flippen (81) which are approximately 12.5 kOe at 55°k and 14 kOe at 63°k. However, the critical field value determined at 33°k was 6 kOe, and a measurement at 20 kOe using the torsion wire magnetometer gave a value for Hc of 19 kOe at 77°k, both values agreeing well with Flippen.

8.8 Holmium: Basal Plane Anisotropy

Since the basal plane anisotropy in the rare earth metals only appears to be observable in the ferromagnetic range, it was expected that torque measurements would only be possible where the critical field could be exceeded. This was found to be the case. In fact it was only possible to obtain torque curves for 55°k and two or three degrees higher (the lowest temperatures obtainable) and field strengths above 12 kOe. Thus the critical field values as determined here appear to be slightly higher than for the C axis specimen.

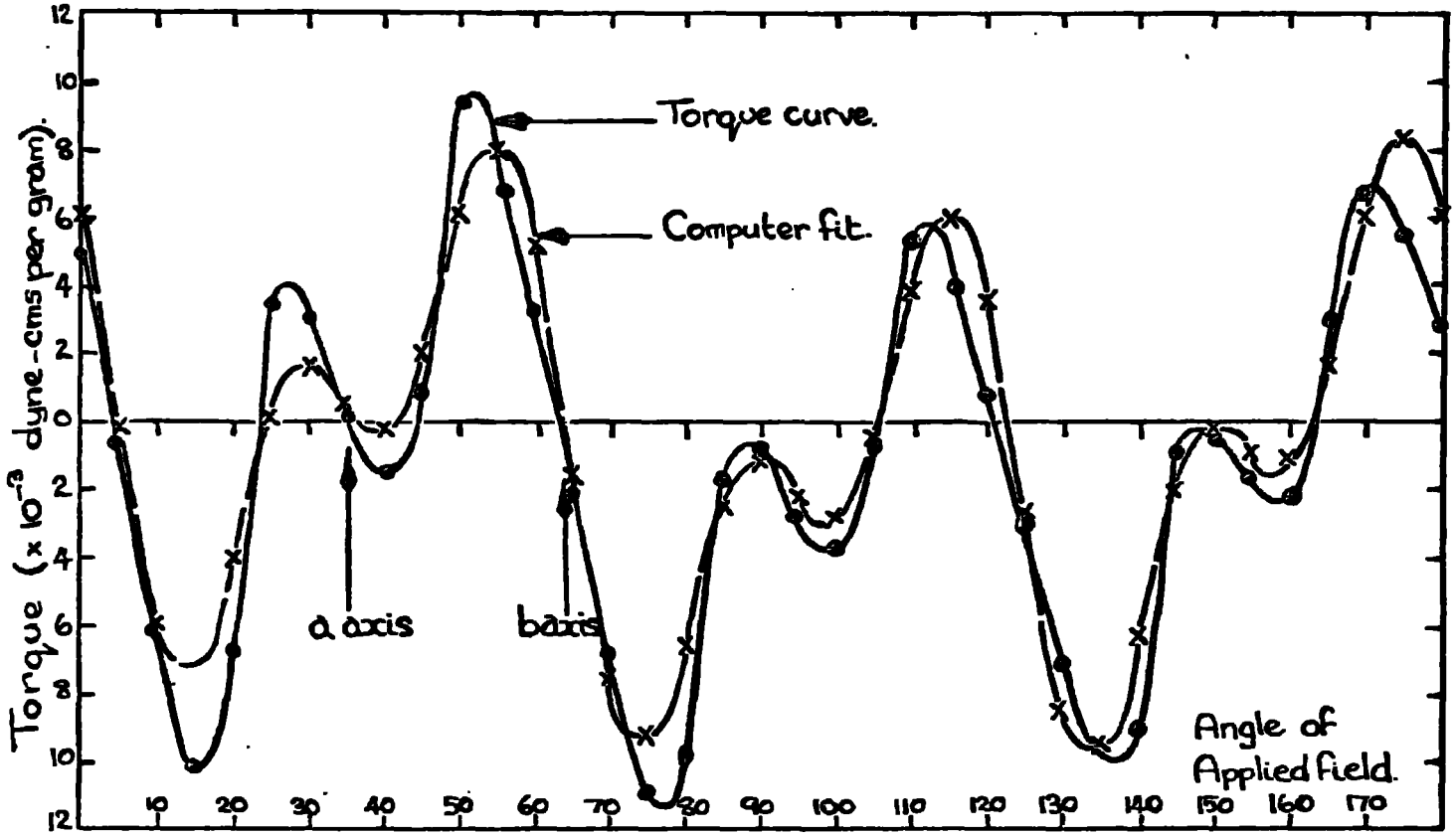

Fig. 8.32 Torque curve obtained for the holmium basal plane specimen at 55°K, 12.5 kOe. Crosses indicate the fit obtained by computer analysis.

Because the torque curves obtained were for fields only just above the critical value, where the magnetisation is increasing very rapidly with field, the curves were not reproducible. However, the shape of the curves was very interesting, in that they exhibited a twelve-fold component. A typical torque curve is shown in Figure 8.32 where it can be seen there is also a sin 2ϕ component present. There was also considerable rotational hysteresis, as was observed in dysprosium just above the critical field.

Because of the sin 12ϕ term the curve had to be analysed using an expression for the anisotropy which included higher terms in ϕ. Expressing the anisotropy energy E_k in spherical harmonics $Y_m^n(\theta,\phi)$ and adding three extra terms of twelfth order to the expression used for the previous calculations:

$$E_k = A_2^0Y_2^0(\theta,\phi)+A_4^0Y_4^0(\theta,\phi)+A_6^0Y_6^0(\theta,\phi)+A_6^6Y_6^6(\theta,\phi)+A_{12}^0Y_{12}^0(\theta,\phi) +A_{12}^6Y_{12}^6(\theta,\phi)+A_{12}^{12}Y_{12}^{12}(\theta,\phi)+\ldots \quad 8.8$$

Of these extra terms only Y_{12}^{12} can include a factor containing 12ϕ, (86); the other terms will have coefficients containing $\mathcal{K}_1, \mathcal{K}_2, \mathcal{K}_3, \mathcal{K}_4$, and two other constants.

$$Y_{12}^{12} = \text{constant} \times \sin^{12}\theta \cos 12\phi. \quad 8.9$$

If this term is added to the energy expression, and the expression for the torque determined using this modified expression, we find:

$$L(\phi) = \theta_c^2\left[\mathcal{K}_1+2\mathcal{K}_2+3\mathcal{K}_3\right]\sin 2\phi + 6\mathcal{K}_4\sin 6\phi + 12\mathcal{K}_5\sin 12\phi + \ldots \quad 8.10$$

assuming that θ_c^2, $\theta_c^2\mathcal{K}_4$ and $\theta_c^2\mathcal{K}_5$ are all negligible. Here $\mathcal{K}_5$ is an additional anisotropy constant required to describe the twelvefold dependence of the basal plane anisotropy.

Computer analysis of the torque curves evaluated $\mathcal{K}_4, \mathcal{K}_5$,

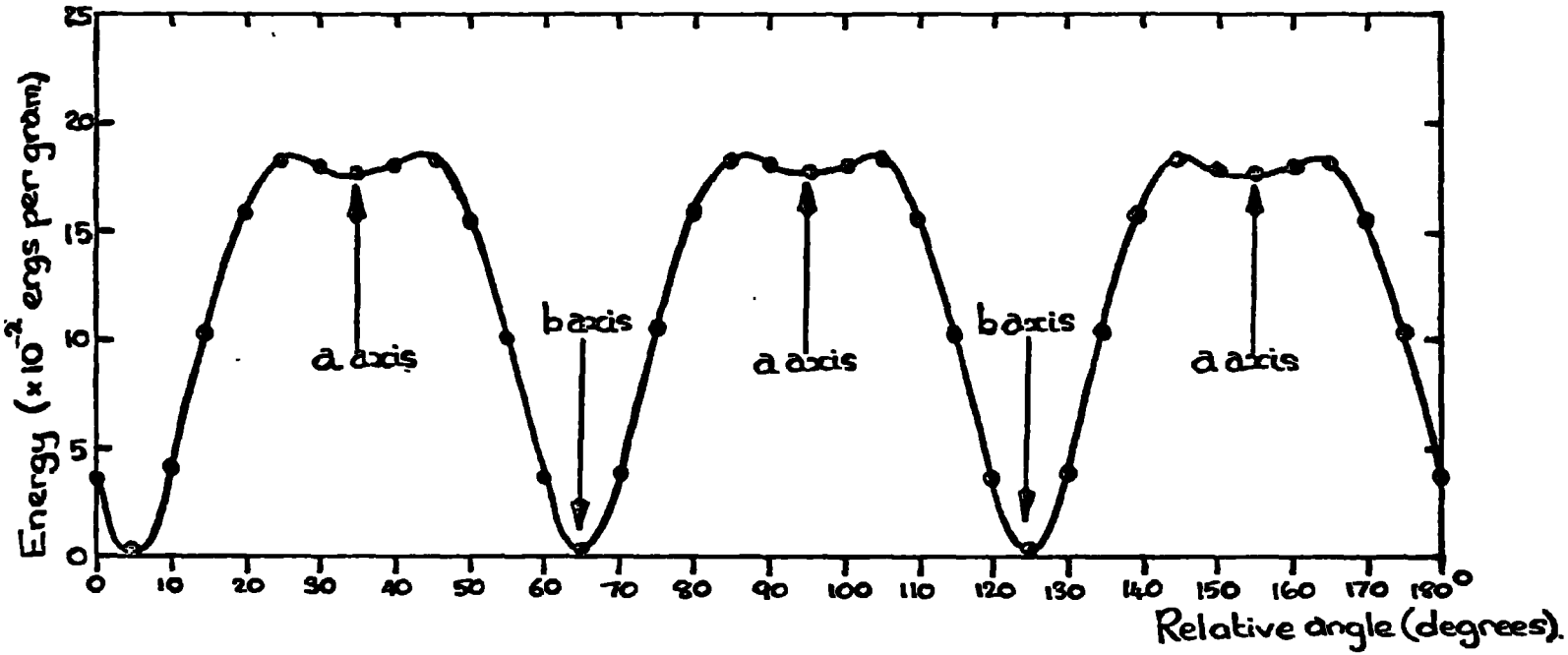

Fig. 8.33 Plot of the anisotropy energy surface in the basal plane of holmium at 55°K, in an applied magnetic field strength of 12.5 kOe, as obtained from integration of the torque curve.

and $\theta_c^2[\mathcal{K}_1 + 2\mathcal{K}_2 + 3\mathcal{K}_3]$ and gave a curve fit indicated in Figure 8.32. A perfect fit cannot be expected, as at the point of measurement the magnetisation, and therefore the torque values, are very sensitive to small changes of temperature or field.

From the computer analysis the contributions of $\mathcal{K}_1$, $\mathcal{K}_2$ and $\mathcal{K}_3$ could be subtracted from the torque curve, leaving only the contributions of $\mathcal{K}_4$ and $\mathcal{K}_5$. Integration of this torque curve gave the shape of the anisotropy energy surface in the basal plane. X-ray orientation of the crystal determined the positions of the a and b axes relative to this curve, which is shown in Figure 8.33, in which it can be seen that although both a and b axes are energy minima, the minimum at the b axis is much deeper than that at the a axis. This agrees with the magnetisation measurements of Strandburg et al (24), in which the approach to saturation is slower for magnetisation in the a axis than in the b axis.

Computer analysis gave a wide range of values for $\mathcal{K}_4$ and $\mathcal{K}_5$ from analysis of different torque curves taken at a nominal 55^{ok} and 12.5 kOe. These values vary from +400 to +1200 ergs per gram for $\mathcal{K}_4$ and from +120 to +500 ergs per gram for $\mathcal{K}_5$, the variation being due to the great sensitivity of the measurement to changes in temperature or field strength.

It must be remembered that these torque curves were obtained on the magnetisation rise occurring at the critical field: it is possible that at magnetisations nearer saturation the energy minima at the a axis will disappear entirely to leave a $\sin 6\phi$ curve as observed for gadolinium, terbium and dysprosium.

8.9 Summary of Results

Because of the limitations on the maximum torque which could be measured, and because the available magnetic fields were insufficient to pull the magnetisation out of the easy direction, only the paramagnetic and antiferromagnetic values of the anisotropy constant K_1 could be evaluated. The K_1 value increased with decreasing temperature in the paramagnetic region, to reach a maximum value at the Néel point for the metals dysprosium and holmium, which show antiferromagnetic behaviour below this temperature. Terbium becomes ferromagnetic at the Néel point, except for very small values of the applied field strength, and the anisotropy became so large at this temperature as to be unmeasurable. For dysprosium and holmium, in the antiferromagnetic region the anisotropy decreases with decreasing temperature, and in the case of holmium the anisotropy constant changes sign from negative to positive, becoming large and negative again as the system becomes ferromagnetic. The magnitudes determined for the critical fields in dysprosium and holmium agree with the measurements of Flippen (81). The maximum value of the critical field in the basal plane of holmium is 26 kOe: presumably if a field is applied in the basal plane to exceed this there will be no antiferromagnetic region, so that as the temperature is decreased the easy direction will remain at all times in the basal plane, the anisotropy increasing rapidly at the Néel point.

As is predicted by Callen and Callen (52) the anisotropy varies as the square of the applied field in the paramagnetic region, and also in the antiferromagnetic region, where the magnetisation appears to be directly proportional to the applied field. In the paramagnetic region

the function $\frac{\partial \mathcal{K}_1}{\partial(H^2)}$, and therefore $\mathcal{K}_1$ at constant field strength, varies linearly with a function of temperature of the type $\frac{1}{(T-\theta)^2}$. However, the value of θ which produced such a dependence was that of the average paramagnetic Curie temperature in the case of terbium and holmium, while for dysprosium the value taken was that of the paramagnetic Curie point for magnetisation along the C axis.

In terbium, dysprosium and holmium the easy direction for magnetisation lies in the basal plane, with the exception of antiferromagnetic holmium below 110^{ok}, where the C axis becomes the easy direction, although this contradicts the neutron diffraction observations of Koehler et al (37).

Determinations of the basal plane anisotropy constant $\mathcal{K}_4$ show that there is no basal plane anisotropy observable in the paramagnetic or antiferromagnetic regions. In all cases the $\mathcal{K}_4$ value increases monotonically as the temperature is decreased, the values becoming vanishingly small well below the Néel temperature. In the case of gadolinium the temperature dependence of $\mathcal{K}_4$ agrees well with the $(\sigma/\sigma_0)^{21}$ dependence as predicted by Zener (50), but this is not so in the case of terbium.

For gadolinium the saturation value of $\mathcal{K}_4$ at 0^{ok} is -800 ergs per gram. The basal plane anisotropy for both terbium and dysprosium is a factor of approximately 500 larger than this.

In the basal plane of dysprosium a change of easy direction from a axis to b axis with increasing field is observed at field strengths just above the critical field, and the transition is field dependent.

Although this agrees in part with the magnetisation measurements of Jew and Legvold (21) there is no evidence of a further transition at higher field strengths in the lower temperature portion of the antiferromagnetic region.

From the single temperature and field value investigated for holmium, the basal plane anisotropy is twelve fold, with a deep energy minimum at the b axis, and a shallow minimum at the a axis. In this case it became necessary to define a further anisotropy constant K_5, adding the term $K_5 \sin^{12}\theta \cos 12\phi$ to the energy expression.

The easy directions for magnetisation were as follows:

Gadolinium	-	a axis (in the basal plane)
Terbium	-	b axis
Dysprosium	-	b axis, changing to the a axis at applied field strengths just above the critical field, as H decreases.
Holmium	-	b axis, with a second energy minimum at the a axis in the ferromagnetic region, changing to the C axis below 110^{ok} in the antiferromagnetic region.

Although in the C axis specimens all the torque curves obtained were of the $\sin 2\theta$ type, it is quite possible that at field strengths which are sufficient to pull the magnetisation well away from the basal plane in the ferromagnetic region, the anisotropy will be such that higher order anisotropy constants than K_1 will be required for analysis, as is found to be the case in gadolinium. From the magnetisation measurements of other workers, however, the anisotropy between the basal plane and the C axis is such that the easy direction will not move far from the basal

plane in terbium, dysprosium and holmium.

8.10 Suggestions for Further Work.

Obviously, the preceding report is far from being a full investigation of anisotropy in the rare earth metals, because of the limitations in the field strengths and temperatures available, and also because the torque magnetometer was unable to measure the maximum torques produced in these experiments. For further work very high field strengths (100 kOe or more) will be required to produce saturation along the hard direction, and a magnetometer capable of measuring very large torques (up to 10^9 dyne-cms) will also be necessary. Such high fields will necessarily be supplied in a solenoid, where the torque axis is perpendicular to the axis of the solenoid, making access difficult. A prototype magnetometer constructed with this intention is described in the appendix.

Such measurements on terbium and dysprosium have very recently been reported by Rhyne and Clark (87). The anisotropy constant K_1 was obtained from the equilibrium orientation of the magnetic moment in applied magnetic fields up to 140 kOe. Measurement of the torques produced was achieved by passing a current through a coil containing the specimen and pivoted in the magnetising field, so bringing the system back to the null position. Measurements were made from 11°K to near the Néel points. The magnitudes of the anisotropy constants K_1 for Tb and Dy were found to be very similar.

The similarity of the magnitudes of the torques per unit mass produced by the Tb and Dy specimens, as measured by the simple torsion balance has already been commented on here: if the gradient at the easy axis of the torque curve for dysprosium is equated to the gradient of $\mathcal{K}_1 \sin 2\theta$ at $\theta=0$, the value obtained for $\mathcal{K}_1$ at $77^{\circ}K$ in an applied field of 17 kOe is 3.5×10^6 ergs/gram, while the saturation value of $\mathcal{K}_1$ at $77^{\circ}K$ as measured by Rhyne and Clark is 5×10^7 ergs/gram. The order of magnitude difference between these values reflects the lack of saturation at the low fields available.

In the same paper Rhyne and Clark report a determination of K_4 for Tb and Dy from magnetostriction data. The values obtained agree satisfactorarily with the values reported here. The value of $\mathcal{K}_4$ at $0^{\circ}K$ for terbium as given by Rhyne and Clark is 2.9×10^5 ergs/gram. The value obtained here was 3×10^5 ergs/gram.

It would appear from the measurements made using the disc-shaped specimens that strain has a large effect on the crystalline anisotropy. This is a point requiring further investigation; a small distortion of the lattice has a very marked effect on the anisotropy, and a systematic distortion of the crystal could provide useful information on the dependence on the lattice parameters of the anisotropy. Similarly, a controlled change in the lattice parameters by the application of large hydrostatic pressures would lead to interesting anisotropy measurements, though in this case the practical difficulties are likely to be severe.

ACKNOWLEDGEMENTS.

I would like to express my sincere thanks to Dr. W. D. Corner, who has supervised and guided me throughout this work. I am also indebted to Dr. K. N. R. Taylor for his assistance in the interpretation of the results, and to Dr. M. I. Darby for advice on the computer analysis of the torque curves.

I am also grateful to Professor G. D. Rochester, F. R. S., for the research facilities made available to me, and to the Physics Department Workshop staff, especially Mr. W. Leslie and Mr. D. Jobling, for the construction of the apparatus. For the loan of the disc shaped terbium and dysprosium specimens I should like to thank Dr. D. M. S. Bagguley of Oxford University Physics Department, and Dr. E. W. Lee of Sheffield University Physics Department.

An acknowledgement is also due to Dr. G. Lidgard, and to each of my fellow research students, M. B. Allenson, H. D. Ellis, D. R. Thompson and G. M. Young, for the discussions and suggestions which are valuable in any research project.

Finally, my thanks are also due to S.R.C. for a Research Studentship from 1963 to 1966.

P. H. B.

June, 1967.

REFERENCES.

1. "Rare Earths", Chemical and Engineering News, 43, 78, (1965).
2. F. H. Spedding & J. E. Powell, J. Metals, 6, 1131, (1954).
3. E. M. Savitskii, V. F. Terekhova, & O. P. Naumkin, Sov. Physics, Uspekhi, 6, 123, (1963).
4. K. A. Gschneidner, "Crystallography of the Rare Earth Metals", Chapter 14 in "The Rare Earths", Spedding & Daane, editors, J. Wiley & Sons, New York, p.190, (1961).
5. S. Chikazumi, "Physics of Magnetism", J. Wiley & Sons, New York, p.450, (1964).
6. P. W. Selwood, "Magnetochemistry", Interscience, New York, (1943).
7. J. H. Van Vleck, "Theory of Electric and Magnetic Susceptibilities", Clarendon Press, Oxford, (1932).
8. K. A. Gschneidner, "Rare Earth Alloys", Van Nostrand & Co., New York, p.22, (1961).
9. M. Griffel, R. E. Skochdopole & F. H. Spedding, Phys. Rev., 93, 657, (1954).
10. J. F. Elliott, S. Legvold &F. H. Spedding, Phys. Rev., 91, 28, (1953).
11. W. E. Henry, J. Appl. Phys., 29, 524, (1958).
12. D. R. Behrendt, S. Legvold & F. H. Spedding, Phys. Rev., 106, 723, (1957).
13. H. E. Nigh, S. Legvold & F. H. Spedding, Phys. Rev., 132, 1092, (1963).
14. H. Leipfinger, Z. Phys., 150, 415, (1958).
15. W. E. Henry, J. Appl. Phys., 30, 99S, (1959).
16. W. C. Thoburn, S. Legvold & F. H. Spedding, Phys. Rev., 112, 56, (1958).
17. D. E. Hegland, S. Legvold & F. H. Spedding, Phys. Rev., 131, 158, (1963).
18. K. P. Belov, R. Z. Levitin, S. A. Nikitin & A. V. Ped'ko, Sov. Phys. JETP, 13, 1096, (1961).
19. D. R. Behrendt, S. Legvold & F. H. Spedding, Phys. Rev., 109, 1544, (1958).
20. S. Legvold, "Rare Earth Research II", E. V. Klebe, editor, Macmillan & Co. Ltd., p.142, (1961).
21. T. T. Jew & S. Legvold, U.S. Atomic Energy Commission Report, IS-867, (1963).
22. W. E. Henry, Bull. Amer. Phys. Soc., 4, 176, (1959).
23. B. C. Rhodes, S. Legvold & F. H. Spedding, Phys. Rev., 109, 1547, (1958).
24. D. L. Strandburg, S. Levgold & F. H. Spedding, Phys. Rev., 127, 2046, (1962).
25. W. Klemm & H. Bommer, Z. anorg. u. allgem. Chem., 231, 138, (1937).
26. R. E. Skochdopole, M. Griffel & F. H. Spedding, J. Chem. Phys., 25, 75, (1956).
27. J. F. Elliott, S. Legvold & F. H. Spedding, Phys. Rev., 100, 1595, (1955).
28. R. W. Green, S. Legvold & F. H. Spedding, Phys. Rev., 122, 827, (1961).
29. S. Arajs, J. Chem. Phys., 32, 951, (1960).
30. D. D. Davis & R. M. Bozorth, Phys. Rev., 118, 1543, (1960).

31. F. Bloch, Z. Phys., 61, 206, (1930).
32. K. Niira, Phys. Rev., 117, 129, (1960).
33. W. E. Henry, J. Phys. Radium, 20, 192, (1959).
34. W. E. Henry, Phys. Rev., 117, 89, (1960).
35. W. C. Koehler, E. O. Wollan, M. K. Wilkinson & J. W. Cable, "Rare Earth Research II", E. V. Klebe, editor, Macmillan & Co. Ltd., p. 149, (1961).
36. J. W. Cable, H. R. Child, W. C. Koehler, M. K. Wilkinson & E. O. Wollan, "Pile Neutron Research in Physics", International Atomic Energy Agency, Vienna, p.379, (1962).
37. W. C. Koehler, J. Appl. Phys., 36, 1078, (1963).
38. K. P. Belov, R. Z. Levitin, S. A. Nikitin & A. V. Ped'ko, Sov. Phys. JETP, 13, 1096, (1961).
39. K. P. Belov & A. V. Ped'ko, Sov. Phys. JETP, 15, 62, (1962).
40. K. P. Belov, I. V. Burov, Yu. V. Ergin, A. V. Ped'ko & E. M. Savitskii, Sov. Phys. JETP, 20, 574, (1965).
41. G. Will, R. Nathans & H. A. Alperin, J. Appl. Phys., 35, 1045, (1964).
42. P. Langevin, J. de Physique, 4, 619, (1905).
43. A. J. Dekker, "Solid State Physics", Macmillan & Co. Ltd., London, (1962).
44. P. Weiss, J. de Physique, 6, 661, (1907).
45. R. M. Bozorth, "Ferromagnetism", D. Van Nostrand, Princeton N.J., p.555, (1951).
46. J. Kanamori, "Magnetism", Vol. I, Rado & Suhl, editors, Academic Press, New York & London, 127, (1963).
47. C. D. Graham, Proceedings of Int. Conf. on Magnetism, Nottingham, England, p.740, (Sept. 1963).
48. G. Mahajani, Phil. Trans. Royal Soc. (London), 228A, 63, (1929).
49. J. H. Van Vleck, Phys. Rev., 52, 1178, (1937).
50. C. Zener, Phys. Rev., 96, 1335, (1954).
51. W. J. Carr, J. Appl. Phys., 29, 436, (1958).
52. E. Callen & H. B. Callen, J. Phys. Chem. Solids, 27, 1271, (1966).
53. F. Keffer, Phys. Rev., 100, 1692, (1955).
54. T. A. Kaplan, Phys. Rev., 124, 329, (1961).
55. R. J. Elliott, Phys. Rev., 124, 346, (1961).
56. K. Yosida & H. Miwa, J. Phys. Soc. Japan, 17, Suppl. BI, 5, (1962).
57. R. J. Elliott, "Magnetism", Vol. IIA, Rado & Suhl, editors, Academic Press, New York & London, p.385, (1963).
58. A. Yoshimori, J. Phys. Soc. Japan, 14, 807, (1959).
59. M. Rudermann & C. Kittel, Phys. Rev., 96, 99, (1954).
60. K. Yosida, Phys. Rev., 106, 893, (1957).
61. T. Kasuya, Progr. Theor. Physics, 16, 45, (1956).
62. P. G. de Gennes, Compt. Rend., 247, 1836, (1958).
63. T. Nagamiya, K. Nagata & Y. Kitano, Progr. Theor. Physics, 27, 1253, (1962).
64. T. Nagamiya, J. Appl. Phys., Suppl. to 33, 1029, (1962).
65. P. G. de Gennes & D. Saint-James, Sol. Stat. Commun., 1, 62, (1963).
66. R. J. Elliott & F. A. Wedgewood, Proc. Phys. Soc., 84, 63, (1964).
67. H. Miwa, Proc. Phys. Soc., 85, 1197, (1965).
68. H. J. Williams, Rev. Sci. Instrum., 8, 56, (1937).

69. W. D. Corner, W. C. Roe & K. N. R. Taylor, Proc. Phys. Soc., 80, 927, (1962).
70. C. D. Graham, J. Phys. Soc. Japan, 17, 1310, (1963).
71. C. D. Graham, J. Appl. Phys., 34, 1341, (1963).
72. R. Birss & P. M. Wallis, Proceedings of Int. Conf. on Magnetism, Nottingham, England, p.744, (Sept. 1964).
73. M. I. Darby & K. N. R. Taylor, Proc. Int. Conf. on Magnetism, Nottingham, England, p.742, (Sept. 1964).
74. C. D. Graham, J. Appl. Phys., 38, 1375, (1967).
75. G. T. Croft, F. J. Donahoe & W. F. Love, Rev. Sci. Instrum., 26, 360, (1955).
76. R. F. Penoyer, Proc. A.I.E.E., Conf. on Magnetism, p.365, (1956).
77. R. F. Pearson & L. Guildford, Mullard Report No. M.R.L./2519, (1957).
78. R. F. Pearson, Mullard Report No. M.R.L./290, (1959).
79. W. C. Roe, Ph. D. Thesis, University of Durham, (1961).
80. Z. Kopal, "Numerical Analysis", J. Wiley & Sons, New York, p.408, (1961).
81. R. B. Flippen, J. Appl. Phys., 35, 1047, (1964).
82. W. C. Koehler, H. R. Child, E. O. Wollan & J. W. Cable, J. Appl. Phys., 34, 1335, (1963).
83. J. J. Rhyne & S. Legvold, Phys. Rev., 138A, 507, (1965).
84. S. Legvold, J. Alstad & J.J. Rhyne, Phys. Rev. Letters, 10, 509, (1963).
85. A. E. Clark, B. F. de Savage & R. M. Bozorth, Phys. Rev., 138A, 216, (1965).
86. Jahnke, Emde & Lösch, "Tables of Higher Functions", 6th. ed., McGraw-Hill, New York, p.110, (1960).
87. J. J. Rhyne & A. E. Clark, J. Appl. Phys., 38, 1379, (1967).

APPENDIX

AN ATTEMPT TO MAKE TORQUE MEASUREMENTS ON RARE EARTH SINGLE CRYSTALS IN LARGE MAGNETIC FIELDS, BOTH PULSED AND STATIC, USING PIEZOELECTRIC TRANSDUCERS.

In the ferromagnetic metals following gadolinium in the rare earth series, applied fields of the order of 80 kOe are necessary to produce saturation in the hard directions. Thus if the torque measurements are made with applied fields in the $(10\bar{1}0)$ plane of terbium, dysprosium or holmium which are considerably less than this magnitude, the magnetisation will not be pulled sufficiently far from the easy direction for a determination of the anisotropy to be made.

The problems involved in a torque determination are:-

(i) The production of the high magnetic fields required.

(ii) Since such a field will only be produced in a solenoid, where access is parallel to the field, the axis of the torque will be perpendicular to the axis of the dewar system used. Thus a system of torque measurement as used previously is eliminated.

The possible solutions to (i) may be listed as:-

(a) A superconducting solenoid. Solenoids are now available which will produce fields of 80 kOe, but only in small useful volumes. Since working temperatures of up to 230^{ok} (for terbium) are required, while the solenoid remains at the temperature of liquid helium, a working volume considerably larger than the volume required by the measuring apparatus is necessary. Thus the superconducting solenoid could not provide sufficient working volume for our purpose.

(b) A high power d.c. solenoid. This would be most satisfactory, but such a system is ruled out for reasons of expense.

(c) A pulsed solenoid. This will provide the necessary field strength in sufficiently large volume, at comparatively low cost. For these reasons it was decided to construct such a system. However, since the field occurs in a pulse of the order of a millisecond duration, difficulties are introduced in the measurement of the torque.

The pulsed magnet was constructed using a bank of 80 x 24 μF capacitors, which could be charged to 2 1/2 kilovolts. The capacitors were mounted in a vertical rack and connected in parallel by long strips of 1/16" thick brass sheet, running on to two 3" x 1/4" brass busbars. The coil used had an inside diameter of 1.1". and an outside diameter of 2.2". It was machined from a solid bar of beryllium copper, by cutting a rectangular thread to a depth of 0.6" with a specially shaped tool, at a pitch of 8 threads to the inch. The bar was then potted in Araldite resin CT200, used without the hardener, so that it could be removed by melting. The core of the coil was drilled and machined to an inside diameter of 1.1", when the coil was removed from the resin. The coil had the form of a helix wound from flat, rectangular strip. 16 turns were cut from the helix, end leads soldered on, and fibre glass washers inserted to insulate the coil. The coil was then compressed on a central mandrel, and the outside wound with many layers of fibreglass yarn, which was then impregnated with Araldite resin to form a strong insulating coating. Two massive stainless steel end plates, with Tufnol insulation, held the coil under compression.

The condenser bank was fired through the coil by a mechanical switch similar to that used by Furth, Levine and Waniek (A1). A wide,

flat brass plate, hinged to one of the bus bars, bridged a gap in the bus bar and could be pushed down upon another flat plate attached to the continuation of the bus bar. Both plates were faced with a thick sheet of molybdenum to reduce surface sputtering, and the edges of the switch were carefully rounded to prevent preferential sparking at the edges. The gap between the two plates when the switch was closed was adjusted by means of spacing bolts to about half a millimetre. The switch was held closed by a strong spring, and opened by an electromechanical solenoid mechanism. Switching off the solenoid fired the switch, the spring reducing contact bounce, and the condenser bank discharged across the small gap, through the coil. The switch was surrounded by fibreglass for sound insulation, but the system was found to be surprisingly quiet. The resultant field produced in the coil was measured to be 100 kOe, lasting for approximately 750 μsec with three or four decaying oscillations after the first. Measurement of the field was by means of an indium arsenide Hall probe; the output was displayed on an oscilloscope and photographed, the induced signal for zero Hall current being determined and subtracted from the signal obtained.

The pulsed magnet was found to be satisfactory, and deterioration of the switch was not very noticeable after some hundreds of firings. Measuring apparatus could be triggered by means of a simple contact switch mounted on the rod which controlled the flat plate switch.

For measurement of torque, piezoelectric transducers were chosen. Because the torque axis is perpendicular to the axis of the solenoid, the apparatus for measurement of the torque must be contained within the solenoid. Piezoelectric ceramics have the small size necessary for this,

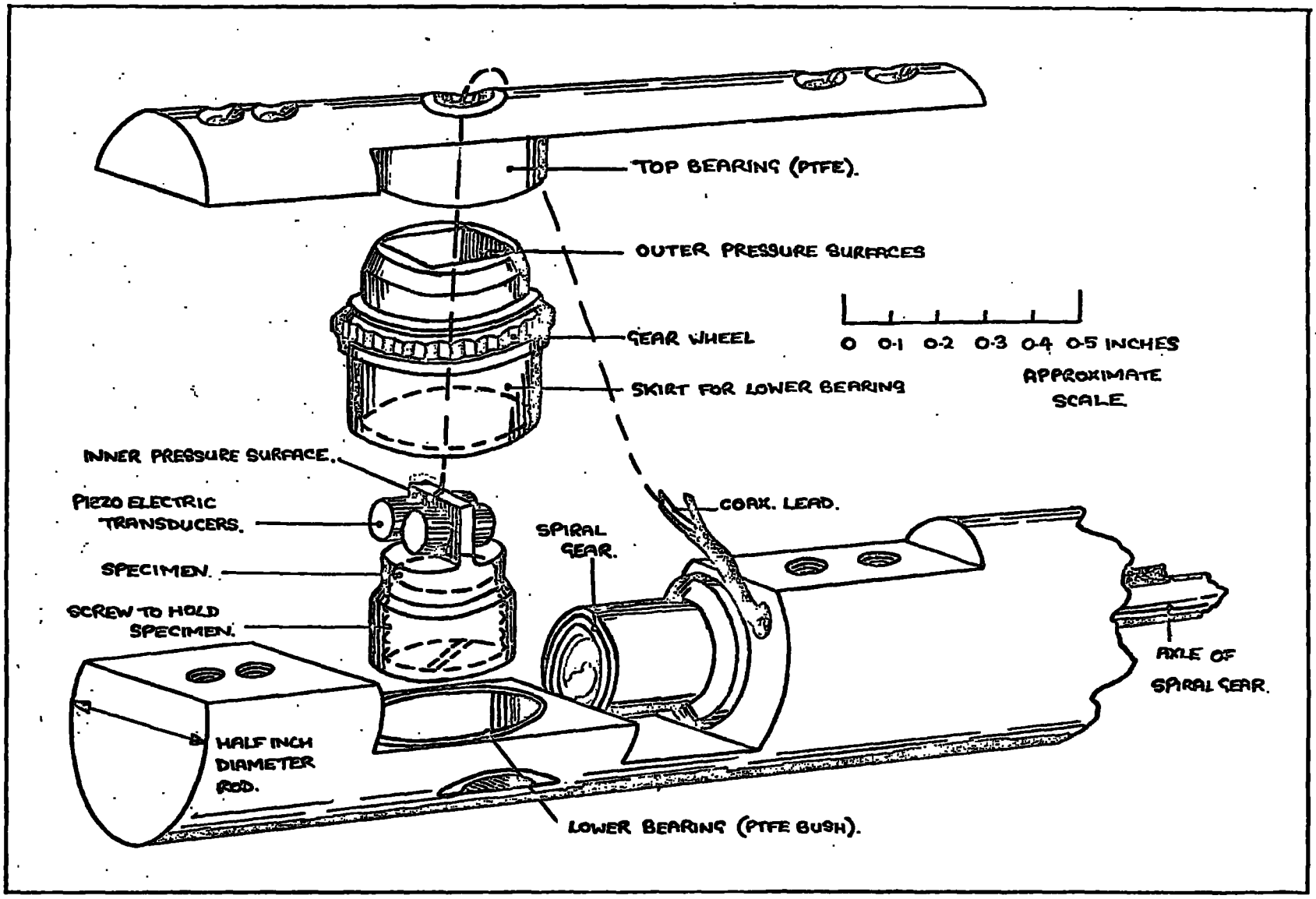

Fig. A.1. High Field Torque Magnetometer.

and because of their high resistance electromagnetic pick-up during the heavy current pulse in the magnet coil will be small. The projected arrangement was one in which the ellipsoidal specimen was contained in a holder with its axis perpendicular to the axis of the magnet solenoid, the piezoelectric ceramics, cylindrical in form, being arrayed around the specimen. It is necessary to vary the orientation of the specimen to the field direction, and the arrangement adopted for this was similar to that designed by Thorsen and Berlincourt (A2) for investigation of the de Haas-van Alphen effect. The specimen holder was surrounded by a gear wheel, which engaged with a spiral cut in the end of a cylinder whose axis lay in the plane of the gear and slightly offset from the diameter. The advantage of this system is that the rotational motion is turned through the necessary right angle with a minimum number of geared components, return action from gearwheel to spiral is small, and Thorsen and Berlincourt claim great precision of movement.

The apparatus is illustrated in Figure A.1. The specimen was contained in a hollow cylinder, a threaded core screwing up on to the ellipsoid to clamp it, and a pressure pad on the end of the cylinder located on the ends of a battery of four piezoelectric ceramics, LZ-2a supplied by the Brush-Crystal Co. (Southampton). Each ceramic was cylindrical, of diameter 0.31 cms and length 0.24 cms. The other ends of the ceramics were contained by two sides of a rectangular hole cut into the body of the gear wheel. Thus torque applied to the specimen holder compressed two of the transducers, reducing the pressure on the other two. The contact faces of each transducer were silver plated, and all the pressure surfaces of the apparatus were faced with thin copper foil, to

which contacts were made so that the piezoelectric ceramics were arranged in parallel. The apparatus had to be non-conducting, because of the transient field applied, and two models were built, each with an overall diameter of 0.55", one of Nylon 66, and the other of P.T.F.E. The latter was not satisfactory, because the spiral gear very quickly showed wear. The nylon model was better, although orientation could not be claimed to better than $\pm$ 2°.

The arrangement was tried in the pulse magnet, but the pick-up due to the large current pulse (which consisted of both electromagnetic and electro static pick-up) was extremely large, and bore little relation to the shape of the field pulse. The output signal as displayed on the oscilloscope contained many secondary oscillations which appeared to be due to mechanical vibrations in the manetometer. The pick-up signal was photographed and proved to be reasonably repeatable, although there was some variation in the higher frequency vibrations. Re-arrangement of the leads reduced the pick-up somewhat, although it was still rather larger than the signal expected from the piezoelectric ceramics for torques of the order of 10^5 dyne-cms. It was at this point that a D.C. solenoid producing 80 kOe in a 2" diameter core, built by the Physics Department of Oxford University, was made available to us. Since it was felt that the magnetometer was likely to produce better results in a steady field, this mode of operation was concentrated upon. Because the apparatus was no longer required to be non-conducting, a third model was constructed from brass: the gear mechanism functioned better when made from this material. The output from the transducers was connected to a o-1 volt vibrating-reed electrometer. The charge produced on the piezoelectric

ceramics by the application of pressure leaked away through the system, so that the signal decayed exponentially. The leakage resistance of the ceramics was 10^{12} ohms, so that the electrometer was used on the 10^{12} ohm range, when a decay time constant of the order of 30 seconds was observed. Since at such high field levels the field could not be suddenly switched on, the torque could only be measured as a change in torque produced when the specimen was rotated from one position to another. The problem experienced here was again one of noise, which obscured any signal produced by a change in torque consequent on rotation. One of the sources of noise was traced to capacitative changes in the leads to the transducers. To combat this the gear wheel and outer pressure pads were earthed, and the signal taken from the pressure pad on the specimen holder via a miniature coaxial cable made from polythene tube extruded over thin copper wire. A braided copper sleeve was stretched on to this insulated wire, and the outside coated with conducting silver paste. This shielded wire was connected to conventional non-microphonic cable a short distance away from the specimen holder. The arrangement, though a big improvement, was not entirely satisfactory, since the cable bent as the holder rotated, the consequent change in capacitance of the cable producing a signal at the electrometer; this could be seen from the fact that the signal was present even when the transducers were replaced by dummies made from P.T.F.E. The main source of noise remaining after these modifications arose, however, from the piezoelectric ceramics themselves. It appeared that rotation of the holder produced vibrations in the system which were picked up by the transducers and appeared as a noise signal. The bearing system was modified in various ways, resulting in a slight improvement,

but the noise was finally ascribed to the vibration produced by the engagement of the two gears. An intermediate gearwheel inserted between the spiral gear and that on the specimen failed to remedy this. Thus it appeared that D.C. operation of a piezoelectric system would involve the complete redesigning of the orienting device. There was not sufficient time available to permit this, and in any case it seems possible that the mechanical vibrations encountered in this system might well be present in other designs.

In view of the large torques produced by magnetocrystalline anisotropy in the rare earth metals, perseverance with the device for use in pulsed fields might be profitable. Re-arrangement of the leads to the transducers,and perhaps of the positioning of the transducers themselves, could be expected to decrease the amount of pick-up signal produced. This was of the order of several volts in the system used. If the pick-up is repeatable, it could possibly be calibrated for against field strength and temperature. In this respect a design in which the transducers were not rotated relative to the field would, however, be at an advantage. It is doubtful that such a magnetometer would be able to measure the torques produced by the rare earth metals in the non-ferromagnetic ranges, but for the C axis anisotropy in the ferromagnetic metals, the measuring system is not required to be sensitive, since torques of the order of 10^6 dyne-cms may be expected. For such torques signals of some 10 volts and more may be produced by the transducers, even though the capacitance of the connectors is comparatively large. Thus a high noise level can be tolerated.

For D.C. measurement, strain gauge measurement of the torque may be preferable to the use of piezoelectric transducers. In this case the

signal is not transient, and mechanical vibrations produced by the rotation of the specimen prior to measurement do not matter. Difficulties might in this case be encountered in producing an apparatus with the necessary small dimensions, although spiral strain gauges of a clock-spring type are now produced, and these might well be usefully employed for this purpose.

REFERENCES

A1. H. P. Furth, M. A. Levine and R. W. Waniek. Rev. Sci.Inst. 28, 949, (1957).

A2. A. C. Thorsen and T. G. Berlincourt, Rev. Sci. Inst., 34, 435, (1963).